DOCTOR OF PHILOSOPHY

LAND COVER CHANGE IMPACTS ON WATER AND ENERGY BALANCE IN EAST AFRICA

Musau, John

Award date:
2021

Awarding institution:
Bangor University

DOCTOR OF PHILOSOPHY

LAND COVER CHANGE IMPACTS ON WATER AND ENERGY BALANCE IN EAST AFRICA

Musau, John

Award date:
2021

Awarding institution:
Bangor University

LAND COVER CHANGE IMPACTS ON WATER AND ENERGY BALANCE IN EAST AFRICA

BY

JOHN MWANZIA MUSAU

A thesis submitted in fulfillment of the requirements for the degree of Doctor of Philosophy in Environmental Science

School of Natural Sciences

Bangor University

2019

Acknowledgements

I am grateful to my supervisors Dr. Sopan Patil, and Dr. Michael Marshall, who have been very supportive throughout all the stages of my research. I have obtained most of my skills through your insights and have been very instrumental in helping me to shape my ideas. I appreciate your dedication and that you were always accessible. Although I was a research student and not based at the university, Dr. Sopan Patil supported me to access all possible student services at the university. I thank Dr. Michael Marshall very much who gave me the opportunity to convert my work as a research fellow at the World Agroforestry Centre (ICRAF) into my PhD research. I also thank Dr. Fergus Sinclair who provided financial assistance during my research. Finally, I would like to thank my family the all the support they provided me during this research. I am eternally grateful to you all.

Table of Contents

List of Tables

List of Figures

Abbreviations

BFAST	Breaks For Additive Season and Trend algorithm
CHIRPS	Climate Hazards group Infrared Precipitation with Stations
ET	Evapotranspiration
FVC	Fractional Vegetation Cover
G	Ground heat flux
GIMMS	Global Inventory Monitoring and Modelling Studies
GLCC	Global Land Cover Characterization Database
H	Sensible heat flux
HFI	Global Human Footprint Index
ITCZ	Intertropical Convergence Zone
LAI	Leaf Area Index
LE	Latent heat flux
LSM	Land Surface Model
LUCCs	Land Use and Land Cover Changes
MODIS	Moderate Resolution Imaging Spectroradiometer
RN	Net radiation
SPEI	Standardized Precipitation Evapotranspiration Index
SYNMAP	Synergetic land cover product
TSE	Thiel-Sen median slope estimator
VIC	Variable Infiltration Capacity model

General Abstract

Terrestrial vegetation plays a key role in land surface-atmosphere interactions as the primary link for moisture (evapotranspiration) and energy (latent) exchange. Consequently, the regional to global effects of historical and expected land use/cover changes (LUCCs) due to both natural and human factors remains a key subject in environmental research. In the East Africa region, LUCC is a key subject as approximately 30% of the region has been converted to cropland or urban areas in the recent past. The recent effects of droughts on vegetation dynamics in the region have also put a spotlight on the potential effects of climate change on ecosystems in the region. This study focuses on the assessment of the vegetation dynamics and effects of land cover changes on the water and energy balance in the East Africa. To address the complexity of the research, an integrated approach was adopted linking climate observations, remote sensing data on vegetation phenology and land surface fluxes, and a land surface model (Variable Infiltration Capacity (VIC) model). Satellite-based Leaf Area Index (LAI) observations over the 1982 to 2011 period showed a significant increasing trend in about 25% of the region while decreasing trend was recorded in 4% of the region. The spatial-temporal vegetation dynamics showed varied relationship with both climate anomalies and human activities. Long-term vegetation dynamics derived from MODIS datasets were used to parameterize VIC model in order to assess the regional sensitivity of the surface water and energy fluxes to varying seasonal and interannual vegetation changes. The results were compared to globally tested datasets on Evapotranspiration (ET), Latent heat and Sensible heat based on FLUXCOM global datasets on surface energy balance as well as MODIS evapotranspiration data. The adoption of vegetation parameter values varying spatially and in time indicated a more realistic representation of the water and energy fluxes in the region. Across the region, the variations in vegetation parameters is found to impose higher standard deviation on mean annual sensible heat (0.3 Wm^{-2}) than on latent heat (0.03 Wm^{-2}) but generally has small effect on ground heat (0.02 Wm^{-2}). However, the percentage of positive variance imposed on ground heat by varying vegetation parameters across the region is higher (33%) compared to 13% and 14% for ET/latent heat and sensible heat, respectively. Using the newly configured VIC model for east Africa, effects of LUCCs were simulated mainly focusing on the potential effects of increased tree cover through afforestation or/and reforestation efforts on regional LAI, FVC and albedo. The land cover changes were simulated using the Dynamic Global Vegetation Model with

managed Land, (LPJmL4) with parameters adapted for the east Africa region. This approach allowed for simulation of increased spread of tree cover in bare areas and areas covered by shrubs and grass, while accounting for habitat suitability for growth of different tree vegetation types. The simulated increase in tree cover across the region showed potential increase in mean LAI and fractional vegetation cover by 1.5 m^2/m^2 and 0.16 respectively, while albedo decreased by 0.02 averaged across the region. The simulated changes in the water balance due to increased tree cover were mainly linked to the increased transpiration and canopy evaporation as well as decrease in soil evaporation. Particularly, increased tree cover led to increased latent and sensible heat while land surface temperature and canopy temperature decreased by -1.0°C and -1.9°C respectively. Based on the findings of the study, increasing forest cover in the region will play a pivotal role in climate change adaptation by inducing a highly needed local cooling effect. However, there is still need for extensive analysis of the potential impacts of natural and human-induced vegetation dynamics in East Africa at a much smaller scale. This will particularly require reduced uncertainties in the region's assessment studies particularly through better parameterization of small-scale variations in vegetation as well improved regional constraining of land surface models using multiple datasets.

Chapter 1: Introduction

1.1 Background of the research

Sustainable management of natural resources is a critical component in the achievement of effective livelihood systems, particularly for the communities most vulnerable to climate change impacts. Among the critical environmental challenges that many communities must address include the Land Use and Land Cover Changes (LULCCs) not only due to their mark on the global environmental change but also because of their effects on ecosystem vulnerability which pose severe impacts on community livelihoods (Olson et al., 2008). Such changes are evident not only in local to global vegetation phenological dynamics, but also through the biophysical and biogeochemical feedbacks between the land surface and the atmosphere. As noted by Lambin et al. (2003), during the 1990's approximately 16.1 million hectares of the world's natural forests were lost by per year on average.

Changes in the structure and density of vegetation through land cover conversions causes dramatic modifications of the water and energy budgets. This occurs through alterations in the biophysical landscape characteristics such as, leaf area, fraction vegetation cover, surface roughness, and canopy conductance at varying spatial and temporal scales (Anderson et al., 2011; Li et al., 2015b). These changes have been associated with biophysical effects composed of both radiative forcing (due to changes in albedo) and non-radiative forcing (due to changes in the hydrological cycle through evapotranspiration rates) on local and regional climate (Davin and de Noblet-Ducoudre, 2010). For instance, compared to rangelands and croplands, forests have lower albedo and more heterogeneous canopies, thus they absorb more sunlight and allow air mixing.

In addition to the direct impacts on the local to regional latent and sensible heat fluxes, LULCC has shown significant impacts on the magnitude of turbulent energy fluxes by altering surface temperatures through changes in evapotranspiration and surface roughness (Davin and de Noblet-Ducoudre, 2010). These competing biophysical effects of LULCC not only vary spatially but also seasonally, with the magnitude of warming or cooling being conditional to the specific vegetation change and background climatic conditions (Duveiller et al., 2018c). What's more, the biophysical effects of LULCC on global climate have shown comparable magnitudes to the biochemical effects, as demonstrated in previous global modelling studies (Davin and de Noblet-Ducoudre,

2010; Devaraju et al., 2015; Pongratz et al., 2010). Consequently, it has been recommended that the biogeochemical considerations mainly adopted in the crediting of forestry projects should be expanded to include the potential biophysical effects of such projects.

1.2 Problem statement

In east Africa, political, economic, demographic, and social factors have been linked to widespread changes in land use/cover, and this is projected to continue. Much of the land that was previously covered by natural ecosystems has been cleared to create room for farmlands, grazing lands, human settlements and urban areas, thus posing a threat to the ecological systems in the region (Brink et al., 2014; Jacobson et al., 2015; Maitima et al., 2009; Pricope et al., 2013). As reported by Jacobson et al. (2015), approximately 30% of the region has been converted to cropland or urban areas, with Burundi and Rwanda showing the highest proportions, 85.99% and 82.27% respectively. Between 1990 and 2010, Brink et al. (2014) found that agricultural area in East Africa (comprising Djibouti, Eritrea, Ethiopia, Kenya, Somalia, Sudan and Uganda) increased by 28% with an alarming shift in the rate of deforestation from 0.2% per year in 1990-2000 period to 0.4% per year in 2000-2010 period. Pricope et al. (2013) addressed the spatial interaction between climate, vegetation variations and degradation, and population density changes in the East Africa Horn's pastoral and agro-pastoral livelihoods zones. They established a potential long-term degradation of rangelands mainly due to population pressures and land use change.

The trade-off in the LULCC for supply of food and fiber is the biophysical impacts on the surface water and energy balance (Li et al., 2015b, 2016; Prevedello et al., 2019). The capacity of ecosystems to supply food for human consumption is influenced by the exchange of water and energy fluxes and therefore, the long-term productivity of these ecosystems is affected by LULCC. Due to the high dependence of livelihoods on rain-fed agriculture, there is high vulnerability to extreme negative effects of climate change in the region (Ayana et al., 2016; Grace et al., 2014; Pricope et al., 2013).

1.3 Justification of the study

Despite the wide range of existing research on the impacts of LULCC, the east Africa region has not been adequately studied. Although the basics of the influence of land surface on water and energy balance are considerably well known, the fragmented and dynamic landscape patterns in East Africa pose substantial challenges and uncertainty in assessment of the potential regional biophysical effects of LULCC. The vegetation dynamics in this region are characterized by highly transient systems which are mainly vulnerable to not only herbivore pressure and fire regimes but also human activities and climate change (Pfeifer et al., 2012). Given the spatio-temporal complexity of the radiative forcing of LULCC, efficient and reliable regional assessments are crucial for adaptive management amid rapid socio-economic and environmental changes.

1.4 Research objectives

1.4.1 General objective

The overall goal of this study was to assess the impacts of land cover change on water and energy balance in East Africa.

1.4.2 Specific objectives

i. To assess the spatio-temporal patterns and trends in vegetation dynamics in east Africa region using time series data derived from Earth observations
ii. To evaluate the water and energy fluxes in east Africa region using the Variable Infiltration Capacity (VIC) model and an improved parameterization of land surface heterogeneity
iii. To assess the impacts of land cover changes on the water and energy balance in East Africa

1.4.3 Research questions

i. Are there any trends in observed vegetation dynamics, and how do they relate to climate anomalies in East Africa? (Chapter 3)
ii. Can we simulate the current water and energy balance in East Africa better using an improved parameterization of spatial and temporal land surface heterogeneity? (Chapter 4)

iii. What are the potential impacts of land cover change on water and energy balance in East Africa region? (Chapter 5)

1.5 Thesis outline

This thesis is structured into six chapters with the first chapter providing a general introduction of the research. Chapter 2 provides a review of literature related to the research topic. Chapter 3 addresses the first objective, namely the spatio-temporal patterns and trends in vegetation dynamics in east Africa based time series data derived from Earth observations. Chapter 4 addresses the second objective that is use of the Earth observations to parameterize vegetation dynamics in a land surface model for simulation of water and energy fluxes. The model was adapted to realistically reproduce the water and energy fluxes in the region by replacing the default climatological statistic vegetation parameter values with time and spatially varying Leaf Area Index, Fractional Vegetation Cover, and albedo derived from various MODIS products covering the period 2001 to 2011. Chapter 5 addresses the third objective that is assessment of land cover change impacts on regional water and energy balance. The last chapter provides a general discussion and conclusions of the study based on the posed research questions.

Chapter 2: Literature Review

2.1 Introduction

The increasingly changing environmental conditions calls for enhanced capacity to both monitor and predict alterations in the carbon and water cycles. Consequently, significant efforts have been exerted on the monitoring and modelling of surface water and energy balance at local, regional and global scales (Hibbard et al., 2010; Mallick et al., 2014; Pitman, 2003; Renner and Bernhofer, 2012). Over the past decades, land surface characteristics have been widely recognized as a crucial factor in the regulation of the local, regional and global land-atmosphere exchanges (Anav et al., 2010; Delire et al., 2011; Foley et al., 1998, 2000; Lee et al., 2015; Snyder et al., 2004). In the soil-vegetation-atmosphere interface, vegetation plays a key role in regulating biophysical and biogeochemical processes and facilitates complex feedbacks varying in space and within a range of timescales (Arora, 2002; Berry et al., 2016; Donohue et al., 2006; Xin and Liu, 2010).

2.2 Modelling land surface water and energy balance

2.2.1 Role of remote sensing data

The monitoring and simulation of water and energy balance components require long-term data of the biochemical and biophysical variables. Measurement of these components at scales relevant to decision makers has been identified as key area of interest (Verma et al., 2015; Williams et al., 2009). Even with access to point measurements, mapping of these quantities at a regional scale is limited as the heat and moisture fluxes across the land-atmosphere interface vary over a range of spatial and temporal scales due to the large heterogeneities in the land surface. Numerous data collection campaigns and inter-comparison studies have been carried out in the recent past which sought to promote eco-hydrological studies through access to datasets at regional and global scales.

Satellite remote sensing has evolved into an exceptional data source for calculating and validating simulated water and energy fluxes at scales relevant for decision making. In the recent past, time series datasets for various biophysical variables spanning 30+ years at various spatial and temporal resolutions have been developed and used to evaluate land surface-atmosphere interactions at regional, continental and global scales (Fensholt and Proud, 2012; Zhu et al., 2013). The availability of long-term, repetitive satellite-derived datasets has greatly improved the monitoring

and characterization of the land surface at varying spatial and temporal scales (Peng et al., 2012; Zhu et al., 2013). Multispectral band combinations of these datasets have aided the retrieval of long time series of land surface variables widely used to examine trends in vegetation dynamics at global, regional and national scales (Bao et al., 2014; Julien and Sobrino, 2009), as well as the impacts of vegetation on water and energy flux (Hu et al., 2009). Routine estimates of precipitation, land surface temperature and emissivity, snow water equivalent and soil moisture, vegetation phenology and land cover change can be readily obtained from data acquired by passive and active sensors orbiting the earth (AghaKouchak et al., 2015; Lakshmi, 2013). This availability of multiple datasets has facilitated water and energy balance studies by increasing the types and number of observations linked to surface parameters that are useful in estimating the land surface-atmosphere interactions (Li et al., 2015a).

2.2.2 Application of land surface models (LSMs)

In the recent past, LSMs have advanced in complexity and applicability in increasingly higher resolutions which has been occasioned by availability of remote sensing data. The present day LSMs have evolved through three distinct generations from the simple bucket model to advanced multilayer soil and plant canopy models (Pitman, 2003; Sato et al., 2015; Yang, 2004; Zhao and Li, 2015). The advances in the development of LSMs is marked mainly by the representation of the carbon cycle and the close coupling of the water and heat exchanges on the land surface including withing canopy and bare areas (Sellers et al., 1996). This coupling of water and heat fluxes and CO_2 was occasioned by the optimization role played by physiological control of evapotranspiration by plants to minimize water loss by closing stomata and maximize carbon fluxes by photosynthesis. In addition, consideration of subgrid-scale variability of land surface characteristics such as elevation, soils and vegetation as well as precipitation is a key highlight in development these models (Bohn and Vivoni, 2016; Guillevic et al., 2002) . Such subgrid variations are likely to affect the accuracy of the simulated surface water and energy budgets by accounting for key non-linear physical processes in the land surface-atmosphere interface. Other crucial developments include a more optimized integration of a cascade of physical and biological processes on the land surface with varying intrinsic time scales through asynchronous coupling thus integrating faster and slower land surface processes (Fatichi and Ivanov, 2014; Ivanov et al.,

2008). However, the appropriate level of complexity, scales and trade-offs in representation of various process in LSMs is still under discussion.

In LSMs, the surface water balance is expressed as follows (Deng et al., 2015):

$$P = E + R + \frac{\partial S}{\partial t} \quad (2.1)$$

Where *P, E, R* and *dS/dt,* are precipitation, evaporation (comprised of evaporation from soil and canopy, and transpiration), runoff, and change of water storage. The water budget in the land surface is mainly controlled by the atmosphere and vegetation/soil through precipitation and evapotranspiration respectively. During high soil moisture conditions, the atmospheric moisture content in the near-surface determines the potential evaporation. When the soil moisture drops below a certain level, physiological mechanism in vegetation reduce water supply from the root layer to the atmosphere thus reducing potential evaporation. During additional precipitation when soil is dry, infiltration is high up to a certain threshold when runoff is generated (Liang et al., 1994; Milly et al., 2014). The ET is mainly driven by not only net radiation and an advection factor given by the saturation deficit but also by physiological control by plants (Bohn and Vivoni, 2016). Thus, ET acts as a crucial link between the water and energy balance. The various ET components are simulated based on the Penman-Monteith equation as follows:

$$E_0 = \frac{\Delta(R_n - G) + \rho_a c_p \delta_e / r_a}{(\Delta + \gamma\left(1 + \frac{r_c}{r_a}\right))L_v} \quad (2.2)$$

Where Δ is rate of change of saturated vapor pressure with temperature, R_n is net radiation, G is ground heat flux, ρ_a and c_p are density and specific heat capacity of dry air, respectively, δ_e is vapor pressure deficit, r_a and r_c are aerodynamic and canopy resistances, respectively, and L_v is latent heat of vaporization. The canopy resistance is calculated as $r_c = r_{arc} + r_s$, where $r_{arc}$is the architectural resistance linked to the canopy structure and r_s is the aggregate stomatal resistance (Bohn and Vivoni, 2016; Guo and Shen, 2015b; Liang et al., 1994).

On the other hand, the energy balances for wet and dry canopy as well as bare soil are used to calculate surface temperature and the sensible and ground heat fluxes. Given a moderately

homogeneous surface, the energy balance equation for a layer of the air column from ground surface to given height in the atmosphere can be expressed as:

$$R_n = H + \rho_w L_e E + G + \Delta H_s \quad (2.3)$$

Where $R_n$is the net radiation, $H$is sensible heat flux, $\rho_w$is the density of liquid water, L_e is the latent heat of vaporization, $\rho_w L_e E$ is the latent heat flux, G is the ground heat flux and ΔH_s is the change in the energy storage in the layer for a given duration over a given unit area. The distribution of net radiation into sensible, latent and soil heat fluxes is influenced by multifaceted inter-dependent processes in the soil-vegetation-atmosphere continuum. Soil heat fluxes are mainly influenced by soil moisture and thermal characteristics of the soil matrix. The net radiation is given by:

$$R_n = (1 - \alpha)R_s + \varepsilon \cdot (R_L - \sigma T_s^4) \quad (2.4)$$

Where α is the albedo of the land surface cover and represents the fraction of the solar radiation reflected by the surface, R_s is the downward shortwave radiation, ε is the emissivity of the land surface cover, R_L is the downward long-wave radiation, $\sigma$is the Stefan-Boltzmann constant and T_s^4 is the temperature of the wet canopy, dry canopy, or bare-soil surface.

Based on the several reviews on the evolution of LSMs, a few conclusions can be drawn. Across the different model structures, only the vertical interactions of the land surface process are well parameterized hence they can be regarded as one-dimensional with little or no explicit horizontal interactions between grid cells. The "big-leaf" approach is the commonly used which basically assumes a homogenous surface type per grid cell (Overgaard et al., 2006). This approach does not capture the surface heterogeneities. In addition, the number and areal coverage of vegetation types and their associated secondary parameters (e.g roughness length, zero-plane displace height, leaf area index, canopy height, minimum stomatal resistance) within a grid cell are often prescribed using static monthly estimates. The choice of any model is often a function of trade-offs between desired realism and complexity. Realistic and consequently complex models provide more realistic outputs at a cost of immense number of parameters which should be accurately estimated at the

scale of the application. Contrary, simple models require less parameters, data and computational demand but their outputs require extensive calibration (Overgaard et al., 2006).

2.2.3 Parameterization of surface heterogeneity in LSMs

The current climate research challenges have led to the development of various land surface-atmosphere schemes to realistically simulated land-vegetation-atmosphere exchanges of water and energy for global and regional climate modeling (Lin and Brunsell, 2013; Maneta and Silverman, 2013). The advancement in the LSMs has mainly focused on varied complexity in the representation of the different components of the soil-vegetation systems. This includes the changes in the number of soil and vegetation layers, grid resolution, description of bio-physical and physiological processes as well as the numerical approaches used (Bronstert et al., 2005). Generally the land-atmosphere interactions are characterized by a wide range of spatial and temporal scales that are highly influenced by the spatial distribution of land surface properties (Giorgi, 1997; Stoll and Porte´-Agel, 2009). Heterogeneities in land surface should therefore be explicitly considered in any efforts to realistically simulate the partitioning of water and energy balance components. According to Giorgi and Avissar (1997), land surface heterogeneities come in form of variations in ecosystem diversity thus different vegetation cover/surface types, terrain morphology, soil characteristics, and climatic forcing.

The traditional lumped model concept assumes that the spatially variable inputs and parameters are homogeneous. Thus, the applicability of lumped-surface parameterizations is undermined as the model response is highly dominated by parameterizations of inputs and parameters at sub-grid scale. An ideal land surface parameterization must both efficiently account for all of the dynamic interaction between the land surface and the atmosphere at sub-grid scale and be computationally realistic. Several studies comparing simulations with and without consideration of subgrid-scale heterogeneity have proven the sensitivity of simulated fluxes to the details of how these variations are represented in very patchy surfaces (Albertson et al., 2001; Arola and Lettenmaier, 1996; Esserya et al., 2003; Guillevic et al., 2002; Koster and Suarez, 1992a; Kure et al., 2011).

Surface heterogeneity can be addressed using approaches ranging from averaging techniques to tile or mosaic approach (Su et al., 1999). A multiplicity of studies has been published on different

averaging techniques which can be used to obtain effective or aggregated parameters to account for the non-linear effects of surface variations (Albertson et al., 2001). Parameter aggregation methods include using either the most prevalent parameter or a weighted mean of the parameters for all surface types within the grid cell to define the effective parameters used in the simulation (Giorgi and Avissar, 1997). To account for local nonlinear processes, additional weighting functions can be included in the parameter averaging (Lhomme, 1992). In addition, theoretical basis for an appropriate parameter averaging can be derived for some parameters. An example is use of the concept of blending height to estimate area-averaged roughness (Claussen, 1991).

The statistical dynamical approach is another commonly used aggregation method which assumes that surface variations in vegetation, soil and climatic conditions can be described by distributions that can be approximated by probability density functions (PDFs) (Avissar, 1992; Kure et al., 2010). The surface fluxes for the grid cell are then estimated by numerical or analytical integration of non-linear terms over the appropriate PDFs. The efficiency and computational cost of this approach is particularly compromised if it is applied to the full set of N parameters in state-of-the-art LSMs which would require numerical solution of integrals of order N and the solution of the whole system over I^N intervals. According to Giorgi and Avissar (1997), three strategies can be adopted to circumvent these challenge. First, based on the assumption that heterogeneity of key parameters is more instrumental than full depiction of biophysical processes, the original set of equations in LSMs can be simplified and the number of independent parameters reduced. Alternatively, the LSMs can be drastically simplified to allow full analytical integration of the model equations over the PDF. The third strategy entails maintaining the entire set of LSM equations and PDF integration only for a few critical variables and over some of the non-linear terms in the equations.

In conditions of moderate heterogeneity, area-averaged effective parameters can be adequate in representing surface heterogeneity. However, in highly heterogeneous areas, the more detailed mosaic, mixture and explicit sub-grid approaches can be used (Seth et al., 1994). In the mixture approach, a tightly coupled mixture of surface types is assumed for an entire grid cell thus accounting for small scale variations in the horizontal and vertical structure of the surface resulting in an homogeneous interface layer (Giorgi and Avissar, 1997). However, as surface fluxes mix in

the interface layer prior to interaction with atmosphere, the dominant sub-area is likely have more effect leading to unrealistic fluxes. The mosaic approach overcomes this challenge. In the mosaic approach, similar vegetation within a grid cell is regrouped into patches which are assumed to be completely covered by the particular vegetation. The patches have independent connections with mean grid cell atmospheric forcing and the separate water and energy balances are computed for each patch and area-weighted mean fluxes calculated for the grid cell. Due to the non-linear dependence of surface fluxes on land surface characteristics, fluxes calculated separately for sub-grids/tiles lead to improved predictions and reduced uncertainties in large-scale applications (Bohn and Vivoni, 2016; Guo and Shen, 2015b). This helps to achieve horizontal complexity and to increase physical rationality of the simulated water and energy fluxes.

Both the mosaic and mixture approaches assume a well-mixed atmosphere hence same atmospheric forcing is used across the grid cell. Unlike these approaches, the explicit sub-grid approach developed by Seth et al., (1994) allows spatially varying atmospheric forcing within a grid. In addition, the similar vegetation patches are not regrouped but instead a higher resolution grid is defined with each sub-grid consisting of single vegetation type or bare soil. This approach therefore maintains the spatial location of the sub-grids hence spatially varying atmospheric forcing can be applied in a physically realistic manner. This is the ultimate strength of this approach since the memory of sub-grid water and energy budgets is maintained across time scales thus ensuring the consistency in the time evolution of surface fluxes. The patches used in the mosaic and explicit sub-grid approaches are assumed to be homogeneous yet some of the some of the characteristics such as roughness lengths and stomatal resistances are obviously heterogeneous. To account for these intra-patch variations, a continuous rather than discrete representation is required hence the statistical–dynamical approach can be used (Avissar, 1991, 1992; Giorgi, 1997; Giorgi and Avissar, 1997; Xinmin et al., 2000). As noted by Avissar (1992) and Brunsell et al. (2011), spatial heterogeneity is fundamentally a question of grid scale with reference to modelling and observation resolution. A large grid cell allows counter balancing feedback mechanisms in different cover types while, on the other hand, large grid size leads to complications in the parameterization of key dynamical processes in the land surface.

2.3 Biophysical impacts of vegetation dynamics

Among the most prominent impacts of human activities is the modification of the land surface through extensive land cover changes, mainly involving the conversion of forests to grassland and cropland (Pongratz et al., 2008). Changes in in land cover properties have been linked to widespread biochemical and biophysical effects with the potential to influence the earth's ecological and environmental systems at varying spatial and temporal scales (Bright et al., 2017; Devaraju et al., 2015; He et al., 2014; Lucia et al., 2017). Vegetation plays a crucial role in the land-atmosphere interface through the regulation of exchanges of water, heat, radiation and momentum. The need to address the increasingly inevitable effects of climate change has therefore been accompanied by an increasingly mounting interest on the role of ecosystems in mitigating climate change impacts. In addition, land cover change has been shown as a major threat to the strength of ecosystems as carbon sinks and threatens to transform these ecosystems into sources of greenhouse gases, thus accelerating global warming. Therefore, reforestation and/or afforestation have been recommended as key strategies for climate change mitigation due to their immense potential in rising and conserving the regional and global terrestrial carbon pools. However, most of the studies addressing this subject have mainly adopted a carbon-centric perspective in evaluating the role of different ecosystem properties in climate change mitigation (Quéré et al., 2018; Sleeter et al., 2018). On the contrary, the biophysical implications of land cover change, particularly at the local to regional level, have been largely overlooked.

The evaluation of the biophysical effects of vegetation on surface fluxes based solely on observations is still a challenge. Multiple studies have applied satellite-based approaches to assess the present-day vegetation impacts on global or regional surface fluxes (Abera et al., 2019; Duveiller et al., 2018c; Li et al., 2015b; Prevedello et al., 2019). On the hand, contribution of land surface models' applications is immense in the current understanding of how vegetation dynamics affect surface fluxes in different regions across the globe (Chen et al., 2012; Duveiller et al., 2018b; Forzieri et al., 2018). In these studies, the main mechanisms proposed to explain the biophysical effects of vegetation are LAI, albedo, evapotranspiration (ET) and surface roughness. While the spatial and temporal vegetation dynamics are highly controlled by climatic conditions, the vegetation also influence climate through bio-geophysical and biogeochemical mechanisms.

Therefore, land surface properties present a high potential to drive not only the local climate but also regional to global atmospheric processes thus regulating the climate through multiple positive and negative feedbacks (Duveiller et al., 2018b; Forzieri et al., 2018). As noted by Bonan (2008), land cover changes modify surface properties such as leaf area index (LAI), fractional Vegetation Cover (FVC), albedo, surface roughness, vegetation height , among others, which in turn affects surface fluxes of moisture, energy, and momentum. Figure 2-1 shows the main local feedbacks involved for changes in physical vegetation characteristics and the consequent effects on portioning of water and energy fluxes. The dominant and sign of these mechanisms varies depending on the geographical regions, seasons, and climate variable of interest.

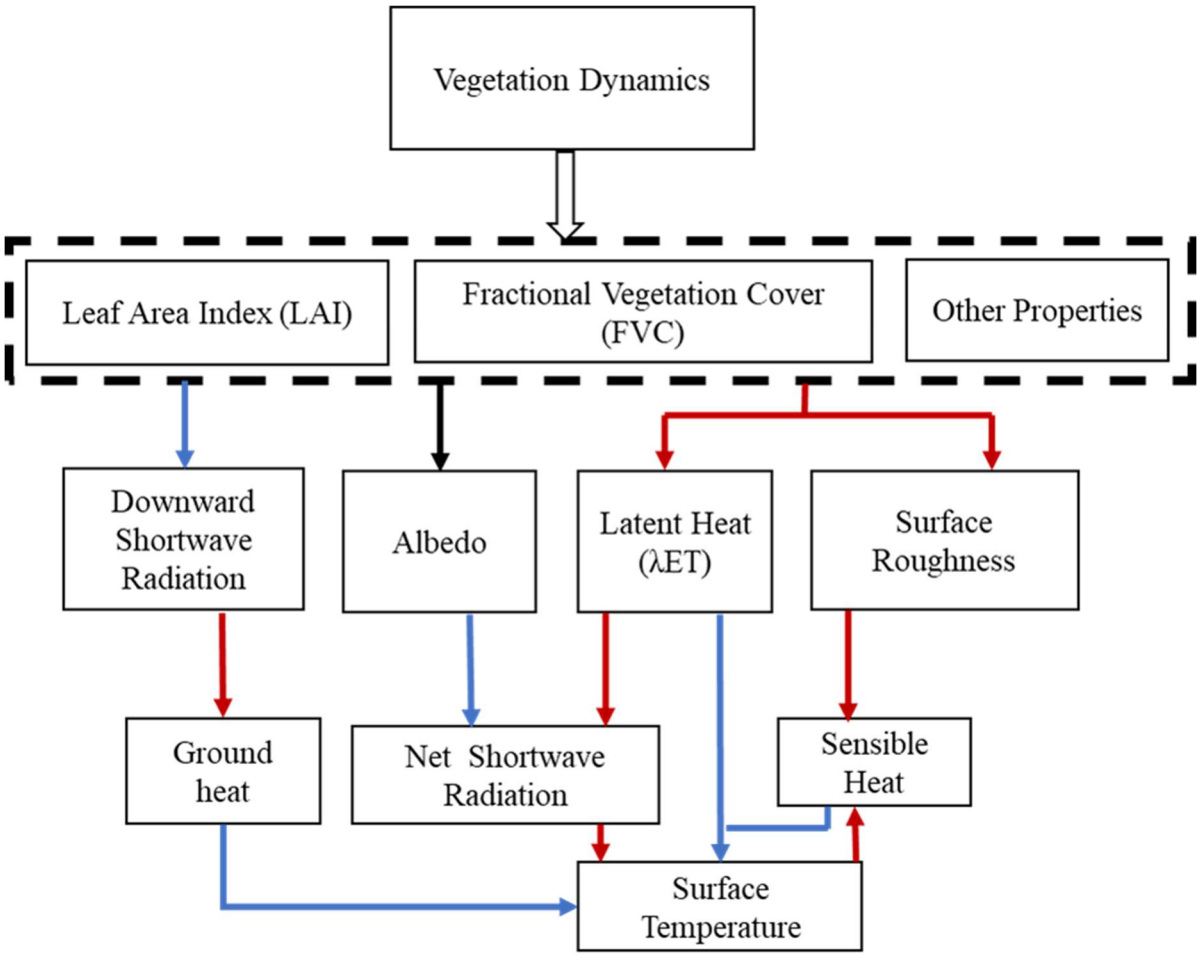

Figure 2-1: Impacts of vegetation dynamics on land surface energy and water balance. The blue (blue) arrows linking variables indicates a positive (negative) response, while the black arrow means that the sign of response depends on other environmental conditions

For instance, changes in vegetation structure due to forestry activities, such as afforestation, reforestation, and forest management are expected to increase leaf Area Index (LAI) and Fractional Vegetation Cover (FVC) as well as influencing other surface properties such as rooting depth. Increased vegetation cover decreases the amount of ground downward incident shortwave radiation which in turn lowers the ground heat flux. Compared to bare areas, vegetation cover has a lower albedo causing an increase in proportion of energy absorbed by the surface which leads to increased surface temperature and potential increase in precipitation through the albedo mechanism. On the other hand, increased vegetation cover leads to enhanced evapotranspiration thus causing increased portioning of energy into latent heat. This causes a decrease in surface air temperature and potential increase in precipitation through the evapotranspiration mechanism. The high roughness length caused by increased vegetation cover leads to an increase in turbulent fluxes (latent heat and sensible heat), which lowers surface temperature. In addition, high roughness length is associated with enhanced mass convergence which increases upward moisture transport and convective clouds. The mechanism leads to increased precipitation and decrease in surface temperature (Chen et al., 2012; Li et al., 2017, 2016; Peng et al., 2014) .

In the recent past, new global estimates of land cover change impacts have been produced (Alkama and Cescatti, 2016; Duveiller et al., 2018a) and multiple approaches developed to assess response to land-use change in various land surface models (Duveiller et al., 2018c, 2018b; Forzieri et al., 2018). The availability of observational datasets and model analysis methods provide analogous metrics at varying spatial scales for the assessment of surface fluxes. However, effective assessment of land cover change impacts has been derailed by substantial model disagreements as well as inadequate observations to constrain the various components of the surface water and energy budgets (Winckler et al., 2017b). The long-term resilience of ecosystems and the fate of their supply of goods and services which support livelihoods of millions is largely contingent on the ecosystem response to environmental changes. The local and regional ecosystem changes extend to larger scales, thus affecting the interregional and global environment. In addition, the physical, chemical, and biological features of the land surface vary across different regions, so the effects of land cover changes are expected to vary significantly. Consequently, assessment of local and regional effects of vegetation dynamics is crucial in understanding environmental change effects.

Chapter 3: Vegetation Dynamics and Responses to Climate Anomalies in East Africa

3.1 Abstract

Across the vast and heterogeneous landscapes in East Africa, vegetation dynamics support a wide range of community livelihoods. Given the potential impacts of climatic changes and human activities, there is a pressing need to adequately evaluate and quantify the variations in vegetation dynamics and their vulnerability to environmental changes in the region. This study aims to provide novel insight into the vegetation trends and responses to climate anomalies using Leaf Area Index (LAI) and Standardized Precipitation Evapotranspiration Index (SPEI). The long-term vegetation trends were assessed based on non-parametric trend test while a liner relationship between LAI and SPEI was used to evaluate vegetation response to climate anomalies. For period 1982 to 2011, about 25% of the region showed significant increasing LAI trend while decreasing trend in LAI was recorded in 4% of the region. However, analysis of the temporal consistency in the LAI trends showed that non-monotonic vegetation changes were widespread in the region, with about 73.2% of the study area (or approx. 93.5% of all cases of significant LAI changes) showing statistically significant ($p<0.05$) abrupt changes (composed of the interrupted and reversed trend classes) in the general long-term LAI trends during the study period. The interrupted trends accounted for 46.9% (composed of 26.6% showing greening with a setback while 20.3% showed browning with a burst) of the area with vegetation cover. On the other hand, reversed trends were identified in 26.3% of the region, composed of greening to browning in 18.4% and browning to greening in 7.8% of region. The timing for the interruptions in the long-term LAI trends was predominantly in 1993 – 1997 for Kenya and after 2002 for Tanzania. The annual average water balance showed higher influence on vegetation resistance to drought anomalies compared to the human footprint. In conclusion, the spatially heterogeneous landscapes of East Africa showed profound transformation driven by both climatic and human factors over the period 1982 to 2011. Management and policy strategies are therefore required to control the utilization of ecosystem resources and to promote sustainability in the region.

3.2 Introduction

Terrestrial vegetation plays a key role in land surface-atmosphere interactions as the primary link for moisture (evapotranspiration) and energy (latent) exchange through its physiological properties

(Leaf Area Index (LAI), rooting depth and stomatal resistance), and its influence on surface roughness, and albedo (Arora, 2002; Bao et al., 2014; Ning et al., 2015). An improved characterization of spatial and temporal vegetation patterns is therefore important to not only assess landscape conditions but also to improve understanding of the vegetation response to climate at varying spatial and temporal scales. Global and regional studies on the causes of variations in vegetation have shown that climatic factors, particularly precipitation and temperature, significantly influence vegetation dynamics (Jiapaer et al., 2015; Liu et al., 2015; Montaldo et al., 2008; Tagesson et al., 2015).

The availability of long-term, repetitive satellite-derived datasets has greatly improved the monitoring and characterization of the land surface at varying spatial and temporal scales (Peng et al., 2012; Zhu et al., 2013). Multispectral band combinations of these datasets have aided the retrieval of long time series of land surface variables widely used to examine trends in vegetation dynamics at global, regional and national scales (Bao et al., 2014; Julien and Sobrino, 2009), impacts of vegetation on water and energy flux (Hu et al., 2009), as well as the correlation between vegetation and climate conditions (Bao et al., 2014). Particularly, LAI, which is defined in broadleaf canopies as the one-sided green leaf area per unit vegetated ground area, and in coniferous canopies as one-half the total needle surface area per unit vegetated ground area, characterizes the physiologically functioning surface area for energy, mass and momentum exchange between the vegetated land surface and the planetary boundary layer. Hence, it is widely used by the global change research community to assess and quantify vegetation dynamics and their effects (Bobée et al., 2012; Cook and Pau, 2013; Ford and Quiring, 2013; Pfeifer et al., 2014; Verhoef et al., 2012).

The East Africa region, covered in this study, exhibits a wide range of climatic and ecological zones leading to diverse land cover types and land cover change dynamics (Brink et al., 2014). Due to the high dependence of livelihoods on rain-fed agriculture, there is high vulnerability to the extreme negative effects of climate change in the region (Ayana et al., 2016; Grace et al., 2014; Pricope et al., 2013). Land cover/use change is a major threat to the ecological systems in East Africa (Brink et al., 2014; Jacobson et al., 2015; Maitima et al., 2009; Pricope et al., 2013). As reported by Jacobson et al. (2015), approximately 30% of the region has been converted to

cropland or urban areas, with Burundi and Rwanda showing the highest proportions, 85.99% and 82.27% respectively. Between 1990 and 2010, Brink et al. (2014) found that agricultural area in East Africa (comprising Djibouti, Eritrea, Ethiopia, Kenya, Somalia, Sudan and Uganda) increased by 28% with an alarming shift in the rate of deforestation from 0.2% per year in 1990-2000 period to 0.4% per year in 2000-2010 period. Pricope et al. (2013) studied the spatial interaction between climate, vegetation variations and degradation, and population density changes in the East Africa Horn's pastoral and agro-pastoral livelihoods zones. They established a potential long-term degradation of rangelands mainly due to population pressures and land use change.

One of the most disastrous and damaging hazards in East Africa is drought. As noted by Ayana et al. (2016), the frequency of drought in the greater horn of Africa has doubled from once every 6 years to once every 3 years, and has partly contributed to the increase in resource-based conflicts in the region. Despite the central role of combined precipitation and temperature effects on vegetation productivity in East Africa, the vegetation trends and the vegetation-climate relationships across the East Africa region have not been adequately evaluated. Investigation of the vegetation trends and its response to the precipitation and temperature conditions across the region will help in better understanding of the impacts on terrestrial ecosystems and identification of emerging vulnerable areas in the region. This is vital for better planning and management to mitigate ecological and economic loss. This study seeks to shed new light on vegetation trends and responses to climate anomalies across East Africa and in different land cover types in the region. In addition, we have evaluated the impacts of biogeographical factors on vegetation response to combined precipitation and temperature index. Specifically, this study aims to: (i) investigate spatiotemporal patterns of long-term vegetation trends based on LAI dataset for the period 1982-2011 at 8 km spatial resolution; (ii) evaluate vegetation response to a simple multi-scalar drought index (the Standardized Precipitation-Evaporation Index (SPEI, (Vicente-Serrano et al., 2010)) that combines precipitation and temperature data at varying time scales, and (iii) understand the relationship of vegetation responses to SPEI and biogeographical factors.

3.3 Materials and Methods

3.3.1 Study area

Our study area spans 2,267,136 km^2 (bounded by 5.52ºN and 11.76ºS latitude, 28.8ºW and 41.92ºE longitude) and comprises the countries of Burundi, Kenya, Tanzania, Rwanda and Uganda, and portions of the Congo, Ethiopia, Malawi, Mozambique, Somalia, South Sudan and Zambia (Figure 3-1). The northward migration of the Intertropical Convergence Zone (ITCZ) in the summer months initiates a bimodal precipitation pattern in the majority of the region with a main rain season during March to May and short (monsoonal) rains during October to November (McNally et al., 2016). A broad overview of the spatial patterns of the key vegetation zones in the region is described in White (1983). The Somalia-Masai ecoregion covers most of Kenya between the highlands and coastal belt as well as the dry lowlands of north and central Tanzania. This ecoregion consists mainly of arid and semi-arid climate with a mean annual rainfall less than 500 mm and high mean monthly temperature of between 25°C and 30°C.

The Sudanian ecoregion extends from South Sudan to West Uganda and it is mainly characterized by a semi-arid and equatorial savanna type of climate with a severe dry season. The highlands and mountain areas of Kenya as well as most of the southern and western parts of Uganda, with more than 1000 mm mean annual rainfall in the forest zone are defined as Afromontane. Along the Kenyan, Tanzania and Southern Somalia coastline is the Zanzibar-Inhambane ecoregion, which consists of forests and Mangroves and is characterized by mean annual rainfall between 800 and 1200 mm. Most parts of Uganda, and some parts of western Kenya, northern Tanzania and Eastern Congo as well as the whole of Eastern Rwanda and Burundi comprise the Lake Victoria ecoregion, which is characterized by rain forest with semi-evergreen forest and woodland/shrubland as the dominant vegetation type.

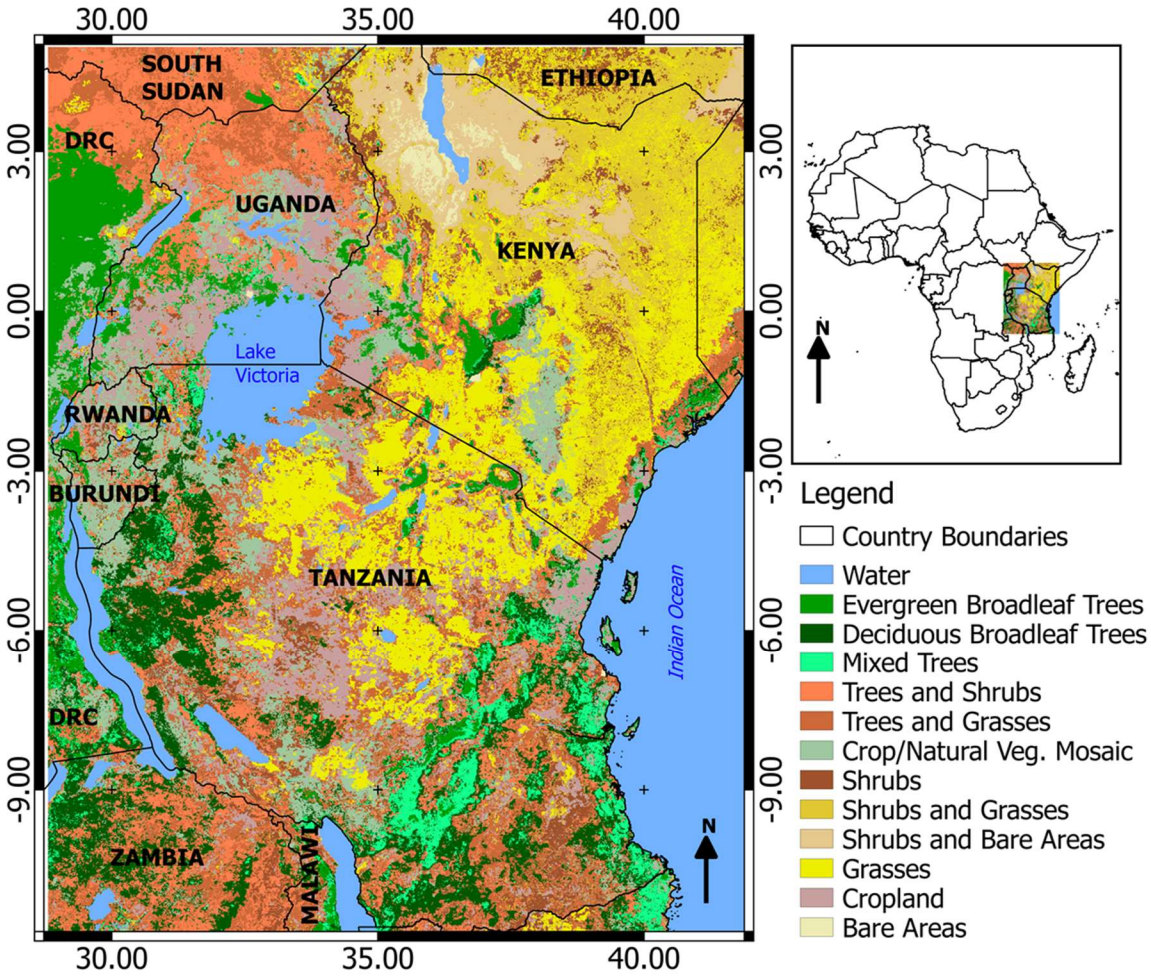

Figure 3-1: Location of the study area and land cover types based on the Synergetic land cover product (SYNMAP) at 1-km spatial resolution.

3.3.2 Data

We used the third generation Global Inventory Monitoring and Modelling Studies LAI (GIMMS LAI3g) dataset spanning the period 1982 to 2011, at approximately 8 km spatial resolution and a 15-day interval, to characterize vegetation dynamics. The dataset was produced by the fusion of GIMMS NDVI3g (Pinzon and Tucker, 2014) and an improved version of the Moderate Resolution Imaging Spectroradiometer (MODIS) LAI using a Feed Forward Neural Network (FFNN) algorithm (Zhu et al., 2013). The GIMMS LAI3g data has been validated using ground based observations measured across East Africa (Pfeifer et al., 2014) and has also been used to study vegetation dynamics at a global scale (Cook and Pau, 2013; Mao et al., 2013; Zhu et al., 2016). To remove superfluous values in the data, the biweekly LAI data were smoothed using an optimized

Savitzky-Golay filter commonly used to correct Earth observation data (Chen et al., 2004). In the Savitzky-Golay filtering process, the seasonality parameter was set to account for areas with two rainfall seasons. The start and end of season was set at around 20% of the seasonal amplitude while median filtering approach was used to detected and smooth the spikes in the data. The smoothed biweekly dataset was then aggregated using the maximum value composites (MVC) approach to create a monthly LAI time series from 1982 to 2011. The MVC approach obtains monthly values as the maximum value per pixel in each pair of bi-monthly datasets.

The climatic data sets used included precipitation, minimum and maximum temperature. The precipitation data was obtained from version 2 of the Climate Hazards group Infrared Precipitation with Stations (CHIRPS) dataset (Funk et al., 2015). The CHIRPS dataset is a 0.05° spatial resolution global gridded dataset of daily precipitation available from 1981 to 2015. It is obtained by merging satellite observations, weighted average precipitation from stations for a given pixel, and precipitation predictors such as elevation, latitude and longitude (Funk et al., 2015). The suitability of this dataset for has been demonstrated through multiple comparisons with other satellite precipitation estimates and observed rain gauge data (Ayehu et al., 2018; Ceccherini et al., 2015; Dembélé and Zwart, 2016; Toté et al., 2015) and has also been widely used in East Africa (Ayana et al., 2016; Pricope et al., 2013). Minimum and maximum air temperature data were obtained from a high resolution daily meteorological dataset developed by the Princeton university hydrology group for East Africa (Chaney et al., 2014; Sheffield et al., 2006). All climatic datasets were also resampled to 1/12 degree * 1/12-degree spatial resolution using the bilinear interpolation method to match the resolution if the LAI data.

The Synergetic land cover product (SYNMAP) (Jung et al., 2006) was used in this study to delineate major land cover classes. This is an improved global land cover product reflecting global land covers around year 2000 at 1-km spatial resolution and consisting of 48 different classes. This dataset was selected particularly for this study as it covers a period approximately at the middle of our study period. The dataset is derived based on fuzzy agreement of different global land cover products, including, Global Land Cover Characterization Database (GLCC), GLC2000, and the 2001 MODIS land cover product, with consideration of individual strengths and weaknesses of mapping approaches. The main land cover types in our study area include evergreen broadleaf

forest (EBF), deciduous broadleaf forest (DBF), mixed forest (MF), shrubs, grasses, crops and bare areas (Figure 3-1). In this study, dynamic land cover changes were not considered, which may bring in uncertainties due to change of vegetation type and land use activities. The land cover data was reclassified in to six main classes namely forest (evergreen broadleaf trees, deciduous broadleaf trees and mixed trees), shrubland (shrubs, trees-shrubs mosaic, and shrub-barren mosaic), wooded grassland (trees-grasses mosaic, and shrubs-grasses mosaic), grassland (grasses), cropland (cropland and cropland/natural vegetation mosaic) and bare areas. The reclassified land cover data was then aggregated to 1/12 degree * 1/12 degree grid cells, using the most prevalent land cover class per grid cell, to be consistent with the resolution of LAI and climate datasets. The Global Human Footprint Index (HFI) dataset (LWP-2) was used as a proxy for anthropogenic effects (WCS and CIESIN, 2005) to assess the human influence on vegetation dynamics and response to climatic conditions. The HFI dataset is derived from the Human Influence Index (HII) normalized by biome and realm. The HII is generated from nine global data layers comprising human population density, land use/land cover and human access datasets.

3.3.3 Long-term trend analysis

We applied the Mann-Kendall (MK) trend test method to verify the existence and direction of significant long-term trends in the data, and Thiel-Sen median slope estimator (TSE) to quantify the strength of the trend. The MK test is a non-parametric method which measures the degree to which a trend is a monotonic increase or decrease over time. Kendall's τ ranges from -1 to 1 where -1 indicates a consistently decreasing trend while 1 indicates a consistently increasing trend and zero indicates no consistent trend. The MK test for the statistical significance ($p<0.05$) of Kendall's τ was considered appropriate since the assumption of normality in data distribution does not affect its validity. The TSE, used to quantify the strength of a trend, is a rank-based regression approach which is resistant to outliers. Its wide application has demonstrated good potential in estimating trends in vegetation and climatic time series data (Fensholt et al., 2012, 2013; Marshall et al., 2012; Teferi et al., 2015).

The serial correlation in high frequency time series data (daily, weekly or monthly) has been shown as a major challenge in long-term trend analysis due to its effects on trend overestimation and detection even when there is none, thereby creating false rejections of the null hypothesis of a trend

test (Wang et al., 2015; Yue and Wang, 2002). To address this, we opted to avoid seasonality in the time series data by using yearly aggregated data, which has been suggested in previous studies (Boschetti et al., 2013; de Jong et al., 2011; de Jong and de Bruin, 2012). Furthermore, the Trend Free Pre-whitening (TFPW) procedure proposed by Yue et al. (Yue et al., 2002) was used to remove serial correlation from the time series based on a lag-one autoregressive (AR1) model. In this procedure, if the slope estimated by the TSE is not equal to zero, a linear trend is removed from the data. A lag-1 serial correlation coefficient of the de-trended data is then computed and the AR(1) component is removed from the data. The pre-whitened residuals and the initially estimated trend are then added, and the MK test is applied to the new series to measure the significance of the trend.

We used monthly LAI values as a proxy for vegetation dynamics in the region. This dataset has been used previously to investigate long-term vegetation trends (Cook and Pau, 2013). The long-term trends were analyzed on per-pixel basis on annual and seasonal basis. The two main rain seasons in the region (long rains: March to May (MAM) and short rains: October to December (OND)) were considered. The spatial heterogeneity in the long-term vegetation trends based on per-pixel analysis of LAI anomalies was particularly preferred to reflect the spatial inconsistencies within the region.

3.3.4 Temporal consistency of LAI trends

We used the Breaks For Additive Season and Trend (BFAST) algorithm (Verbesselt et al., 2010) to identify shifts in the trend and seasonal components of the LAI time series. This algorithm iteratively splits the time series into seasonal, trend, and residual components, while trend and seasonal breakpoints and their associated confidence intervals are estimated for the seasonality and trend components. This allows extraction of the anomaly time series while explicitly accounting for the non-stationarity (gradual and abrupt changes) in the trend and seasonal components of the time series. Based on the information output by BFAST, the largest magnitude break was detected, and its sign was used to characterize the non-stationarity of LAI trends. These trends were categorized into the following 8 classes while non-significant ($P < 0.05$) breakpoints are not shown: (i) monotonic increase, (ii) monotonic decrease, (iii) monotonic increase (with a positive trend break), (iv) monotonic decrease (with a negative trend break), (v) interruption: increase with

negative trend break, (vi) interruption: decrease with positive trend break, (vii) reversal: increase to decrease, and (viii) reversal: decrease to increase (De Jong et al., 2013). The trend breaks represent abrupt positive or negative changes in long term trend slope.

3.3.5 Characterizing drought/wetness conditions

We used the Standardized Precipitation-Evaporation Index (SPEI) (Vicente-Serrano et al., 2010), which is based on precipitation and Potential Evapotranspiration (PET) data, to characterize the drought/wetness conditions in a given area at dynamic time-scales. Compared to climatic indices based on precipitation or temperature data alone, SPEI is considered a superior climatic indicator as it considers the effect of temperature on water balance through its influence on the atmospheric evaporative demand. SPEI is multi-scalar and can therefore be calculated at a range of time-scales (1 to 48 months) to assess water deficit impacts at short- and long-time scales. A user-defined calibration period (reference period) is used to calculate the average water balance while the deviations from this average are determined at varying time-scales. Positive SPEI values represent wet conditions, whereas negative values represent drought conditions. Due to differences in physiological or edaphic factors, some vegetation types may respond to short-term soil water deficit periods, while others may be more resistant and only respond to soil water deficits of longer durations. Therefore, at a regional scale, time scales of optimum SPEI-vegetation correlation are expected to vary spatially (Vicente-Serrano et al., 2013). We used the climate data described in section 2.2 to compute PET based on a modified-Hargreaves (MH) method, which includes a rainfall term (Droogers and Allen, 2002; Hargreaves, 1994). SPEI was then estimated using the climatic water balance defined as precipitation minus PET (Vicente-Serrano et al., 2010, 2013) in R software using the SPEI package.

3.3.6 Short-term vegetation response to climate

We analyzed vegetation response to climatic conditions using LAI anomaly obtained from BFAST analysis to account for the breakpoints in the trend and seasonal components of the time series. In addition, SPEI obtained at a three-month timescale (i.e. SPEI calculated on cumulative water balance over previous 3 months) was used. Although the maximum LAI-SPEI correlation is characterized by variations in the SPEI timescales in different vegetation types, we used a three-

month time-scale to assess the short-term vegetation response. Following De Keersmaecker et al. (2015), three response metrics were used to described the short-term vegetation response: (i) variance metric (the standard deviation of the LAI anomaly time series); (ii) resistance metric (the association between the LAI anomaly and SPEI time series); and (iii) resilience metric (the auto-correlation at lag one of the LAI anomaly).

To obtain the latter two metrics, we used a lag-1 autoregressive (AR1) model (De Keersmaecker et al., 2015, 2017) to compute the linear relationship between monthly LAI anomalies and SPEI at three-month timescale defined as follows.

$$\boldsymbol{LAI_t = \alpha \cdot SPEI_t + \phi \cdot LAI_{t-1} + \varepsilon_t} \qquad (3.1)$$

Where LAI_t is the standardized LAI anomaly at time *t,* $SPEI_t$ the standardized SPEI at time *t*, and ε_t is the residual term at time *t*. α and ϕ are the model's coefficients. α is an indicator of the extent to which the vegetation deviates from its equilibrium due to droughts anomalies, thus expressing the resistance against drought. Similarly, ϕ relates to vegetation resilience as it gives an indication of the dependency of the anomalies on previous values. Large absolute values of α indicate a low resistance to droughts anomalies, hence a large vegetation response to short term droughts anomalies. On the other hand, large absolute values of ϕ imply that the anomalies are strongly determined by the anomaly at time *t−1* and indicate a low resilience, i.e. a slow return to ecosystem equilibrium after disturbance. The time series were standardized to assure comparability between the model coefficients.

In addition to the response metrics obtained for the entire study period, a twelve-year moving window was used to obtain time series of response metrics. The trend of these time series (obtained using the non-parametric Kendall τ rank correlation coefficient) was used to define the temporal non-Stationarity of the short-term vegetation response to climatic conditions. To reveal the climatic impacts on LAI variance metric, we applied a similar approach on monthly SPEI data to obtain the time series of climatic variance. We further calculated the Kendal τ rank correlation coefficient between the vegetation and climatic variance time series.

As noted by Hawinkel et al. (2016), vegetation response to climate variability in East Africa is influenced by a set of biogeographical factors. We therefore analyzed the spatial variations in the

vegetation response metrics based on their relationship with the annual average climatic water balance (precipitation minus PET) and human activities. As the vegetation response is not linearly related to all explanatory factors, we used a generalized additive model with integrated smoothness estimation (Hastie and Tibshirani, 1990). The effect of these factors on vegetation response is modelled using data across the region as well as per land cover type.

3.4 Results

3.4.1 Long-term trends in LAI and climatic conditions

Figure 3-2 shows the spatial heterogeneity in LAI trends. Considering only the statistically significant pixels ($p \leq 0.05$) and the total vegetated area in the region, the increasing and decreasing annual LAI trends accounted for 25.37% and 3.94% respectively. During the MAM season, positive trends showed a wider coverage at 31.04% compared to 3.87% for the negative trends. Compared to annual and MAM trends, the OND season shows more widespread declining vegetation trends at 12.68% while positive trends covered 18.91% of the area.

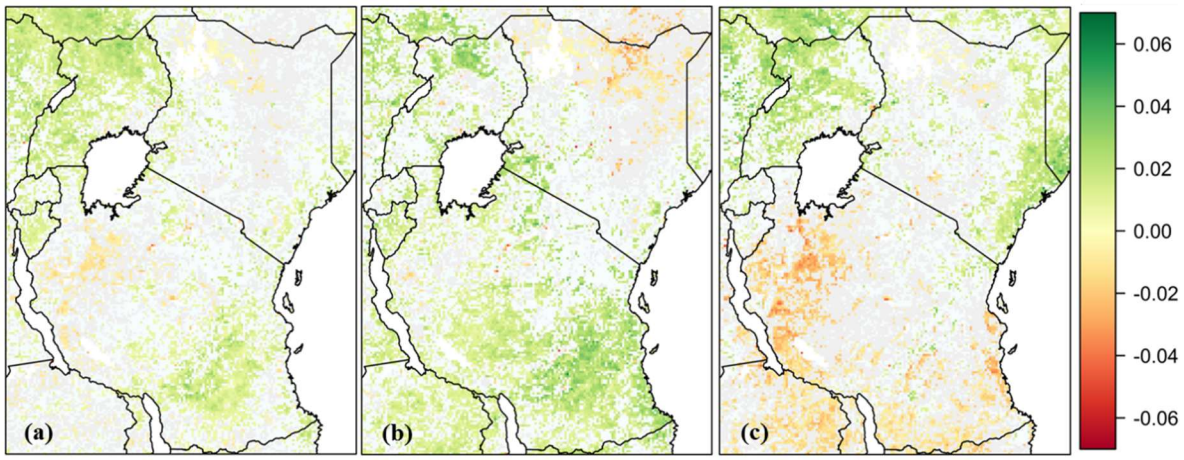

Figure 3-2: Spatial patterns of long term (a) annual, (b) MAM, and (c) OND LAI trends. Significance of the trends is based on 95% confidence level. Non-significant (p=0.05) positive and negative trends are represented in grey.

Northern parts of Kenya show significant negative LAI trends, while increasing trends are prevalent in the East Sudanese Savanna (extending from South Sudan to North Uganda and mainly composed of trees and shrub cover) and the southern parts of Tanzania (mainly covered by deciduous broadleaf and mixed trees) for annual and MAM season. During the OND season, negative trends are prevalent in the deciduous broadleaf and mixed tree covered areas in Tanzania

and Malawi. Along the coast region of Kenya (mainly composed of Evergreen broadleaf trees, tree/grass mosaic and cropland) and the East Sudanese Savanna significant positive trends were prevalent during the OND season.

3.4.2 Temporal consistency of LAI trends

Based on the BFAST trend analysis, about 78% of the study area showed statistically significant ($p<0.05$) LAI changes for the study period (Table 3-1 and Figure A. 1). As shown in Table 3-1, across the areas with significant LAI trend, pixels with significant interrupted trends were composed of 26.3% showing greening with a setback while 20.2% showed browning with a burst. In comparison, reversed trends were identified in 26.1% of the region, composed of greening to browning in 18.3% and browning to greening in 7.8%. On the other hand, 5.3% of the study area showed monotonic greening (4.9%) and monotonic browning (0.4%). The observed trend types in the region were therefore dominated by, in a descending order, increasing trend with negative break, decreasing trend with positive break, reversed increase (increase to decrease) and reversed decrease (decrease to increase).

Large patches of decreasing trend with a positive break were particularly noted in the North-eastern Kenya and Tanzania (Figure A. 1), areas mainly covered by grass and xeric shrubs. Interruptions of decreasing trends were mainly recorded in the 1993-1997 period. Majority of the areas with significant change in both segments was characterized by an increasing trend with a negative break. Large areas showing significant change only in the second segment mainly showed a decreasing trend with a positive break while their timing of the break was predominantly 1993 – 1997 for Kenya and after 2002 for Tanzania. When compared across the region, these two classes of timing of trend shifts appeared to be the most common. A detailed analysis of significance of the trend segments showed that more than 25% of the respective total coverage of cropland, forest, wooded grassland and shrubland showed significant trends in both segments or no break and significant change. In addition, irrespective of the land cover type, pixels with significant change in only one of the two segments often showed significant trend in the second segment. This analysis also revealed that major changes observed in the LAI trends across the region occurred recently. Irrespective of the land cover type, about 25% of the shifts in the LAI dynamics were noted in the period after 2002 while the periods before 1988 and between 1988 and 1992 are

characterized by the lowest proportions of the detected trend shifts at 2.1% and 8.9%, respectively. Trends shifts in the 1998 – 2002 period were predominantly composed of increasing trend with negative break and reversed increasing trend (increase to decrease).

Table 3-1: Frequency of (a) Type, (b) timing and (c) significance of trend shift in monthly LAI time series across the study area. Trends and breaks are considered as significant when P-value is below 0.05. Pixels with no significant (P < 0.05) change for all segments and/or no significant (P < 0.05) breakpoint are not shown. The trend shifts types in (a) are: (1) monotonic increase, (2) monotonic decrease, (3) monotonic increase (with positive break), (4) monotonic decrease (with negative break), (5) interruption: increase with negative break, (6) interruption: decrease with positive break, (7) reversal: increase to decrease, and (8) reversal: decrease to increase. The significance classes are: (1) both segments significant (or no break and significant), (2) only first segment significant, and (3) only 2nd segment significant.

(A) Break Type	Frequency (%)	(B) Break Timing	Frequency (%)	(C) Significance Classes	Frequency (%)
1	2	Before 1988	2.1	1	29.2
2	0.3	1988-1992	8.9	2	19
3	2.9	1993-1997	20.5	3	29.7
4	0.1	1998-2002	21.4		
5	26.3	After 2002	25		
6	20.2				
7	18.3				
8	7.8				

3.4.3 Vegetation response to climatic conditions

Figure 3-3 shows the spatial pattern of long-term average water balance (i.e., precipitation minus PET) across East Africa. The water balance shows values increasing from the north-east to the south-west of the region. In northwest Kenya the long-term average water balance is below -1500 mm being a typical arid area also characterized by rock outcrops and bare areas. Semi-arid areas are shown extending from south Ethiopia through central Kenya into north and central Tanzania. These areas are mainly composed of grasslands, cropland, wooded grassland and shrubland. The humid and semi-humid areas are found in west of the region, western Kenya and southern parts of the region. These areas are mainly composed of forests, tress/shrub/grass mosaics and cropland.

We selected twelve regions representatively, shown by solid boxes in Figure 3-3, for case studies on LAI-SPEI correlation at various timescales.

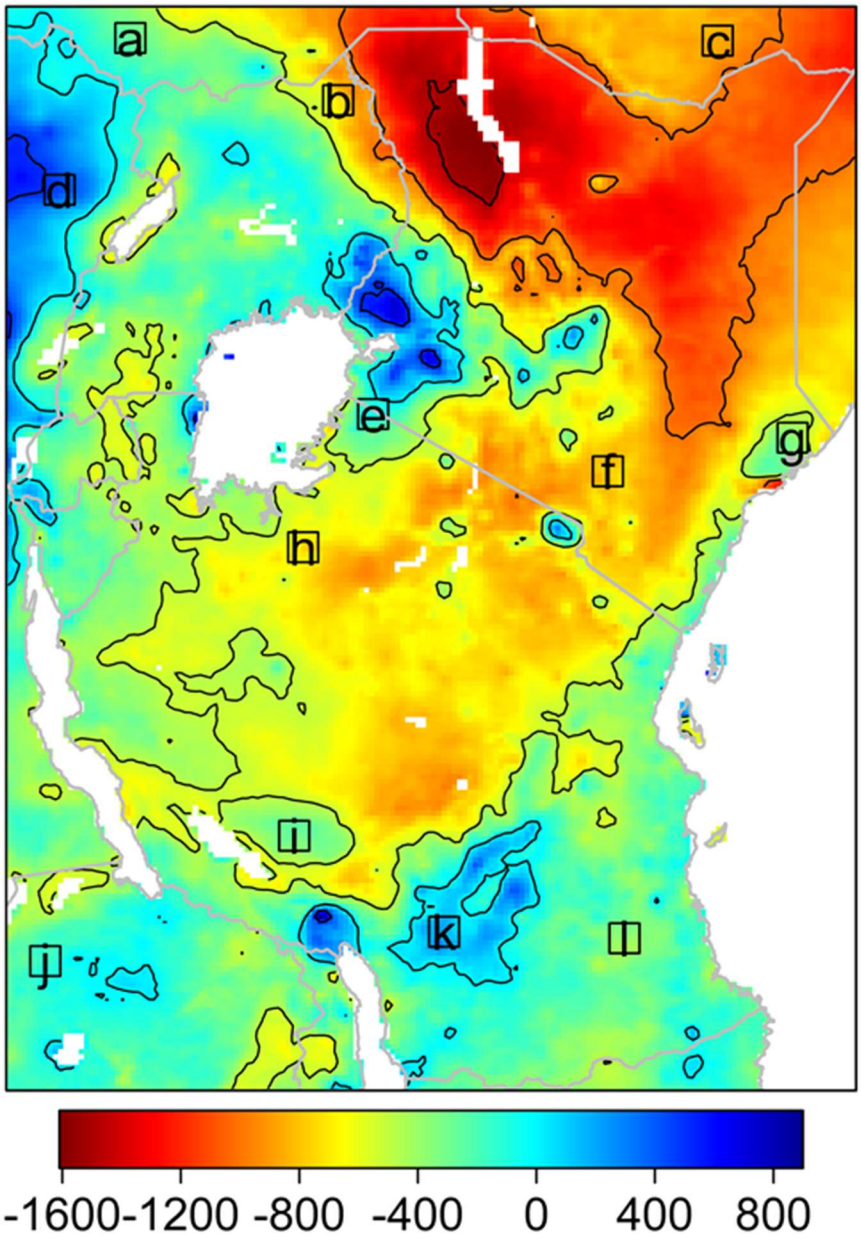

Figure 3-3: Spatial distribution of average annual water balance (mm) during the period of 1982–2011. Regions circled by thick solid box are denoted as the typical water balance regions selected for case studies on LAI-SPEI correlation at various timescales.

Although a three-month time scale was selected for vegetation response analysis in our study, the maximum LAI-SPEI correlation is expected to occur at varying timescales across the region. Figure 3-4 shows the variations in LAI-SPEI correlation at different time-scales for the selected

case study areas (shown in Figure 3-3). While these selected locations represent different water balance regions in the study area, they also coincide with different land cover types. As shown in this figure, differing vegetation response to SPEI time-scales is evident in different water balance regions. Particularly, locations b, d, e, f, g and i show stronger positive LAI-SPEI correlation while locations a, k and l shows strong negative LAI-SPEI correlation. Weak correlation is shown in locations c, h, and j at varying time-scales. Location a, which comprises of trees-grass mosaic is characterized by prevalent negative correlations while potential weak positive relationship is indicated during the March-May season across all the time-scales. Both locations c and j, which are characterized by semi-arid and semi-humid climatic conditions as well as shrubs and trees-shrub mosaic land covert types, respectively, do not show distinctive patterns in the LAI-SPEI correlations. Locations f and h, which are respectively covered by crop-vegetation mosaic and grassland, showed a similar pattern in the LAI-SPEI correlation characterized by low correlation values in the May-August period.

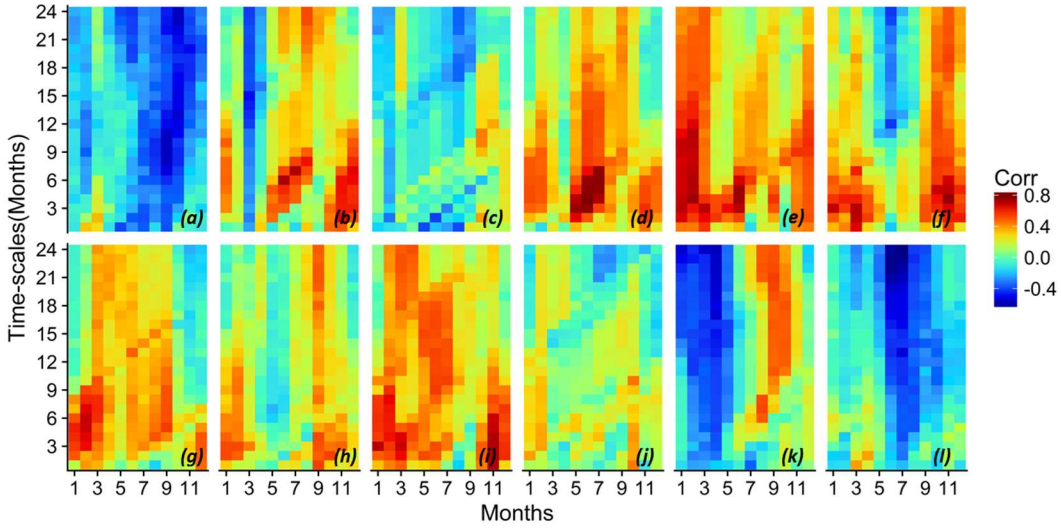

Figure 3-4: Correlation coefficients (R) between LAI and multi-timescale SPEI at points sampled across the study area as shown in Figure 3-3. The SPEI timescales (shown in the vertical axis) range from 1 to 24 months while the horizontal axis represents seasonal cycle (January to December).

Figure 3-5(a) shows the increase/decrease in LAI anomaly variance given by the Kendall τ coefficient for the standard deviation derived over a twelve-year running window. The trend in vegetation variance/stability is positive and statistically significant in most parts of the region. Figure 3-5(b) shows the Kendall τ rank correlation coefficient between the LAI and SPEI variance

time series. As shown in this figure, variations in vegetation stability can be linked to climatic conditions. Most of the pixels indicated a positive relationship between the LAI and SPEI variances which implies that an increase/decrease in vegetation variance is linked to increase/decrease in climate variability. Stronger positive trend in vegetation variance shows a similar spatial pattern compared to the LAI-SPEI stability correlation, implying widespread influence of precipitation on vegetation trends in the region.

A correlation analysis between the two metrics (i.e. Kendall τ coefficient for LAI variance time series and Kendall τ rank correlation coefficient between the LAI and SPEI variance time series) showed that, although not strong (r = 0.44), the spatial relationship between both coefficients was positive and significant. This indicates that positive SPEI variance trends tend to favor positive LAI variance trends across the region. The spatial variations in vegetation stability and relationship between vegetation and SPEI variance also reflect differences in land cover types. The LAI variance shows widespread increasing trend across all the land cover types but predominantly in the grasslands and wooded grasslands. A similar pattern is indicated in the correlation between LAI variance and SPEI variance. However, a decrease in this correlation is prevalent in forests, shrubland and cropland which also showed large proportions of decreasing trend in LAI variance.

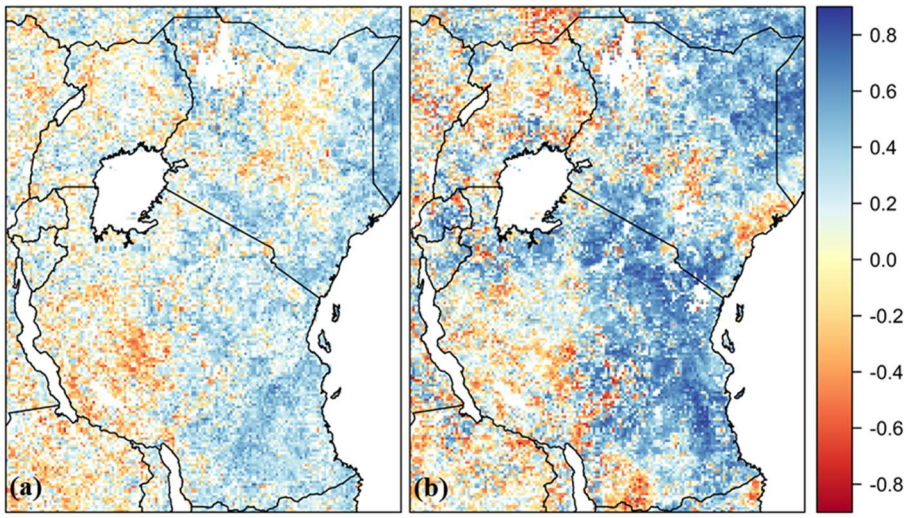

Figure 3-5: Spatial overview of the Kendall τ coefficient for (a) LAI standard deviation time series derived over a twelve-year running window and (b) correlation between the LAI and SPEI twelve-year running window standard deviation time series. Only significant pixels are shown.

Figure 3-6 shows the spatial distribution of vegetation drought-resistance and resilience coefficients over the complete period (1982 to 2011) computed using the AR1 model. Although the model converged effectively with RMSE <0.9 in all pixels, coefficients were not significant in some pixels at 95% confidence level, which were masked from the analysis. Vegetation drought-resistance coefficients were positive and largely significant, emphasizing the influence of moisture availability on vegetation in the region. The spatial distribution of this coefficient generally reflects the spatial patterns of the different land cover types in the region. High and significant drought-resistance coefficient is evident in the stretch extending from south-eastern area of South Sudan to east of Uganda and western Kenya into northern parts of Tanzania. This is indicative of the low resistance thus large vegetation response to short term drought anomalies in these areas. These areas are mainly composed of grassland, cropland and crop/natural vegetation mosaic land cover types. However, some areas showed insignificant drought-resistance coefficients, mainly in western and southern parts of the region that composed of deciduous and evergreen broadleaf and mixed tree cover.

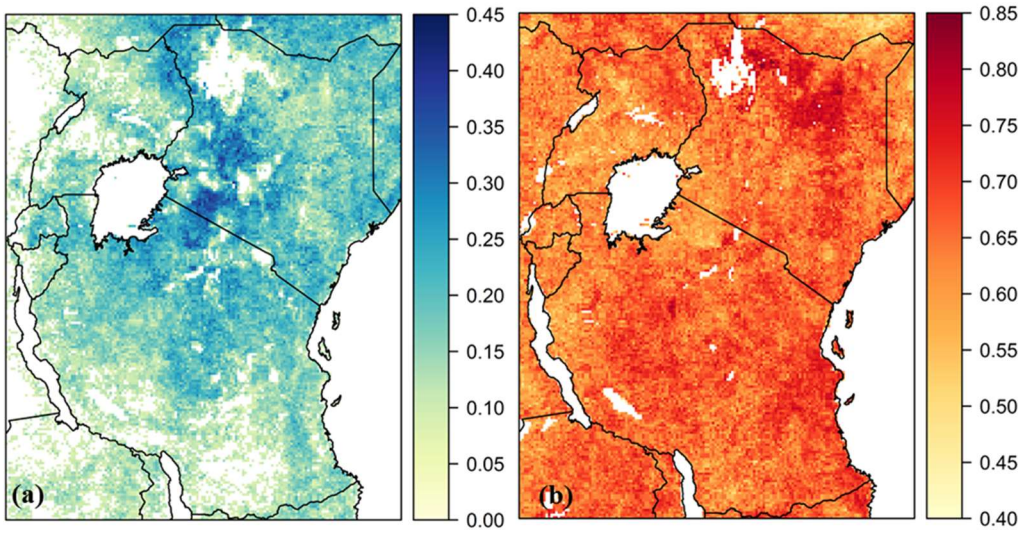

Figure 3-6: Spatial patterns of vegetation (a) drought-resistance coefficient and (b) resilience coefficient obtained using the AR-1 model. The pixels with insignificant coefficients are masked.

On the other hand, resilience coefficients were positive and significant across the region. High vegetation resilience coefficients were prevalent in Kenya, Tanzania and eastern parts of Uganda, which implies slow return to ecosystem equilibrium after potential disturbance in those areas. In addition, the two coefficients (vegetation resistance and resilience) showed widespread contrast in

their spatial distributions. The areas with low drought-resistance coefficients (i.e. high resistance to drought) also show high resilience coefficients (i.e. low resilience) and vice versa. For instance, the north-eastern Kenya region (mainly composed of grassland and shrubland) showed low drought resistance coefficient and a high resilience coefficient.

The sensitivity of vegetation response to water balance and human footprint index in different land cover types was compared to the regional sensitivity across East Africa (Figure 3-7). Across the region, vegetation dynamics are dependent on the climatic conditions, human activities as well as the intensity and structural features of the vegetation itself. As shown in Figure 3-7a and b, vegetation resistance coefficient is significantly and negatively related to the annual water balance across the region which shows that vegetation in the drier areas is more sensitive to drought anomalies compared to relatively humid areas. The sensitivity of the resistance coefficient in different land cover types across the region also shows significant variations. Areas dominated by herbaceous vegetation cover (wooded grassland, grassland and croplands) show larger overall sensitivity to short-term SPEI anomalies in arid and humid areas. Particularly, cropland show higher sensitivity compared to the regional curve in the areas with annual water balance less than -750 mm and greater than -200 mm while resistance in grassland shows high sensitivity beyond -750 mm of annual water balance (Figure 3-7a). On the other hand, drought resistance in grassland and wooded grassland shows a higher sensitivity to human influence while cropland shows a lower sensitivity compared to the regional curve. In shrublands, the impact of annual average water balance on vegetation resistance approaches the average regional curve with a decreasing sensitivity beyond -250 mm of annual water balance. Drought resistance in forests shows a consistently lower sensitivity to both annual water balance and human influence.

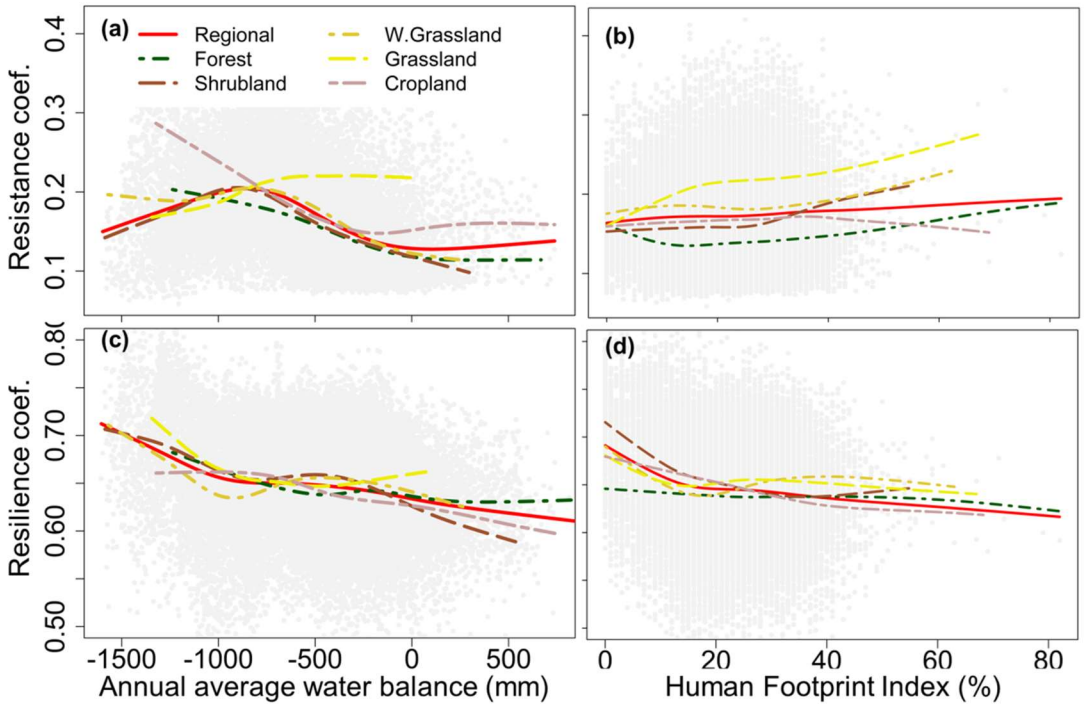

Figure 3-7: The effect of mean annual water balance and human footprint index on the inter-annual vegetation response to SPEI anomalies. The local response in different land cover types is compared to the overall curve for East Africa (red line).

On the other hand, vegetation resilience coefficient is negatively related to both annual water balance and human footprint index in the region (Figure 3-7c and d). Unlike the resistance coefficient, the sensitivity of vegetation resilience to both factors does not vary widely across different land cover types. Except in cropland, the different land cover types show a rapid decreasing sensitivity of vegetation resilience coefficient to water balance below -1000 mm. Both shrubland and wooded grassland show a relatively complicated sensitivity of resilience to water balance. On the other hand, except in cropland, human influence on vegetation resilience is relatively higher in other land cover types compared to the regional curve. Sensitivity of forest resilience is fairly constant across the region.

In addition to the vegetation response across the complete period of analysis, the temporal changes in the drought resistance and resilience coefficients were also analyzed. Figure 3-8 shows the spatial heterogeneity in the temporal variations of vegetation drought-resistance and vegetation resilience coefficients. The vegetation resistance metric shows the largest increase in forest, wooded grassland and grasslands. These land cover types are also characterized by the largest

increase in the resilience metric. Forests and cropland showed the highest spatial variance in the trend of resistance metric while the trend of resilience metric varied widely in wooded grassland and grasslands.

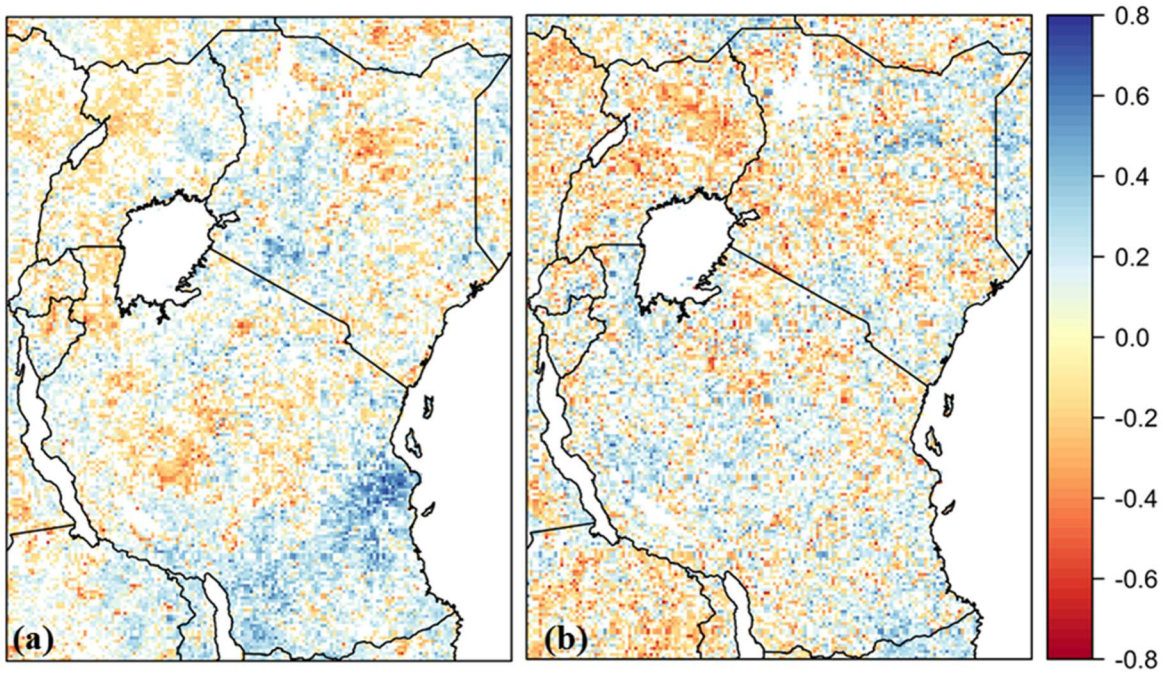

Figure 3-8: Spatial overview of Kendall τ coefficient for (a) vegetation drought-resistance coefficient, and (b) vegetation resilience coefficient for the period 1982-2011. Only significant pixels are shown.

3.5 Discussion

3.5.1 Spatio-temporal variations in vegetation

The east Africa region, which is mainly characterized by vast dryland ecosystems, was focused in this study. These ecosystems are often over-utilized for pastoral grazing and mixed cereal cropping systems thus exacerbating their vulnerability to extended drought occurrences leading to severe negative implications on food security and community livelihoods (Hoscilo et al., 2015; Landmann and Dubovyk, 2013; Pricope et al., 2013). The results presented here provide a view of vegetation dynamics that could be used to fully appreciate where significant changes in ecosystem functioning have occurred in the region. Vegetation trend analysis based on LAI time-series showed a significant increase in the annual vegetation condition in over 25.37% of study area for the period 1982–2011. In northern parts of Uganda and DRC, increasing LAI trends were found in the annual

and MAM time series. These areas are characterized by savanna-forest transition land cover types mainly composed of grassland, shrubland and wooded grassland. These areas were also identified in a global NDVI trend analysis by Mueller et al. (2014) as part of eco-regional extremes for NDVI increase. As noted by Kim et al. (2013) this increase has been linked to land use planning and reforestation activities targeting the northern Congo basin which is designated as a high-priority conservation zone. The southern parts of Tanzania, particularly the Tanzania's Eastern Arc mountain ranges, also showed increasing annual LAI trends which was linked to increasing vegetation greenness during the MAM rain season. Widespread decreasing LAI trend found in Tanzania during the OND season coincides with Vrieling et al. (2013) finding of a decrease in the length of growing season. The significant and persistent negative trends in north-central and southern Kenya coincide with a significant decline in precipitation and can be attributed to climatic effects, as also reported by Hoscilo et al. (2015). In addition, the decline in LAI shown in our analysis could also be a combined effect of climate as well as replacement of shrubs by grass and crops with lower LAI values in areas characterized by intensive pastoral activities.

The temporal non-stationarity of LAI trends derived over the complete study period varies spatially and depends on the land cover type. Although the regional variations in LAI are closely linked to climatic and human-induced factors, it is still unclear how the increasing and decreasing trends shown from the timeseries analysis are influenced by the different land-use changes in the region. A wide coverage of significant reversed increasing trends (increase to decrease), particularly in Kenya and Tanzania, coincides with both significant and non-significant decreasing trend in the long-term trend analysis. This indicates the need to consider potential turning points in long-term vegetation index time series analysis. Interrupted positive trends (increase with negative break) across the region leads to a decline in areas identified as indicating increase in long-term trends. Further analysis of the potential effects of sensor errors in the data is recommended to provide the clear link between the trend breaks and climatic conditions and human activities.

3.5.2 Vegetation response to climate

The stability of natural and productive ecosystems and their flow of services is crucial especially amid potential climate change impacts. Assessment and quantification of this stability has been largely aided by the availability of regional to global scale and long-term time series of vegetation

indices derived from readily available remote sensing datasets. The vegetation response metrics derived in this study revealed contrasting spatial patterns. For instance, a sample set of pixels representing different land cover types under varied water balance regions across the study area showed highest LAI-SPEI monthly correlations at various time-scales.

The vegetation variance, resistance, and resilience metrics varied across the study area, signifying the influence of land cover types on vegetation response to short-term droughts and memory effects. The fact that vegetation response is stronger for a given range of annual water balance emphasizes also the effects of different vegetation formations. The vegetation resistance coefficient in forest environments was evidently very small and statistically insignificant, which implies that the greenness of trees is not largely influenced by short-term variations in the water balance. This corresponds with the findings of Camberlin et al. (2007) based on NDVI-rainfall regression analysis in tropical Africa. In addition to the lack of vegetation response to inter-annual water balance variability, seasonal LAI variations in most of these areas do not match seasonal rainfall variability. In these areas, leafing can be induced by rainfall amounts even lower than average while the effects of moisture deficit are hampered by the capability of the vegetation to tap deep soil water resources. In addition, the lack of significant vegetation response in such vegetation formations may be attributed to other biases in the LAI time series such as cloud contamination as well as predominance of other vegetation growth constraints (Huxman et al., 2004)

The annual average water balance emerged as the key factor determining the level of vegetation resistance to drought anomalies compared to the human footprint. A high sensitivity of vegetation resistance coefficient across the region coincides with intermediate water balance areas (-1000 to -500 mm). The major peak of the vegetation resilience sensitivity to water balance is shown at -750 mm. This relates with findings of Huxman et al. (2004) based on the correlation analysis of net primary production and annual precipitation data at sites sampled from major global biomes. However, the influence of annual average water balance on vegetation resistance coefficient is somewhat intricate: a positive effect is shown in areas with annual average water balance below -750 mm, which changes to decreasing influence between -750 mm and 0 mm and then to relatively constant sensitivity in areas with annual average water balance greater than 0 mm. The low

sensitivity in drier areas has been linked to vegetation drought resistance strategies such as low specific leaf area, high root–shoot ratio and low stomatal conductance (Paruelo et al., 1999). While in wetter areas, the vegetation is also well-adapted to the temporary seasonal constraint in water availability (Camberlin et al., 2007).

In addition to response metrics derived across the complete study period, this study also quantified the magnitude and direction of temporal changes in vegetation response to climate. The temporal changes in the vegetation response metrics imply the effects of both natural and anthropogenic factors. Therefore, the assumption of stationarity in whole time series is not realistic for the analysis of vegetation dynamics. However, this study did aim to disentangle the separate effects induced by human and natural factors on vegetation dynamics. In addition, results are likely to differ significantly depending on the time series length as well the data sources (De Keersmaecker et al., 2017).

3.6 Conclusions

This chapter focused on understanding the spatial-temporal variations in LAI during 1982-2011 period over East Africa based on robust non-parametric trend tests. Our results show extensive spatial variability in LAI trend with both increasing and decreasing trends during 1982–2011 period. Most parts of East Africa show significant increasing trend in MAM and OND seasons as well as in the annual time series over the 30-year period. We also found hotspots with significant LAI declines over the last 30 years, thus signifying potential degradation of vegetation cover and thus increased vulnerability to climate change in the future. Although vegetation degradation linked to climatic factors has been cited in these areas, other factors such as population pressures and declining land health should be considered in future studies in the region. In addition, LAI trends showed multi-year variations, showing widespread abrupt changes in the long-term trends particularly between 1992 and 2000. More than 70% of the region show changes in long-term trends characterized by interrupted monotonic trends and reversed trend types. The region is mainly characterized by sparse vegetation that is composed of grass and shrubs. At the 1/12-degree spatial resolution used in this study, some gradual and abrupt vegetation changes may have been masked. We therefore recommend further analysis at higher spatial resolution. The BFAST decomposition is a useful approach for the detection of abrupt intra-annual changes within the

trend and seasonal components and their time of occurrence, as well as the quantification of the magnitude of these abrupt changes detected during the study period. This approach provides valuable support in decision-making on potential ecosystem degradation hot-spots and further unravelling of human and climatic related disturbances to ecosystem functioning.

The vegetation-climate regression analysis provided a view of the interactions between vegetation and climate. However, due to the coarse spatial resolution of the data, the obtained vegetation response is comprised of the response by the dominant vegetation type as well contamination by spurious signal attributed to other vegetation types in the pixels. In addition, there is need for further analysis of the multifaceted connection between vegetation production patterns to human and climatic drivers in the region to account for the individual and coupled effects of both natural and anthropogenic determinants of terrestrial ecosystem functioning. The significant correlation between climatic water balance and the vegetation drought-resistance and resilience coefficients emphasizes the role of variations in vegetation structure and type in adaption to changes in climatic conditions. Despite the coarse resolution of the dataset used, our findings demonstrate that climate variations are crucial in vegetation dynamics across the region. Further analysis is required to precisely explain and quantify the influence of climatic factor and human activities as well as their interaction on vegetation changes in the region.

Chapter 4: Modelling Water and Energy balance in East Africa Using Multi-year Vegetation Parameters

4.1 Abstract

The role of vegetation, particularly its spatial and temporal dynamics, is often understated in the land surface water and energy balance simulations. Land Surface Models (LSMs) have been used to assess the global role of land surface heterogeneity in portioning of surface water and energy budgets. However, the regional validity of this studies is not guaranteed. This work puts emphasis on the connections of vegetation dynamics to water and energy balance in East Africa by considering their linkages at seasonal and interannual time scales. Two long-term simulations with the Variable Infiltration Capacity (VIC) model are conducted: an experimental simulation (EXP) with varying Leaf Area Index (LAI), Fractional Vegetation Cover (FVC) and albedo obtained from MODIS products over 2001 – 2011 period, and a control simulation (CTL) based on the climatological means of these land surface parameters. The EXP simulation reproduced the spatial patterns of ET, latent, and sensible heat fluxes over East Africa comparatively well although some biases exist in comparison to MODIS ET and FLUXCOM energy balance data. The variation in vegetation parameters was found to impose more than half of the variance in the evapotranspiration in the study area. Across the region, the variations in vegetation parameters is found to impose higher standard deviation on mean annual sensible heat (0.3 Wm^{-2}) than on latent heat (0.03 Wm^{-2}) but generally has small effect on ground heat (0.02 Wm^{-2}). However, the percentage of positive variance imposed on ground heat by varying vegetation parameters across the region is higher (33%) compared to 13% and 14% for ET/latent heat and sensible heat, respectively. The model setup adopted in this study provides a starting point for assessing the potential impacts of land cover change on water and energy balance in the region

4.2 Introduction

Over the past decades, land surface characteristics have been widely recognized as a crucial factor in the regulation of the local, regional and global land-atmosphere exchanges (Anav et al., 2010; Delire et al., 2011; Foley et al., 1998, 2000; Lee et al., 2015; Snyder et al., 2004). In the soil-vegetation-atmosphere interface, vegetation plays a key role in regulating biophysical and biogeochemical processes and facilitates complex feedbacks varying in space and within a range

of timescales (Arora, 2002; Berry et al., 2016; Donohue et al., 2006; Xin and Liu, 2010). Vegetation properties (e.g leaf area index (LAI) and fractional vegetation coverage (FVC)) as well as the surface radiative properties (e.g albedo) significantly regulate the land-atmosphere exchanges of water and energy fluxes. LAI and FVC has been shown to significantly influence water balance by affecting rainfall interception, canopy evapotranspiration, throughfall, surface runoff, baseflow and soil moisture (Kim et al., 2005; Twine et al., 2004). On the hand, surface albedo affects the energy balance by impacting the portioning of sensible, latent and ground heat fluxes (Bright et al., 2015; Burakowski et al., 2018).

The structure and distribution of vegetation across the globe is subject to the effects of human activities, increased atmospheric CO_2 concentration as well as changes in climatic conditions (Cuo et al., 2016; Hély et al., 2006; Pricope et al., 2013). Therefore, vegetation characteristics are expected to vary spatially and over time due to only phenological patterns but also due to changes caused by human and natural disturbances such as forest management, overgrazing, deforestation and wildfires. However, application of dynamic vegetation properties in modelling surface water and energy fluxes is still underexplored. This has been attributed to several factors including oversimplified representation of the water and energy balance components, as well as inadequate validation of the models using observed flux datasets (Murray et al., 2011; Ren et al., 2013). Although there is recognized need to prescribe realistic temporal and spatial variations in vegetation properties in land surface models (LSMs), few of these models have the capability to simulate dynamic vegetation conditions with reasonable seasonal and interannual variability as well as spatial heterogeneity. The significance of time-varying vegetation conditions on the simulation of water and energy balance in East Africa has not been studied. Particularly, the combined effects of the time-varying vegetation properties (i.e LAI and FVC) and albedo in East Africa have not been explored.

Use of such time-varying land surface properties is expected to significantly influence simulated surface water and energy balance. This motivated us to apply the Variable Infiltration Capcity (VIC) model explicitly for the region with improved vegetation properties and albedo derived from MODIS products to test the effects on simulated water and energy fluxes. Therefore, this study hypothesizes that using realistic spatially and temporally varying LAI, FVC and albedo strongly

impact the simulations of seasonal and inter-annual evapotranspiration, surface energy fluxes in East Africa. We first developed continuous high-quality surface properties datasets from MODIS products over East Africa at 0.05° spatial resolution and daily time-step for the 2001 – 2011 period. These datasets were prescribed to the Variable Infiltration Capacity (VIC) model to simulate water and energy balance in the region. Two modeling experiments were designed to systematically assess the combined impacts of the derived surface properties. The study region, VIC model, and methodology for deriving the land surface parameters as well as the experimental design are described in section 4.3. Section 4.4 presents the results on the developed datasets and comparison to a control model setup while section 4.5 and 4.6 provide further discussion and conclusions of the study, respectively.

4.3 Materials and Methods

4.3.1 Study Region

We focused our analysis on the region spanning approximately 2,267,136 km^2 (bounded by N5.52 and S11.76 latitude, W28.8 and E41.92 longitude) and encompassing the countries of Burundi, Kenya, Tanzania, Rwanda and Uganda, and portions of the Congo, Ethiopia, Malawi, Mozambique, Somalia, South Sudan and Zambia (Figure 4-1). A broad overview of the relation between climate and the key vegetation zones in the region is described in White (1983). The northward migration of the Intertropical Convergence Zone (ITCZ) in the summer months initiates a bimodal precipitation pattern in the majority of the region with a main rain season during March to May and short (monsoonal) rains during October to November (McNally et al., 2016). The Somalia-Masai ecoregion covers most of Kenya between the highlands and coastal belt as well as the dry lowlands of north and central Tanzania. This ecoregion consists mainly of arid and semi-arid climate with a mean annual rainfall less than 500 mm and high mean monthly temperature of between 25°C and 30°C. The Sudanian ecoregion covers extends from South Sudan to West Uganda. It is mainly characterized by a semi-arid and equatorial savanna type of climate with a severe dry season. The highlands and mountain areas of Kenya as well as most of southern and western parts of Uganda with more than 1000 mm mean annual rainfall in the forest zone are defined as Afromontane. Along the Kenyan, Tanzania and Southern Somalia coastline is the Zanzibar-Inhambane ecoregion, which consists of forests and Mangroves and characterized by

mean annual rainfall between 800 and 1200 mm. Most parts of Uganda, and some parts of western Kenya, northern Tanzania and Eastern Congo as well as the whole of Eastern Rwanda and Burundi comprise the Lake Victoria ecoregion, which is characterized by rain forest with semi-evergreen forest and wood- and shrubland as the dominant vegetation. This area receives high and well distributed rainfall.

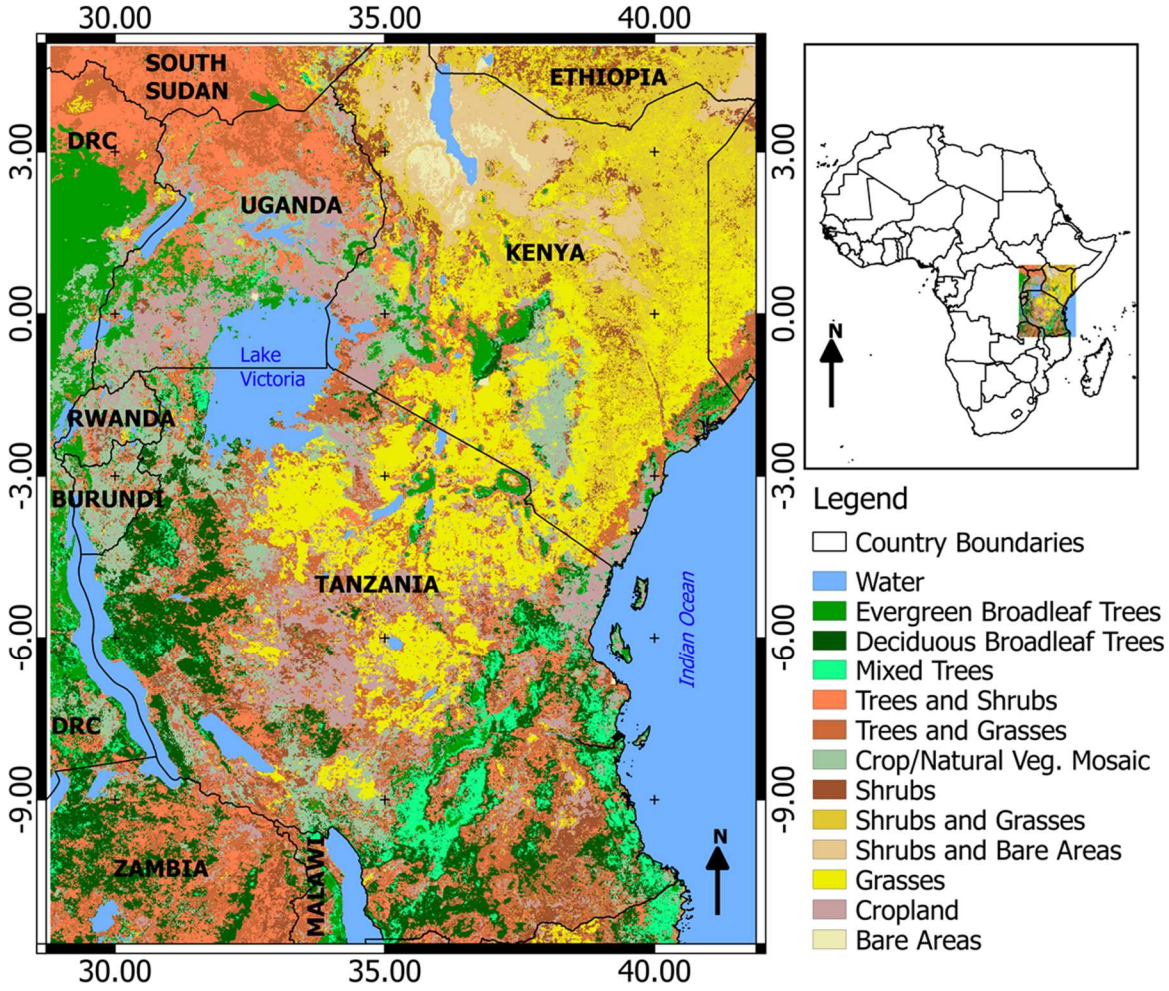

Figure 4-1: Location of the study area and land cover types based on the Synergetic land cover product (SYNMAP) at 1-km spatial resolution.

4.3.2 Model description

We applied the three-layer Variable Infiltration Capacity (VIC) model (Liang et al., 1994) version 4.2.d in this study. The VIC model is a grid-based, semi-distributed process-based land surface and hydrologic model which can be forced with meteorological data in an offline mode or directly

coupled to General Circulation Models (GCMs). This model has been widely applied and evaluated at global and continental levels as well as across large river basins. In this study, the model was preferred due to its three main features: (1) a simple conceptual rainfall–runoff model that enables the representation of spatial heterogeneity based on gridded topography, infiltration rate, soil properties, climate variables, and land covers; (2) consideration of both infiltration and saturation excess runoff generation mechanisms; and (3) improved algorithms on bare soil evaporation in the sparsely vegetated land covers such as open shrubland and grassland which are prevalent in the East Africa region (Bohn and Vivoni, 2016). The following paragraphs give a summary of the model's main computation steps, with special emphasis on processes related to LAI, albedo and FVC.

The vertical energy and moisture fluxes at each grid cell are calculated in the model by resolving full water and energy balances based on the vegetation properties and coverage as well as soil characteristics. Land surface heterogeneity is represented in the model through consideration of multiple vegetation classes within a single grid cell as vegetation mosaics. For each land cover tile, biophysical parameters (LAI, FVC, albedo, root fraction and depth, etc.) are assigned inform of climatological means or as daily time series. The simulated fluxes from each land cover mosaic within a grid cell are then combined as weighted sum for a given grid cell. The adopted VIC version also includes modified vegetation formulation which accounts for vegetated and non-vegetated area fractions in each vegetation tile based on a "clumped" approach. This alteration approximates the effects of exposed soil between plants thus allowing for a time-variant bare soil area and accounting for the effects of shading and wind attenuation from nearby vegetation (Bohn and Vivoni, 2016).

The ET components are simulated based on the Penman-Monteith equation which computes evaporation rate, E_o,as:

$$E_o = \frac{\Delta(R_n - G) + \rho_a c_p \delta_e / r_a}{\left(\Delta + \gamma\left(1 + r_c / r_a\right)\right) L_v}, \qquad (4.1)$$

Where Δ is rate of change of saturated vapor pressure with temperature, R_n is net radiation, G is ground heat flux, ρ_a and c_p are density and specific heat capacity of dry air, respectively, δ_e is

vapor pressure deficit, r_a and r_c are aerodynamic and canopy resistances, respectively, and L_v is latent heat of vaporization. The canopy resistance is calculated as $r_c = r_{arc} + r_s$, where $r_{arc}$is the architectural resistance linked to the canopy structure and r_s is the aggregate stomatal resistance calculated as:

$$r_s = r_{s.o}/\left(LAI.f_{sm,sr}f_T f_R f_{vp}\right), \qquad (4.2)$$

Where $r_{s.o}$ is the minimum stomatal resistance per unit leaf area, LAI is the leaf area index, while the functions $f_{sm,sr}, f_T, f_R \; and \; f_{vp}$, represent the dependence of r_s on root zone soil moisture, air temperature, solar radiation and vapor pressure deficit, respectively, and they all range from 0 to 1 (Liang et al., 1994). The canopy evaporation, E_{can} is then estimated as:

$$E_{can} = \left(\frac{w_{can}}{w_{can,max}}\right)^{2/3} E_o, \qquad (4.3)$$

Where w_{can} represents the water intercepted by canopy water, $w_{can,max}$ is the canopy storage capacity proportional to LAI, and $E_o$is obtained using equation (1) with r_s set to 0. Likewise, transpiration is calculated as:

$$T = \left(1 - \left(\frac{w_{can}}{w_{can,max}}\right)^{2/3}\right) E_o, \qquad (4.4)$$

where E_o is calculated from equation (1) using r_s determined by equation (2). Lastly, soil evaporation in unvegetated classes, such as bare soil, is computed as:

$$E_{soil} = E_o f_{sm,soil}, \qquad (4.5)$$

where E_o is calculated with equation (1) with r_{arc} and r_s set to 0, while $f_{sm,soil}$ is a function applied to the top soil layer (10 cm depth) and ranges from 0 (signifying completely dry conditions) to 1 (at saturation) (Franchini and Pacciani, 1991). To account for evaporation in the canopy gaps or exposed soil between plants in sparsely vegetated land cover types, Bohn and Vivoni (2016b) developed a "clumped" vegetation formulation which, based on the provided FVC, splits each vegetation tile into vegetated (f_v) and non-vegetated ($1 - f_v$) area fractions. Then, in each grid cell the spatial average of LAI ($\overline{LAI}$) is scaled by a factor of ($1/f_v$) to obtain the plant-specific LAI in

the vegetated fraction of the tile (f_v). Total ET is then computed as a weighted average over the vegetated and non-vegetated fractions of the tile as:

$$ET = f_v(E_{can} + T) + (1 - f_v)E_{soil}, \qquad (4.6)$$

The energy balances for wet and dry canopy as well as bare soil are used to calculate surface temperature and the sensible and ground heat fluxes. Given a moderately homogeneous surface, the energy balance equation for a layer of the air column from ground surface to given height in the atmosphere can be expressed as:

$$R_n = \rho_w LE + H + G + \Delta H_s \qquad (4.7)$$

Where $R_n$is the net radiation, $\rho_w$is the density of liquid water, $\rho_w LE$is the latent heat flux to the atmosphere, $H$is sensible heat flux into the atmosphere, G is the ground heat flux and ΔH_s is the change in the energy storage in the layer for a given duration over a given unit area. The net radiation is given by:

$$R_n = (1 - \alpha)R_s + \varepsilon \cdot (R_L - \sigma T_s^4) \qquad (4.8)$$

Where α is the albedo of the land surface cover, R_s is the downward shortwave radiation, ε is the emissivity of the land surface cover, R_L is the downward long-wave radiation, $\sigma$is the Stefan-Boltzmann constant and T_s^4 is the temperature of the wet canopy, dry canopy, or bare-soil surface. The latent heat flux, which is the link between the water and energy balances, is obtained as:

$$\rho_w LE = \frac{\rho c_p}{\gamma(r_c + r_{av})}(e^*(T_l) - e_a) \qquad (4.9)$$

Where ρ is the density of air, c_p is the specific heat of air at constant pressure, γ is the psychometric constant, r_c is the canopy resistance, r_{av} is the aerodynamic resistance, $e^*(T_l)$ is the saturation vapor pressure at the surfacet emperature T_l and e_a is the vapor pressure at a given height above the canopy or soil surface. The sensible heat flux is expressed as:

$$H = \frac{\rho c_p}{r_h}(T_l - T_a) \qquad (4.10)$$

Where r_h the aerodynamic resistance to heat flow and T_l is the surface temperature, and $T_a$is the air temperature. Bohn and Vivoni (2016b) modified the attenuations of wind and radiation fluxes through the canopy to include the influence of plant shading and turbulence over nearby unvegetated areas. The fraction τ_o of solar radiation transmitted through the vegetative canopy to the ground is expressed as:

$$\tau_o = f_v \exp\left(-k\left(\frac{\overline{LAI}}{f_v}\right)\right) + (1 - f_v) \qquad (4.11)$$

where k is a canopy extinction coefficient and set to 0.5 for all land cover types.

4.3.3 Data

4.3.3.1 Forcing data

VIC model simulations require various forcing data sets comprising of meteorological, vegetation and soil parameters. The precipitation data was obtained from version 2 of the Climate Hazards group Infrared Precipitation with Stations (CHIRPS) dataset (Funk et al., 2015). The CHIRPS dataset is a 0.05° (~5 km) spatial resolution global gridded dataset of daily precipitation obtained by merging satellite observations, average precipitation from stations, and precipitation predictors such as elevation, latitude and longitude. Minimum and maximum temperature, as well as wind speed datasets were obtained from a high resolution daily meteorological dataset developed by Princeton university hydrology group for East Africa (Chaney et al., 2014; Sheffield et al., 2006). This dataset is created by downscaling the National Centers for Environmental Prediction–National Center for Atmospheric Research (NCEP–NCAR) reanalysis, adjusting for temporal inconsistencies and assimilating quality controlled and gap-filled Global Summary of the Day (GSOD) in situ measurements to remove random errors. The model was set up using three soil layers with varying depths. For each grid cell, the soil classes and properties at top and subsurface layers were obtained from the Africa Soil Information Service (AfSIS) project database (http://africasoils.net) while the root zone depth and fraction of root zones of each vegetation type were estimated according to Zeng (2001). The pedo-transfer functions of Saxton and Rawls (2006) were used to estimate the saturated hydraulic conductivity for each soil layer. Spatial variation in elevation were estimated using SRTM dataset (Jarvis et al., 2008). All the input datasets obtained

from different sources at different resolutions were processed to 0.05º spatial resolution for the VIC model simulation.

4.3.3.2 Time-varying vegetation parameters

In VIC model, the effects of vegetation phenology on water and energy balance can be parameterized using either constant climatological vegetation parameter values (i.e., no year-to-year variability) or a time series of spatially varying vegetation parameter values. To improve the representation of spatial and temporal land surface heterogeneity and realistically capture the vegetation phenology, MODIS Version 6 products were used to derive time varying vegetation properties at ~500m for the period spanning 2001 to 2011 following Bohn and Vivoni (2016 & 2019). Compared to version 5 MODIS products, the Version 6 products feature improvements such as use of daily Level 2 Gridded (L2G)-lite surface reflectance as input instead of a MODIS daily aggregated surface reflectance product used in Version 5. Also, the products are generated at native resolution of 500 meters based on an improved multi-year land cover product thus not only account for the interannual variability in vegetation phenology but also the impacts of land cover conversion.

The LAI values were derived from 8-day MOD15A2H.006 product for the period spanning 2001-01-01 to 2002-03-30 and the MCD15A2H.006 product for the period 2002-04-07 to end of 2011. The MCD15A2H was preferred as the adopted algorithm selects the best pixel available from all the acquisitions of both MODIS sensors located on NASA's Terra and Aqua satellites from within the 8-day period. However, MOD15A2H was used to provide data for the missing dates in MCD15A2H in the years 2001 and 2002. The Enhanced Vegetation Index (EVI) data from the 16-day MOD13A1.006 product was used to derive the fractional vegetation cover (FVC) for the entire period 2001-2011 using the "Mosaic Pixel" approach. This approach assumes that the quantity ($\emptyset$) measure in a pixel can be understood as a mosaic with linear contributions from the vegetated area (σ_V) and bare soil (1-σ_V):

$$\emptyset = \emptyset_V \sigma_V + \emptyset_S (1 - \sigma_V) \quad (4.12)$$

where the subscripts v and s represent values for fully vegetated and bare soil areas, respectively. Based on this equation, we derived the FVC as follows:

$$FVC = \begin{cases} 0, & EVI \leq EVI_{min} \\ \left(\frac{EVI - EVI_{min}}{EVI_{max} - EVI_{min}}\right), & EVI_{min} \leq EVI \leq EVI_{max} \\ 1, & EVI \geq EVI_{max} \end{cases} \quad (4.13)$$

Where EVI_{min} and EVI_{max} were seasonally and spatially invariant values set at 0.05 and 0.85 to correspond to the yearly minimum EVI of bare areas in northern Kenya, and yearly maximum EVI recorded at Congo Forest, respectively.

The albedo values for 2001-2011 period were obtained from "White-Sky Albedo from shortwave broadband" variable in the daily MCD43A3.006 product (Schaaf et al., 2002). In order to ensure consistency with LAI data, the albedo observations for the days corresponding to the 8-day LAI were used. We computed land cover fractional areas from the MCD12Q1v006 product which provides global land cover types at yearly intervals (2001-2017) based on six different classification schemes. To account for land cover variations in East Africa during our study period we considered land cover maps for the period 2001- 2011 and selected the most frequent land cover class in each pixel and used this to determine time invariant land cover fractions in each 0.05° by 0.05° grid cell. Since the land cover and phenology data was defined at same spatial resolution (500m), each phenology pixel therefore corresponded to a single land cover pixel. Pixels classified as bare areas were not considered in our analysis.

The Quality Control (QC) files provided with each of the considered MODIS products were used to exclude pixels with poor retrievals due to various contaminations, thus leading to missing values in some pixels for one or more acquisition dates. These gaps were therefore filled using several steps for all biophysical variables. First the climatological mean and standard deviation were derived and any pixel with fewer than 5 observations in a particular day of the year across the 2001 – 2011 period was set as missing for that particular day. These gaps were interpolated spatially from values of the same land cover class in neighboring cells. Using the gap-filled climatological mean and standard deviation, we derived standardized anomalies for all pixels. In cases where the first- or last-time steps in the anomaly time series were missing or where the nearest valid data

points were more than 2 intervals away, such cases were set to 0, and remaining gaps approximated using linear interpolation. The anomaly time series was then recombined with climatological mean and standard deviation to obtain the final gap-filled time series. The gap-filled variables were then aggregated from the 500m resolution to 0.05° simulation grid size by calculating a spatial average value for each land cover class in each 0.05° grid cell as follows (Bohn and Vivoni, 2019):

$$\bar{x}(c,t,i,j) = \frac{1}{N_l(c)} \sum_{k_l=1}^{N_l(c)} x(k_p(k_l),t) \qquad (4.14)$$

Where x is a vegetation phenology variable, k_l is an index of the set of $N_l(c)$ land cover pixels of class c within the 0.05°grid cell, $k_p(k_l)$ is the index within the cell of the MODIS pixel containing land cover pixel k_l,, t is the time index (at 8-day intervals), and i and j are the row and column indices of the grid cell.

4.3.4 Experimental design and analysis

To address the aim of the study, we considered two modeling experiments at 0.05º spatial resolution based on climatological mean of vegetation parameters as well as freely varying vegetation parameters derived from MODIS time series data. For simplicity, the VIC simulation based on climatological vegetation parameters is hereafter referred to as the control run (CTL) while that using timeseries MODIS data is the experimental run (EXP). The EXP simulation adopts the most realistic land surface conditions by using the spatially and temporally varying vegetation properties derived from MODIS data and therefore provides the reference for VIC model validation and sensitivity analysis of the water and energy balance to vegetation dynamics. Uncertainty in the initial states of the water and energy balance can significantly affect simulation in the long-term. We therefore repeated the 11-year simulation (2001-2011) three times based on final states from the previous simulation as initial conditions to for the next simulation until the change in the selected fluxes was within 1% tolerance both CTL and EXP simulations.

In both simulations, the model was initialized using the forcing data described in section 4.3.3. The full energy mode in VIC model was used in which surface temperature is iterated to close the surface energy balance unlike the water balance mode which assumes land surface temperature to be equal to the surface air temperature. Further model configurations adopted in both simulations

included closed energy balance calculations, ARNO baseflow parameterization, and implicit solution for soil heat flux equation. In addition, the initial 2 years are used as a spin-up period and not considered in the analysis of model results.

4.3.4.1 Model evaluation

To evaluate the model performance, we compared the ET, latent heat and sensible heat from the EXP simulation with gridded estimates over the 2003 – 2011 period. The EXP simulation was specifically used for model evaluation as it is based on the more realistic representation of the land surface temporal and spatial heterogeneity. The model evaluation datasets used in this study have been widely evaluated and exhibit acceptable quality and reliability in multiple regions. The MODIS ET product (Mu et al., 2011, 2013) is based on an improved Remote Sensing-Penman-Monteith (RS-PM) approach which accounts for not only plant transpiration but also soil and canopy evaporation. The latent and sensible heat datasets are based on the FLUXCOM energy balance products (www.fluxcom.org) developed using an ensemble of machine learning models trained using global flux data (Jung et al., 2018). Two complementary approaches are used in the development FLUXCOM datasets. The first is a remote sensing approach in which energy fluxes are estimated exclusively from Moderate Resolution Imaging Spectroradiometer (MODIS) satellite data. The second approach includes meteorological data as covariates. In this study, we averaged latent and sensible heat data derived from both approaches to obtain empirical data for evaluation of the energy balance fluxes simulated in this study. We use several statistical measures, including the percent bias (PBIAS), root mean squared error (RMSE) and coefficient of determination (R^2), to evaluate the EXP simulation results. These measures indicate the average error magnitude as well as direction of the error bias between the VIC model results and validation data

4.3.4.2 Analysis of impacts of vegetation parameter variability

The contribution of inter-annual vegetation dynamics on water and energy balance variability were objectively quantified using a variance analyses approach. The two experiments we adopted enable separation of the effect of vegetation dynamics on the interannual variability of a surface water

and energy $\mathcal{M}$ variable from the other factors. First, we analyzed the difference in standard deviation of mean seasonal $\mathcal{M}$.

$$\Delta sd_{\mathcal{M}} = \sigma_{\mathcal{M}}(EXP) - \sigma_{\mathcal{M}}(CTL) \quad (4.15)$$

Where $\sigma_{\mathcal{M}}(CTL)$ and $\sigma_{\mathcal{M}}(EXP)$ represent the interannual standard deviation of seasonal mean $\mathcal{M}$ in the CTL and EXP simulations, respectively. $\Delta sd_{\mathcal{M}}$ provides a spatially varying measure of absolute influence of vegetation dynamics on seasonal water and energy balance variability. We also computed a percentage parameter $PV_{\mathcal{M}}$which measures the relative influence of vegetation dynamics on seasonal water and energy balance variability.

$$PV_{\mathcal{M}} = \frac{\sigma^2_{\mathcal{M}}(EXP) - \sigma^2_{\mathcal{M}}(CTL)}{\sigma^2_{\mathcal{M}}(EXP)} \quad (4.16)$$

Where $\sigma^2_{\mathcal{M}}(CTL)$ and $\sigma^2_{\mathcal{M}}(EXP)$ represent the interannual variance of seasonal mean $\mathcal{M}$ in the CTL and EXP simulations, respectively. $PV_{\mathcal{M}}$ represents the fraction of the variance of a specific water and energy balance variable in CTL simulation that results from interannual vegetation dynamics.

4.4 Result

4.4.1 Time-varying vegetation parameters

The fractional contribution of different MODIS land cover types per 0.05° grid box is shown in Figure 4-2. An evaluation of the dominant cover types from the MODIS land cover product shows that Evergreen forest are dominant in DRC and west Uganda while in Kenya the dominant cover types were open shrubland, Savanna and grassland. Across Tanzania, the dominant cover types are wooded Savanna, Savanna and crop/natural vegetation mosaics. In the north of Lake Victoria and extending into south Uganda savanna and crop/natural vegetation mosaic are dominant while open and closed shrubland types dominate in the northern parts of Kenya.

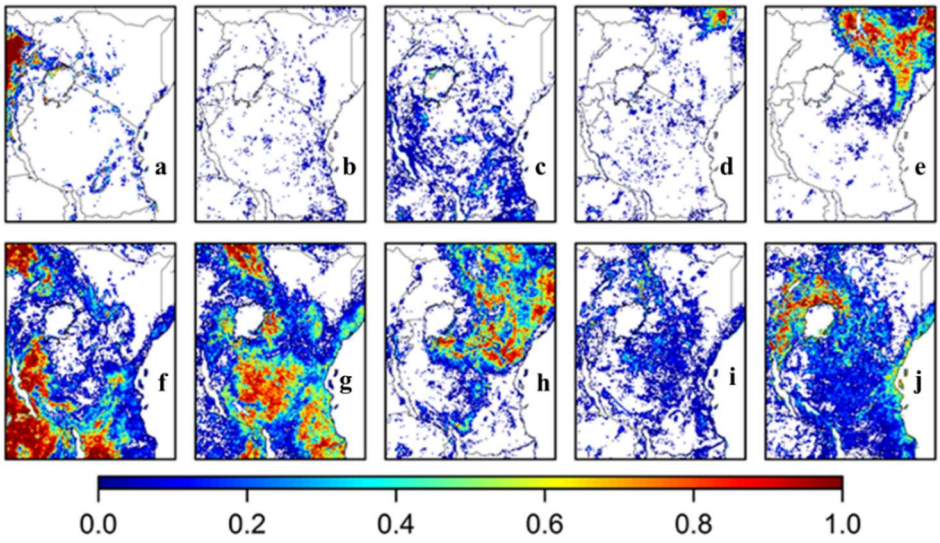

Figure 4-2: Fractional contribution per 0.05° grid box of MODIS land cover types (a) Evergreen broadleaf forest, (b) Deciduous broadleaf forest, (c) Mixed forest, (d) Closed Shrubland, (e) Open Shrubland, (f) Wooded Savanna, (g) Savanna, (h) Grassland, (i) Cropland, and (j) Cropland/natural mosaic

We first examined the differences between the default LAI, FVC and albedo and the corresponding time-varying datasets derived from MODIS data. Although the default parameter values represent inter-annual averages of monthly climatology of the MODIS data for the 2001 – 2011 period, there are significant differences to the time-varying parameters. These differences are attributable to temporal variations linked to natural and human activities affecting the not only the vegetation phenology but also vegetation type in the study area. Figure 4-3 show the spatial distributions in seasonal coefficient of variation for LAI, FVC and albedo during the January-February, March-May, June-September and October-December seasons. The long-term LAI data shows higher variance in most of the region during MAM and OND seasons, particularly in northern Kenya and Tanzania. The coefficient of variation of time-varying FVC generally corresponds to the LAI variations. The coefficient of variation in the time-varying albedo data is small across all seasons. As shown in Figure 4-3 the coefficient of variation for the albedo data varies between 0.0 to 0.4. compared to 0.0 to 1.45 for LAI and FVC.

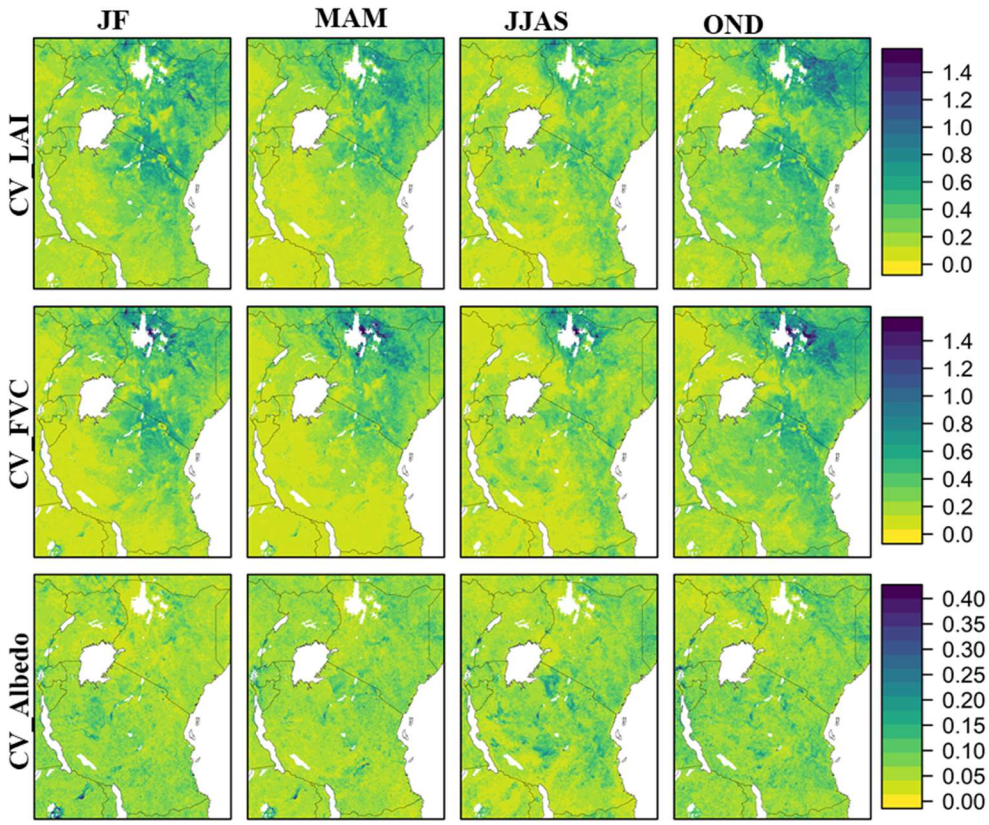

Figure 4-3: Spatial variations in seasonal coefficient of variation for LAI, FVC and albedo during the January-February, March-May, June-September and October-December seasons.

4.4.2 VIC Model evaluation

To evaluate the simulated water and energy balance, we compared the EXP simulation with multiple datasets for 2003 – 2011 period. Figure 4-4 shows mean and standard deviation of monthly ET in the EXP simulation and MODIS ET product. Overall, the VIC model simulated well the geographical distribution of monthly mean ET in the study region with RMSE of 19.6, PBIAS of -20.4%, and R^2 of 0.59. Both simulated and MODIS ET datasets show a clear gradient along the equator with high ET exhibited along the coast, Lake Victoria basin, Congo forest and Arc mountains in southern Tanzania. On the hand, low ET in both datasets is shown in an area extending from southern Ethiopia through Kenya to north eastern Tanzania. Across the region, high ET fluxes occurred in the Evergreen forests and cropland/natural vegetation mosaic (>35 mm/month) signifying that these ecosystems are vital ET source areas in the region, while low ET amounts (<20 mm/month) were found in grassland and open shrubland. The ET variability shows

a similar pattern to that of mean ET in both the observations and the EXP simulation. Overall, the EXP simulation represents well the ET variability in comparison to the MODIS ET with RMSE of 6.3, PBIAS of 10%, and R^2 of 0.72. While the simulated ET variability is overestimated in the northern and eastern parts of the region, the EXP simulation underestimates ET variability over the north western and south eastern parts of the region, which also exhibited large mean ET values.

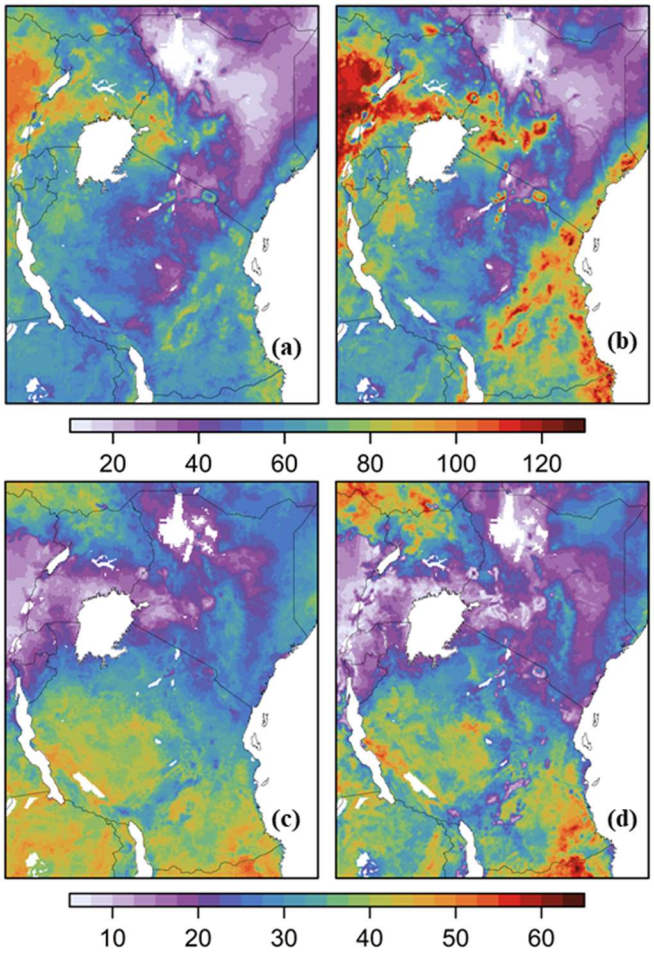

Figure 4-4: The mean and standard deviation of monthly ET (mm/month) in (left) EXP simulation and (right) MODIS data: (a, b) mean and (c, d) standard deviation

The monthly mean and standard deviation of latent and sensible heat from the EXP simulation and FLUXCOM datasets is shown in Figure 4-5. With regard to the spatial patterns, a general agreement is exhibited between mean latent and sensible heat in the EXP simulation and FLUXCOM data with RMSE of 37.4, PBIAS of -40.5%, and R^2 of 0.6 for latent heat, and RMSE

of 21.9, PBIAS of 46.2%, and R^2 of 0.5 for sensible heat. However, the VIC model underestimated the latent heat flux and overestimated the sensible heat across the region. In addition, the VIC model reproduced effectively the regional gradients in energy balance fluxes as well as simulating realistically the magnitude of the interannual variability in the latent and sensible heat fluxes. The standard deviation of both latent and sensible heat is smallest in the Congo forest, north of Lake Victoria, norther Kenya and along the coast.

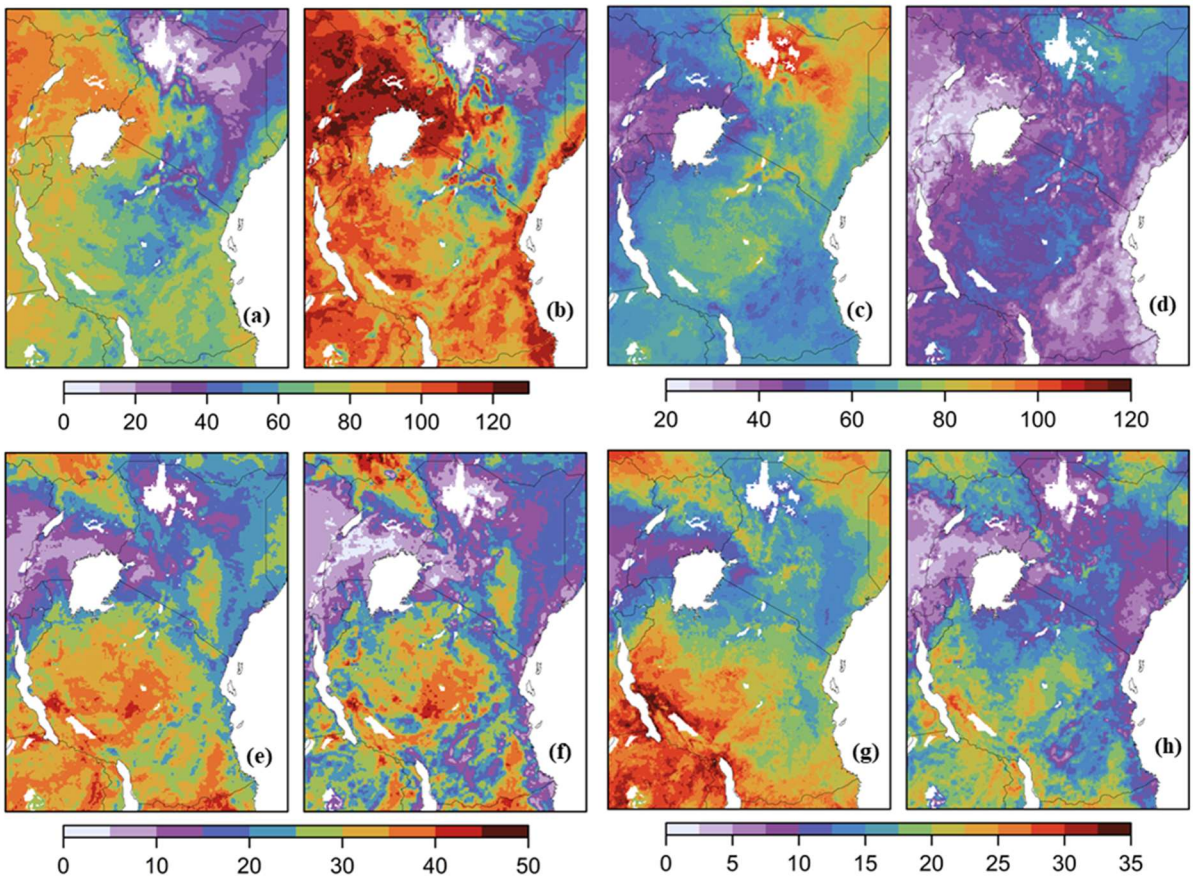

Figure 4-5: The mean and standard deviation of latent heat and sensible heat (Wm^{-2}): (a, e) mean and standard deviation of EXP simulation latent heat, (b, f) mean and standard deviation of FLUXCOM latent heat, (c, g) mean and standard deviation of EXP simulation sensible heat, and (d, h) mean and standard deviation of FLUXCOM sensible heat

4.4.3 Influence of vegetation dynamics on water and energy balance

In this section, we examined the effects of the vegetation parameters on water and energy balance components as simulated with the mean climatological and long-term vegetation parameters

during 2001-2011 period. By comparing the variability of evapotranspiration, latent heat, sensible heat, ground heat and vegetation canopy temperature fluxes from the CTL and EXP simulations, we evaluated the influence of the interannual vegetation parameters on the simulated water and energy balance components across the region.

4.4.3.1 Effects on Evapotranspiration

Figure 4-6 presents differences in standard deviations of seasonal mean daily evapotranspiration (mm/day) between EXP and CTL simulations (Δsd_{ET}) for JF, MAM, JJAS and OND seasons. Since the variability of land surface parameters is removed in the CTL simulation, the differences seasonal ET variability indicate changes in ET due to interannual vegetation variations. Across the seasons, the interannual variability of seasonal ET is generally enhanced by time-varying vegetation parameters over the northern Uganda, western Kenya and north eastern Tanzania during the January-February and March-May seasons. Particularly, during the MAM and OND seasons, ET variability shows widespread enhancement by to time-varying vegetation parameters as exhibited by positive $\Delta \mathrm{sd}_{\mathrm{ET}}$. The proportions of areas in which varying parameters were found to increase seasonal ET variability were 75%, 81%, 64% and 92% during the JF, MAM, JJAS, and OND seasons, respectively. Decrease in ET variability in the EXP simulation is mainly shown in JJAS, particularly in areas with increased variability during the MAM and OND seasons.

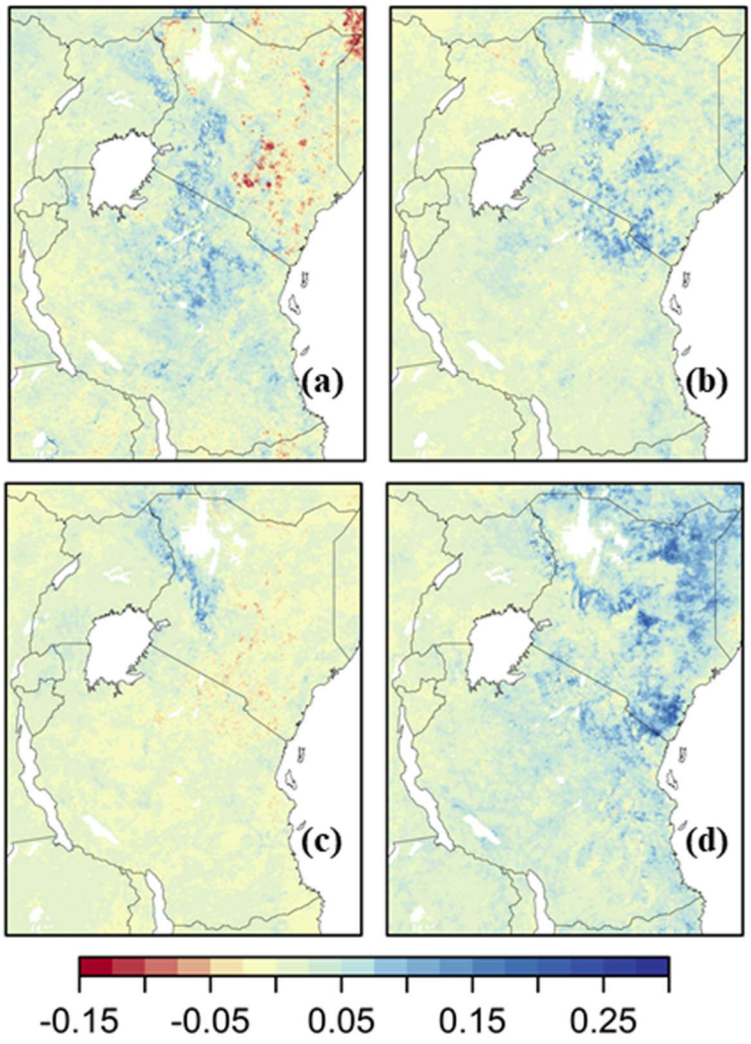

Figure 4-6: Difference in standard deviation of seasonal Evapotranspiration (mm/day) between EXP and CTL simulations (Dsd_{ET}): (a) JF, (b) MAM, (c) JJAS and (d) OND.

To address the heterogeneity in effects of vegetation parameters on ET, we computed the percentage of interannual variance caused by varying vegetation parameters during the MAM and OND seasons (Figure 4-7). This measure shows that the vegetation dynamics amplifies evapotranspiration variability during the rain seasons across the region except in western parts of the region, mainly characterised by evergreen forest cover. Interannual variations in land surface parameters accounted for 16%, 12%, 23% and 15% of the positive variance in ET across the region in the respective seasons. Therefore, although the spatial coverage of positive influence on ET variability is higher during the rain seasons (i.e MAM and OND) than in dry seasons, the magnitude of the influence is higher during dry season than in rain seasons. Although the positive

vegetation influence on ET is predominant across the region, at 76% and 81% of the region during MAM and OND respectively, there are negative signs particularly in western parts of the region.

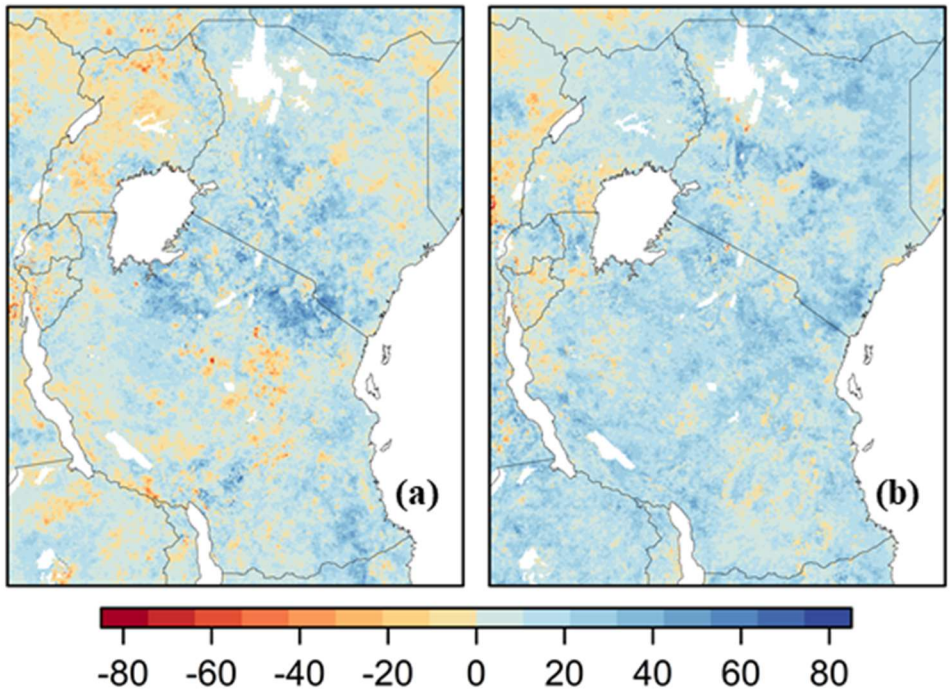

Figure 4-7: Percentage of interannual evapotranspiration variance due to vegetation dynamics (PV_{ET}) during (a) MAM and (b) OND seasons.

4.4.3.2 Effects on latent heat

The differences in standard deviations of Latent heat flux between EXP and CTL simulations for JF, MAM, JJAS and OND seasons are shown in Figure 4-8. The differences indicate the influence induced by interannual vegetation variations since dynamic vegetation properties are a disabled in the CTL simulation. The results show enhanced variability in Latent heat in the EXP simulation. During the JF season, which mainly dry across the region, large variations in Latent heat due to dynamic vegetation properties are particularly simulated in most of central and eastern parts of Kenya, Northern parts of Uganda and southern parts of Tanzania, with magnitude of 5 – 20 Wm^{-2}. These areas are particularly composed of wooded savanna, grassland and shrubland land cover types. However, the areas with enhanced LE during the JF season show contrasting results in OND season. On the other hand, vegetation variations generally play a minimal role in influencing LE variability in JJAS season. In this period, vegetation variations exert negative influence on LE

standard deviation over the North western parts of the region with magnitude of up to -10 Wm^{-2}. These areas also show increasing LAI trend as indicated in Figure 3-2. During the rain seasons (MAM and OND), interannual vegetation variations exert negative influence on LE in most parts of the region.

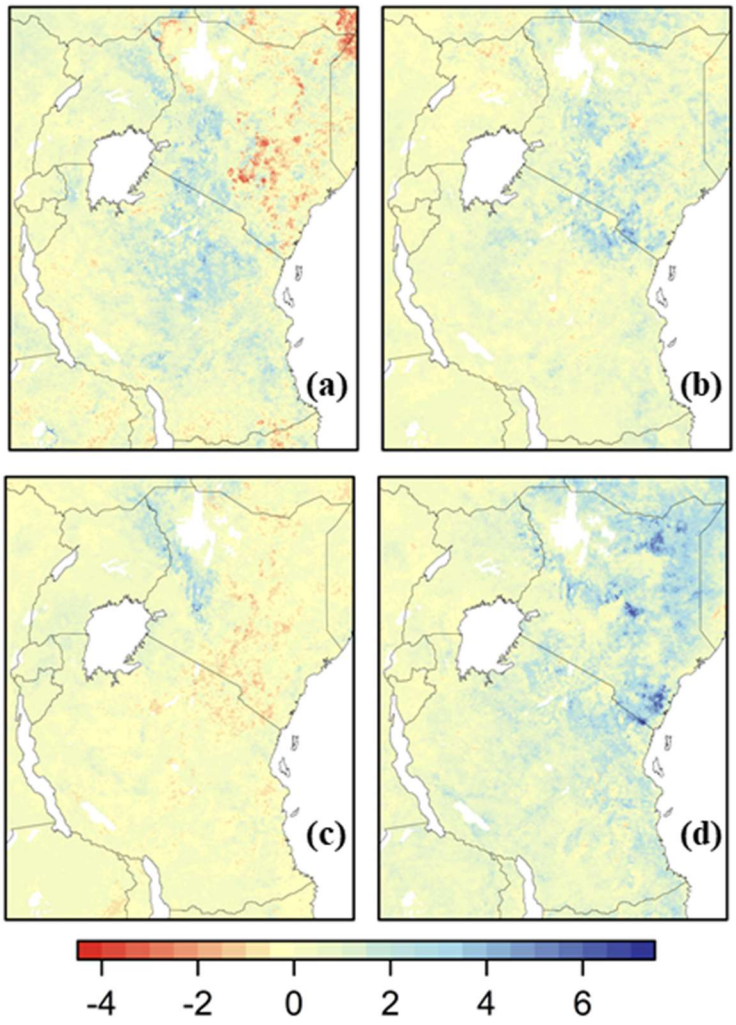

Figure 4-8: Difference in standard deviation of seasonal Latent heat (Wm^{-2}) between EXP and CTL (Dsd_{LE}) simulations: (a) JF, (b) MAM, (c) JJAS and (d) OND.

4.4.3.3 Effects on sensible heat

Figure 4-9 shows differences between EXP and CTL in standard deviations of sensible heat during JF, MAM, JJAS and OND seasons. Generally, time-varying vegetation parameters results in an increase in standard deviation of seasonal sensible heat, particularly over a region extending from

western Kenya to norther Tanzania to southeast Tanzania. We further calculated the role of the vegetation dynamics on interannual seasonal sensible heat variability using the variance method (Figure 4-10). This parameter shows that interannual vegetation variations exert a strong influence on sensible heat variability in the Lake Victoria basin and northern Tanzania during MAM season, and an area extending from central to the Kenya coastline as well in Rwanda and Burundi during the OND season, accounting for about 40–80% of the total interannual sensible heat variance.

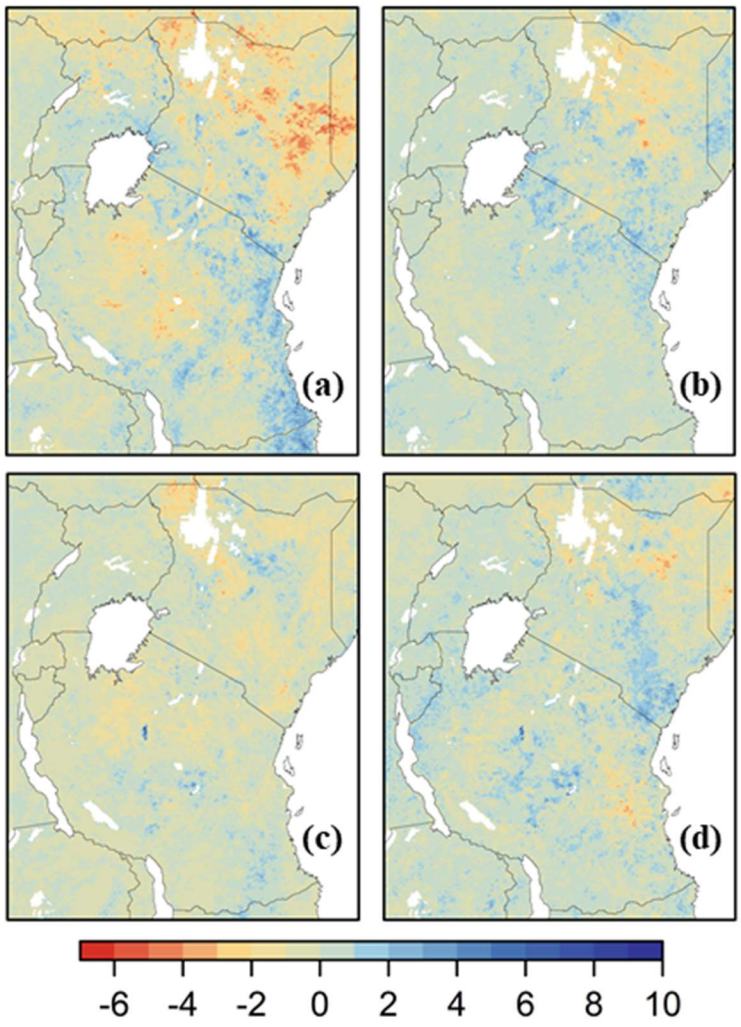

Figure 4-9: Difference in standard deviation of seasonal Sensible heat (Wm^{-2}) between EXP and CTL (Dsd_H): (a) JF, (b) MAM, (c) JJAS and (d) OND.

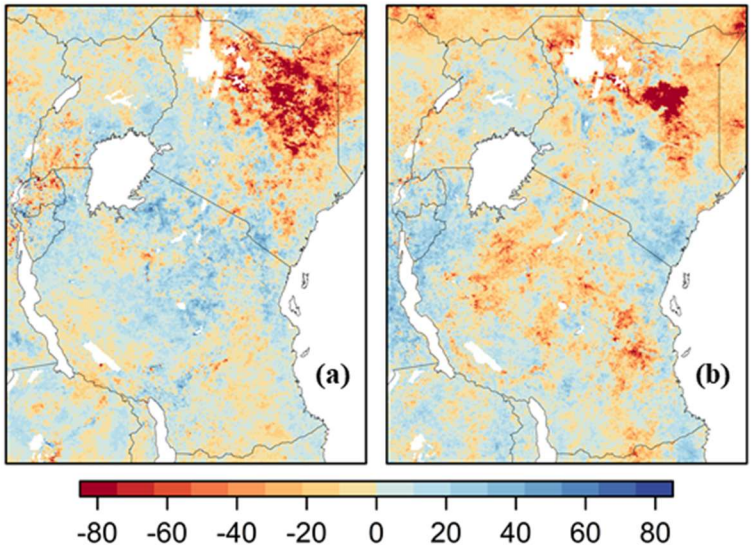

Figure 4-10: Percentage of interannual sensible heat variance due to vegetation dynamics (PV_H) during (a) MAM and (b) OND seasons.

4.4.3.4 Effects on ground heat

Figure 4-11 shows the differences between CTL and EXP in standard deviations of ground heat flux. Generally, the varying vegetation parameters causes an increase in interannual seasonal variability of ground heat over north eastern Uganda, central Kenya, and northern Tanzania. Across the region, proportion of areas showing positive effects are 43%, 71%, 78%, and 65% for the JF, MAM, JJAS and OND seasons respectively. Therefore, positive effects show strong dominance across the region for MAM and JJAS seasons. The magnitude of ground heat variability over the region are generally small as compared to latent and sensible heat variability changes. Figure 4-12 shows the percentage of ground heat interannual seasonal variance due to varying vegetation parameters. This measure reinforces the strong contribution of vegetation parameters on ground heat interannual seasonal variability accounting for about 17%, 31%, 35%, and 31% of the interannual ground heat variance during the JF, MAM, JJAS and OND seasons respectively.

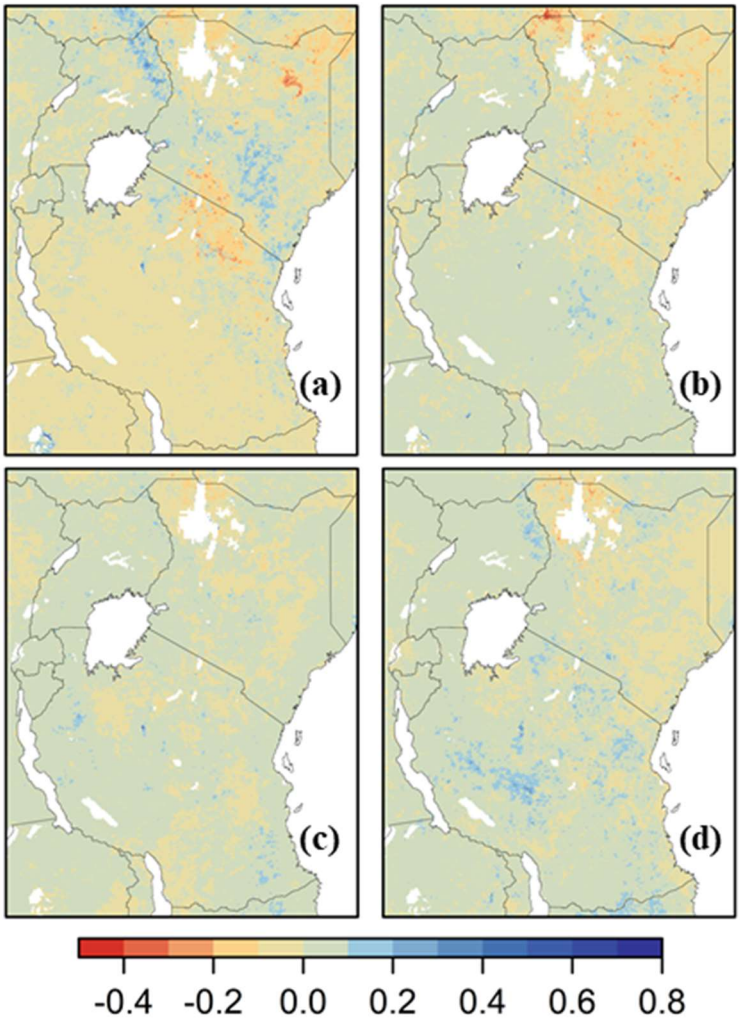

Figure 4-11: Difference in standard deviation of seasonal Ground heat (Wm^{-2}) between EXP and CTL (Dsd_G): (a) DJF, (b) MAM, (c) JJA and (d) SON.

4.5 Discussion

The application of land surface models is vital particularly in the assessment of the potential effects of environmental changes as well as in assessment of effectiveness of different climate change impact mitigation measures adopted at varying spatial scales. One of the crucial steps in application of these models is realistic parameterization of the land surface characteristics in the models and thus reducing uncertainties due to prescribed land surface parameters. In this study, two simulations (CTL and EXP) were conducted with the same meteorological forcing data covering the 2001 – 2011 period. The EXP simulation allows the land surface parameters to vary over time while in the CTL simulation the variability in land surface parameters is disabled by

prescribing the climatology of the surface parameters used in EXP. We therefore isolated the effects of interannual variations in vegetation on water and energy balance by comparing the two simulations.

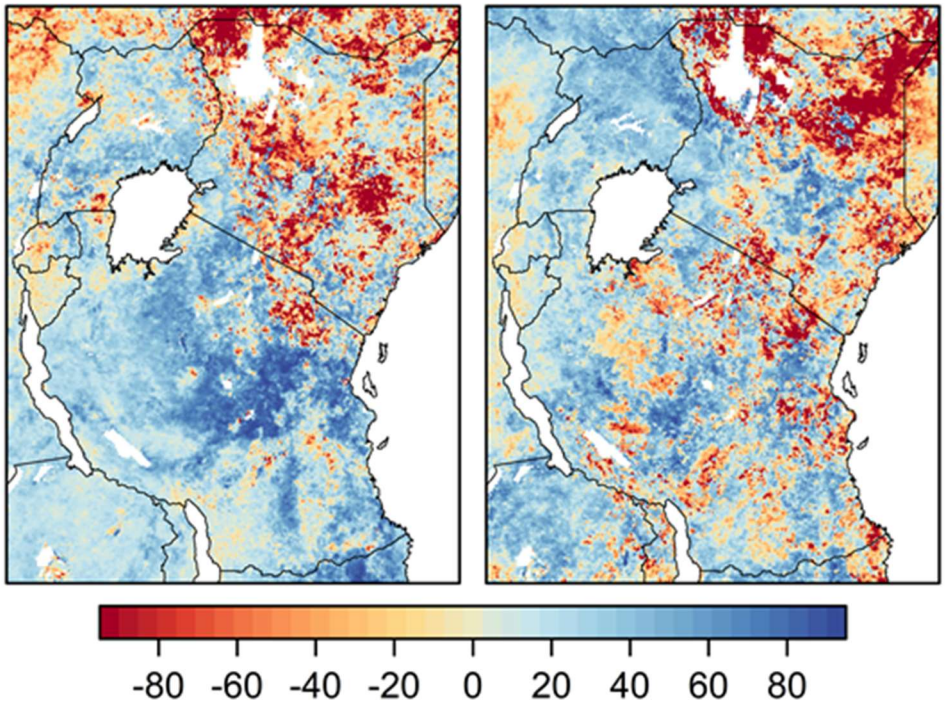

Figure 4-12: Percentage of interannual ground heat variance due to vegetation dynamics (PV_G) during (a) MAM and (b) OND seasons.

VIC simulations of evapotranspiration, latent heat, and sensible heat were improved by the incorporation of time varying LAI, FVC and albedo data into the model, as demonstrated by the RMSE and R^2 values between simulated and validation datasets. The model evaluation results shows performance statistics comparable to previous studies on regional water balance simulation (Ghilain et al., 2012; Guo and Shen, 2015a; Moriasi et al., 2007). As shown in Figure 4-6 to Figure 4-12, using time varying land surface parameters accounts for increased variance in simulated water and energy fluxes. Although both the CTL and EXP simulations reproduced the seasonal characteristics of the land surface water and energy balance in the East Africa, the EXP simulation captured the interannual variance in these land surface fluxes more ardently. The findings of this study advance the greater knowledge on the impacts of time-varying land surface parameters on

the performance of VIC model, which is valuable for many applications, particularly for land surface and climate modelling.

The spatial and seasonal patterns of the effects of vegetation dynamics on water and energy fluxes differ across the region. Compared to changes in standard deviation of sensible and ground heat, varying vegetation parameters shows larger effects on latent heat variability. However, despite the weaker influence on sensible and ground heat, the vegetation influence on these fluxes is still vital over many parts of the region as shown in Figure 4-10 and Figure 4-12. Although vegetation dynamics mainly enhance variability in seasonal water and energy balance, it also shows dampening effect in some parts of the region. For instance, vegetation dynamics may lead to decreased ET variability over north western parts of the region as well as other isolated areas in central Tanzania during the MAM and OND seasons and decreased sensible heat variability over the areas from North Uganda to eastern part of Kenya during MAM and OND seasons. Nevertheless, the negative differences between EXP and CTL simulations are limited to relatively small areas.

The results of this study emphasis that improved modeling practices which consider the physical realism of spatial and temporal vegetation dynamics adequately represent surface water and energy balance as also concluded in multiple previous studies (Molod and Salmun, 2002; Pitman, 1991; Seth et al., 1994; Wood et al., 1992). The following key questions arising from the results of the study are discussed below: (1) Are the MODIS LAI, FVC and albedo datasets appropriate for water and energy balance modelling in East Africa? (2) What is the link between the new parameterization scheme and improved water and energy predictions? and (3) What are the key modelling factors affecting use of time-varying vegetation parameters in VIC model? These questions are addressed in the following sections.

Are the MODIS LAI, FVC and albedo datasets appropriate for water and energy balance modelling in East Africa?

In addition to meteorological forcing and soil parameters, the VIC model requires vegetation parameters (i.e LAI, FVC and albedo) which can be prescribed either as long-term monthly means or as a monthly time-series covering the period of study. The spatio-temporal variations in these

variables is a key underlying factor in the variations of land surface water and energy partitioning at local and regional scales as also concluded in multiple previous studies (Ke et al., 2012; Su et al., 1999). In this study, we used the widely applied VIC model to assess the effects of time-varying LAI, FVC and albedo input data on water and energy balance in East Africa. Most previous applications of the VIC model are based on the Advanced Very High-Resolution Radiometer (AVHRR) datasets at spatial resolutions greater than 0.05° and temporal resolutions of 1 month. In addition, these applications use the dominant land cover type in a grid to characterize the entire grid cell. Consequently, MODIS datasets provide a capability for reliable and consistent characterization of the land surface properties at higher spatial resolutions compared to the AVHRR data.

What is the link between the new parameterization scheme and improved surface water and energy predictions?

In order to improve simulation of surface fluxes, land surface parametrization schemes must address two crucial aspects: (1) sub-grid spatial variability in vegetation parameters, and (2) inter-annual variability of the vegetation parameters due to both climatic and human factors. As the regional surfaces over the typically resolvable scales in land surface models are extremely heterogeneous, surface parameterizations that assume homogeneity do not accurately characterize the surface forcing. The two types of sub-grid spatial heterogeneities accounted for in this study are differences between vegetation "tiles" and intra-tile heterogeneity. The former is considered through accounting for fractional coverage of different land cover types (e.g Evergreen deciduous forest, shrubs, and cropland) per grid cell while consideration of canopy gaps or exposed soil between plants in a particular tile accounts for the latter through a clumped vegetation scheme. In addition, vegetation parameters for a particular land cover type are allowed to vary from one grid cell to another based on MODIS data. Contrary to the "dominant" approach to land cover characterization (where the parameters of most dominant land cover type per grid cell are assumed to cover the entire cell), the "mosaic" approach adopted in this study allows for the water and energy fluxes to be calculated explicitly for every vegetation tile and the fluxes for each grid cell to be calculated as weighted averages of the tiles (Koster and Suarez, 1992a, 1992b; Melton and Arora, 2014). The inter-annual variability in land surface properties was captured more

realistically by using a time series of LAI, FVC and albedo obtained from various MODIS products following Bohn and Vivoni (2016 & 2019).

What are the key modelling factors affecting use of time-varying vegetation parameters in VIC model?

The efficient use of satellite remote sensing data in land surface modelling is dependent on not only the quality of the data but also the interoperability between the model and data (Kumar et al., 2006; Rajib et al., 2020). The interoperability between the VIC model and MODIS data was addressed in terms of compatibility of the derived datasets with the model architecture (Bohn and Vivoni, 2019). Using this approach, MODIS data can be assimilated in VIC model across other regions in the Africa continent for improved simulation of surface water and energy balance. However, the optimum level of complexity required in parameterization of spatial and temporal land surface heterogeneities is still an unresolved issue. This is a crucial subject due to the trade-off between higher resolution parameterization of land surface and the computation feasibility for continental to global simulations. On other hand, there is need for extensive sensitivity analysis of the potential advective effects between the different patches within a grid cell and they may affect long-term simulation of water and energy balance.

4.6 Conclusion

In the current study, we create and evaluate the usefulness of a long-term MODIS-based land surface parameter data set using the VIC model over the East Africa region. As shown in our results, the use of time-varying land surface datasets in VIC model improves its capacity to accurately simulate the interannual variability in surface water and energy balance in East Africa. In addition, due to the land cover/use changes in East Africa, the long-term parameter set provides a better representation of the dynamic vegetation properties and is therefore more suitable for water and energy balance simulations. Nevertheless, prior to adopting the MODIS parameters in land surface simulations, it is crucial to compare the vegetation parameters derived from MODIS data to field observations and therefore link their differences to the variations in simulated regional water and energy fluxes.

In this study, we first derived a new vegetation parameter set based MODIS datasets for period 2001-2011 which were then used in the simulation of regional water and energy balance fluxes. The derived parameter set showed that MODIS land cover provided significant variations in dominant vegetation covers compared to other regional land cover products over East Africa and specifically in the northern Uganda, and norther Kenya through to Tanzania which are areas mainly characterized by cropland/natural mosaic, savanna and shrubland cover types. In addition, the long-term LAI and FVC parameters showed significant spatial and temporal variations. As a result of the large discrepancies between the long-term and seasonally averaged vegetation parameters, the simulated regional water and energy fluxes during 2001 – 2011 period differ significantly between the two simulations.

Based on our results, the use of long-term parameters in VIC model considerably increases the model performance in ET simulation across the study domain and particularly over the central Kenya and north west and central Tanzania, which are characterized by intensive human effects on vegetation dynamics through agriculture and livestock keeping activities. In addition, the strong coupling between land surface characteristics and regional water and energy balance is further demonstrated by the differences between the surface sensible heat fluxes simulated based on the two parameter sets. In southern parts of the region characterized by sparse savanna vegetation, long-term vegetation parameters lead to a decrease in evapotranspiration which increases the sensible heat flux, and this has the potential to increase in surface temperature in the area.

Regardless of the improvements in the EXP simulation, both the CTL and EXP simulations are characterized by uncertainties attributed to not only errors in forcing meteorological data but also uncertainties in physical or empirical parameterizations in the model. In addition, the validation datasets used are characterized by uncertainties emanating from the empirical upscaling algorithms used to derive them. These uncertainties call for further analysis to improve regional water and energy balance simulations in East Africa.

Chapter 5: Effects of Land Cover Change on Water and Energy Balance in East Africa

5.1 Abstract

Changes in land cover characteristics due to human and natural causes affects not only the carbon storage capacity of the terrestrial ecosystems but also the biophysical characteristics of the earth's surface. Particularly, increasing tree cover though afforestation, reforestation and other forest management practices affects not only the surface albedo, but also roughness length and the evaporative capacity. In this study, we evaluated the potential biophysical implications of extensive increase in tree cover across East Africa. Based on simulated evapotranspiration, latent and sensible heat, land surface temperature (LST), and vegetation canopy temperature, we assessed the potential effects of land cover change on water and energy balance in the region. The land cover changes showed an increase in mean LAI and fractional vegetation cover by 1.5 m^2/m^2 and 0.16 respectively, while albedo decreased by 0.02 averaged across the region. As a result, total evapotranspiration was simulated to increase by 1.6 mm/month which is attributed to increased transpiration and canopy evaporation by 2.6 mm/month and 3.9 mm/month, respectively, and a decrease in bare soil evaporation by 4.9 mm/month. On the other hand, increased tree cover led to increased latent and sensible heat while land surface temperature and canopy temperature decreased by -1.0°C and -1.9°C respectively. Based on the findings of the study, increasing forest cover in the region will play a pivotal role in climate change adaption by inducing a highly needed local cooling effect. However, there is need for further analysis of the net effect from not only local afforestation efforts but also teleconnections due changes taking place in the surrounding regions.

5.2 Introduction

Among the most prominent impacts of human activities is the modification of the land surface through extensive land cover changes mainly involving conversion of forests to grassland and cropland (Pongratz et al., 2008). These changes have been linked to widespread biochemical and biophysical effects with the potential to influence the earth's ecological and environmental systems at varying spatial and temporal scales (Bright et al., 2017; Devaraju et al., 2015; He et al., 2014; Lucia et al., 2017). Vegetation plays a crucial role in the land-atmosphere interface through the regulation of exchanges of carbon, water, heat, radiation and momentum. However, land cover

change has been shown as a major threat to the capacity of ecosystems to perform their provisioning and environmental regulation functions. Consequently, reforestation and/or afforestation have been recommended as key strategies for climate change adaptation and mitigation due to their immense potential in regulating local hydroclimatic conditions while rising the regional and global terrestrial carbon pools. However, most of the studies addressing the subject on impacts of land cover change have mainly adopted a carbon-centric perspective (Quéré et al., 2018; Sleeter et al., 2018). The biophysical implications of land cover change, particularly at the local to regional level, have been largely overlooked. The focus of this study is therefore to assess the local biophysical effects of land cover change on water and energy balance in East Africa. Understanding the potential effects of land cover change on partitioning of water and energy balance is particularly crucial for water resource management in the vast arid and semi-arid areas in East Africa, where potential evapotranspiration far surpasses precipitation.

For instance, changes in land cover types disrupts surface properties such as albedo, leaf area index, fraction vegetation cover, surface roughness, and canopy conductance at varying spatial and temporal scales (Anderson et al., 2011; Li et al., 2015b). These changes have been associated with biophysical effects composed of both radiative forcing (due changes in albedo) and non-radiative forcing (due to changes in the hydrological cycle through evapotranspiration rates) on local and regional climate (Davin and de Noblet-Ducoudre, 2010). Compared to bare areas, vegetation cover has a lower albedo causing an increase in proportion of energy absorbed by the surface which leads to increased surface temperature and potential increase in precipitation through the albedo mechanism (Meng et al., 2014). On the other hand, increased vegetation cover leads to enhanced evapotranspiration thus causing increased portioning of energy into latent heat. This causes a decrease in surface air temperature and potential increase in precipitation through the evapotranspiration mechanism. (Chen et al., 2012; Li et al., 2017, 2016; Peng et al., 2014). These competing biophysical effects of land cover changes not only vary spatially but also seasonally, with the magnitude of warming or cooling effect determined by specific vegetation changes and climatic conditions (Duveiller et al., 2018c). What's more, the biophysical effects of LUCC on global climate have shown comparable magnitudes to the biochemical effects as demonstrated in previous global modelling studies (Davin and de Noblet-Ducoudre, 2010; Devaraju et al., 2015; Pongratz et al., 2010). Consequently, it has been recommended that the biogeochemical

considerations mainly adopted in the crediting of forestry projects should be expanded to include the potential biophysical effects of such projects.

As noted by Lucia et al. (2017), assessment land cover change impacts on surface water and energy balance can be observation-driven or model-based. In the observation-driven assessments, in-situ measurements from flux sites can be used (Lee et al., 2011; Zhang et al., 2014). However, due to insufficient spatial coverage of such stations, regional and global studies have mainly relied on satellite remote sensing products (Alkama and Cescatti, 2016; Duveiller et al., 2018c). These products provide biophysical variables such as albedo (Schaaf et al., 2002), land surface temperature and emissivity (Li et al., 2013; Wan, 2014) which can be used to estimate land surface water and energy balance. On the other hand, model-based assessment involves data-driven land surface models which are used to estimate changes in land surface fluxes by imposing different land cover scenarios based on observed or idealized land cover changes (Duveiller et al., 2018b; Forzieri et al., 2018).

In this study, we assess the potential bio-geophysical effects emanating from alterations in the physical properties of the land surface in East Africa based on a land surface model. We primarily focused on land cover alterations due to increased tree cover through forestation and/or afforestation activities which are crucial strategies for climate change adaptation and mitigation across the east Africa following the extensive deforestation in the region (Brink et al., 2014). The changes in LAI, albedo, fractional vegetation cover due to the increase in tree cover were simulated by a dynamic vegetation model accounting for vegetation disturbance factors such as drought. This approach is more realistic for this particular region as it provides spatially and temporally explicit information for a better understanding of the geographic and seasonal patterns of the potential effects (Duveiller et al., 2018c). The simulated vegetation changes were then prescribed into the Variable Infiltration Capacity (VIC) model to assesses local biophysical impacts with particular emphasis on evapotranspiration (ET), latent and sensible heat as well as land surface temperature (LST) and vegetation canopy temperature.

5.3 Model description and experiments design

5.3.1 The LPJ-mL dynamic vegetation model

In this study, the Dynamic Global Vegetation Model with managed Land (LPJ-mL, Schaphoff et al., 2018) was used to simulate dynamic vegetation growth. This model has been evaluated at numerous sites spread across the globe and representing different vegetation types and has been shown to reasonably simulate spatial-temporal vegetation dynamics and carbon pools (Forkel et al., 2014, 2019). In LPJ-ml, vegetation composition per grid cell is a function of the fractional coverage of populations of various plant functional types (PFTs) which are normally prescribed based on existing land cover data. The natural PFTs represents vegetation aggregated into classes depending on leaf type (broadleaf, needleleaf), phenology (summergreen, evergreen, raingreen), and preferred climatic conditions (boreal, temperate, tropical). Some of the key vegetation growth processes are summarized below while additional details about the model are presented by Schaphoff et al. (2018). The Leaf Area Index (LAI) for individual PFTs is related to leaf biomass ($C_{leaf,ind}$), Specific Leaf Area (SLA, m^2 gC^{-1}), and crown area (CA_{ind}) as follows:

$$LAI_{ind} = \frac{C_{leaf,ind} \cdot SLA}{CA_{ind}} \qquad (5.1)$$

The SLA is derived using an empirical relationship with leaf longevity (α_{leaf}) which determines whether certain climatic conditions will favor growth of deciduous or evergreen phenology PFTs. As suggested by Smith et al. (2014), the equation of SLA for needle-leaved and broadleaved PFTs is as follows:

$$SLA = \frac{2X10^{-4}}{DM_c} \cdot 10^{\beta_0 - \beta_1 \cdot \log(\alpha_{leaf})/\log(10)} \qquad (5.2)$$

Where parameter β_0 is adapted for broadleaved (β_0= 2.2) and needle-leaved trees (β_0 = 2.08) and for grass (β_0 = 2.25), and β_1 is set to 0.4. The dry matter carbon content of leaves (DM_c) is set to 0.4763 (Schaphoff et al., 2018).

The foliar projective cover (FPC_{ind}, which is defined as the vertically-projected percentage coverage of photosynthetic foliage) is essential in determining canopy transpiration and radiation

interception. The LAI_{ind}, can be converted into FPC_{ind}using the canopy light-absorption model (Lambert–Beer law) as follows:

$$FPC_{ind} = 1 - e^{(-0.5LAI_{ind})} \qquad (5.3)$$

In a grid cell, the entire FPC is computed by multiplying FPC_{ind} by the crown area (CA) and population density (P):

$$FPC_{total} = CA \cdot P \cdot FPC_{ind} \qquad (5.4)$$

Where crown area (CA) is obtained by applying the stem diameter (D) based on the inversion of Reinecke's rule (Zeide, 1993) with k_{rp} as the Reineke parameter (Schaphoff et al., 2018):

$$CA = \min\left(k_{allom} \cdot D^{k_{rp}}, CA_{max}\right) \qquad (5.5)$$

On the other hand, Albedo (β), which is the average reflectivity per grid cell, is determined by several drivers such as land surface conditions as well as assumed albedo values for bare soil, plant functional types, and snow (Forkel et al., 2014; Schaphoff et al., 2018; Strengers et al., 2010). The grid cell albedo in LPJ-ml can be expressed as:

$$\beta = \sum_{PFT=1}^{nPFT} \beta_{PFT} \cdot FPC_{PFT} + F_{bare} \cdot \left(F_{snow} \cdot \beta_{snow} + (1 - F_{snow}) \cdot \beta_{soil}\right) \qquad (5.6)$$

Where β_{PFT} is the albedo of each existing PFT, FPC_{PFT} is the foliage projective cover of the respective PFT, F_{bare} and F_{snow} are the coverage of bare soil and snow on top of bare soil in a grid cell and β_{soil} and β_{snow} are the soil and snow albedo parameters, respectively. The albedo of the different PFTs is the sum of leaf, stem/branches and litter (background) albedo. The albedo of green leaves depends on the daily phenology status (FPC_{PFT}), and the PFT-dependent leaf albedo parameter ($\beta_{leaf,PFT}$). The albedo of stems and branches is determined based on the fractional coverage of the ground by stems and branches and a PFT-dependent stem albedo parameter ($\beta_{stem,PFT}$). The β_{PFT}, β_{soil} and β_{snow} parameters were based on optimized results from multiple previous studies (Forkel et al., 2014; Schaphoff et al., 2018; Strengers et al., 2010).

The forcing data used in LPJ-mL consisted of Climate Hazards group Infrared Precipitation with Stations (CHIRPS) dataset (Funk et al., 2015), frequency of rain days derived from the CHIRPS data, mean temperature and cloud fraction obtained from a high resolution daily meteorological dataset developed by Princeton university hydrology group for East Africa (Chaney et al., 2014; Sheffield et al., 2006). The soil information was obtained from the Africa Soil Information Service (AfSIS) project database (http://africasoils.net). Area fractions for different land cover types per grid cell are also part of the model input datasets thus the MODIS land cover data (MCD12Q1v006) for the year 2005 was used in this study. Although this product provides land cover data at yearly interval from 2001 to 2017 in six different classification schemes, we selected the data for 2005 with the IGBP classification. In LPJ-mL land cover is specified in terms of the maximum annual FPC per PFT. However, the establishment and survival rates for the PFTs are based on bioclimatic limits, heat and cold stress, competition among PFTs, as well as fire disturbance. The fractions of different land cover types per 0.05° x 0.05° grid cells were converted into FPC as described in section 5.3.3.

5.3.2 Variable infiltration capacity (VIC) model

The vegetation parameters (LAI, FVC, and albedo) from the LPJ-mL were used as inputs in in three-layer Variable Infiltration Capacity (VIC) model (Liang et al., 1994) version 4.2.d to assess the effects of simulated changes in vegetation dynamics on surface water and energy balance. The VIC model is a grid-based, semi-distributed process-based land surface and hydrologic model which can be forced with meteorological data in an offline mode or directly coupled to General Circulation Models (GCMs). This model has been widely applied and evaluated at global and continental levels as well as across large river basins (Bohn and Vivoni, 2016; Crow et al., 2003; Wu et al., 2011; Zhao et al., 2013). The vertical energy and moisture fluxes at each grid cell are calculated in the model by resolving full water and energy balances based on the vegetation properties and coverage as well as soil characteristics. Land surface heterogeneity is represented in the model through consideration of multiple vegetation classes within a single grid cell as vegetation mosaics. The simulated fluxes from each land cover mosaic within a grid cell are then combined as weighted sum for a given grid cell. The adopted VIC version also includes modified vegetation formulation which accounts for vegetated and non-vegetated area fractions in each

vegetation tile based on a "clumped" approach. This alteration approximates the effects of exposed soil between plants thus allowing for a time-variant bare soil area and accounting for the effects of shading and wind attenuation from nearby vegetation (Bohn and Vivoni, 2016). For each land cover tile, vegetation parameters (LAI, FVC, and albedo) were assigned inform of daily time series for each land cover scenario.

The forcing datasets used in VIC model comprised of meteorological, vegetation and soil data. The precipitation data was obtained from version 2 of the Climate Hazards group Infrared Precipitation with Stations (CHIRPS) dataset (Funk et al., 2015). Minimum and maximum temperature, as well as wind speed datasets were obtained from a high resolution daily meteorological dataset developed by Princeton university hydrology group for East Africa (Chaney et al., 2014; Sheffield et al., 2006). This dataset is created by downscaling the National Centers for Environmental Prediction–National Center for Atmospheric Research (NCEP–NCAR) reanalysis, adjusting for temporal inconsistencies and assimilating quality controlled and gap-filled Global Summary of the Day (GSOD) in situ measurements to remove random errors. The model was set up using three soil layers with varying depths. For each grid cell, the soil classes and properties at top and subsurface layers were obtained from the Africa Soil Information Service (AfSIS) project database (http://africasoils.net) while the root zone depth and fraction of root zones of each vegetation type were estimated according to Zeng (2001). The pedo-transfer functions of Saxton and Rawls (2006) were used to estimate the saturated hydraulic conductivity for each soil layer. Spatial variation in elevation were estimated using SRTM dataset (Jarvis et al., 2008). All the input datasets obtained from different sources at different resolutions were resampled to 0.05º spatial resolution for the VIC model simulation.

5.3.3 Land cover change scenarios

One of the key input datasets in LPJ-mL is the annual maximum FPC which defines the possible maximum fraction for different PFTs simulated per grid cell. However, the land cover classes in existing global and regional land cover datasets are not directly comparable with PFTs used in vegetation growth models. We therefore reclassified the MODIS land cover classes following Ottlé et al. (2013) into two tree PFTs (Tropical broadleaf Evergreen, and Tropical broadleaf raingreen trees) and tropical herbaceous PFT (which characterized grass, shrub and cropland). In addition,

although we translated the land cover types into fractions of PFTs per 0.05x 0.05 grid cell, these fractions do not represent FPC. Thus, a grid cell in land cover maps can be classified as covered by 100% deciduous broadleaf forest while this grid cell may contain only 80% trees while the rest is covered by herbaceous plants. The tree PFTs (e.g Deciduous broadleaf forest) in every grid cell were therefore converted into annual maximum FPC using the MODIS Vegetation Continuous Fields dataset (Townshend et al., 2011) for the year 2005 as follows (Forkel et al., 2014):

$$FPC_{PFT} = LC_{PFT}\, X \frac{F_{Tree}}{\sum_{PFT=1}^{PFT=n} LC_{PFT}} \qquad (5.7)$$

Where LC_{PFT} is the fraction covered by a tree PFT in a 0.05x 0.05 grid cell, F_{Tree} is the fraction of tree cover in the grid cell based on MODIS Vegetation Continuous Fields dataset and n is total number of tree PFTs in the 0.05x 0.05 grid cell. To obtain the hypothetical land cover change scenario, the bare areas fraction in the MODIS Vegetation Continuous Fields was considered as converted to tree cover and the annual maximum FPC for each PFT re-calculated as explained above. This is a hybrid diagnostic-dynamic approach to simulation of land change where increasing annual maximum FPC for tree cover types allows increased establishment and survival of tree PFTs in a particular grid cell while the vegetation growth and mortality is determined by the allocation rules in LPJ-mL (Forkel et al., 2014). Recent studies on the parameterization of the LPJ-mL were used to adapt the model for the East Africa region using parameter values obtained in previous global calibration studies (Forkel et al., 2014, 2019). The differences between current and simulated LAI, FVC and albedo are shown in Figure 5-1.

5.3.4 Experimental design

The East Africa region was considered in this study, an area spanning approximately 2,267,136 km^2 (bounded by N5.52 and S11.76 latitude, W28.8 and E41.92 longitude). This area comprises the countries of Burundi, Kenya, Tanzania, Rwanda and Uganda, and portions of the Congo, Ethiopia, Malawi, Mozambique, Somalia, South Sudan and Zambia (Figure 3-1). A four-step methodological approach was adopted as follows: (a) simulation of water and energy balance based on present-day land surface parameters derived from multiple MODIS products (section 4.3.3), (b) preparation of land cover change scenarios reflecting increased tree cover over the study

region and simulation of the corresponding LAI, FVC and albedo over the 2001 – 2011 period using LPJ-mL, (c) simulation of the water and energy balance using simulated LAI, FVC and albedo as inputs in VIC model and (d) evaluation of the local impacts of land cover change on water and energy balance based on ET, latent heat, sensible heat, land surface and vegetation canopy temperature. All data processing and analysis was performed in R software.

5.4 Results

The results in this study provide details of potential impacts of increasing tree cover per 0.05° grid cell across the East Africa region. The effects of land cover change were assessed on annual and seasonal basis for selected water and energy fluxes. It is noteworthy that changes in multiple land surface biophysical properties including albedo, surface roughness and evaporative capacity may induce contrasting impacts on the overall water and energy balance components.

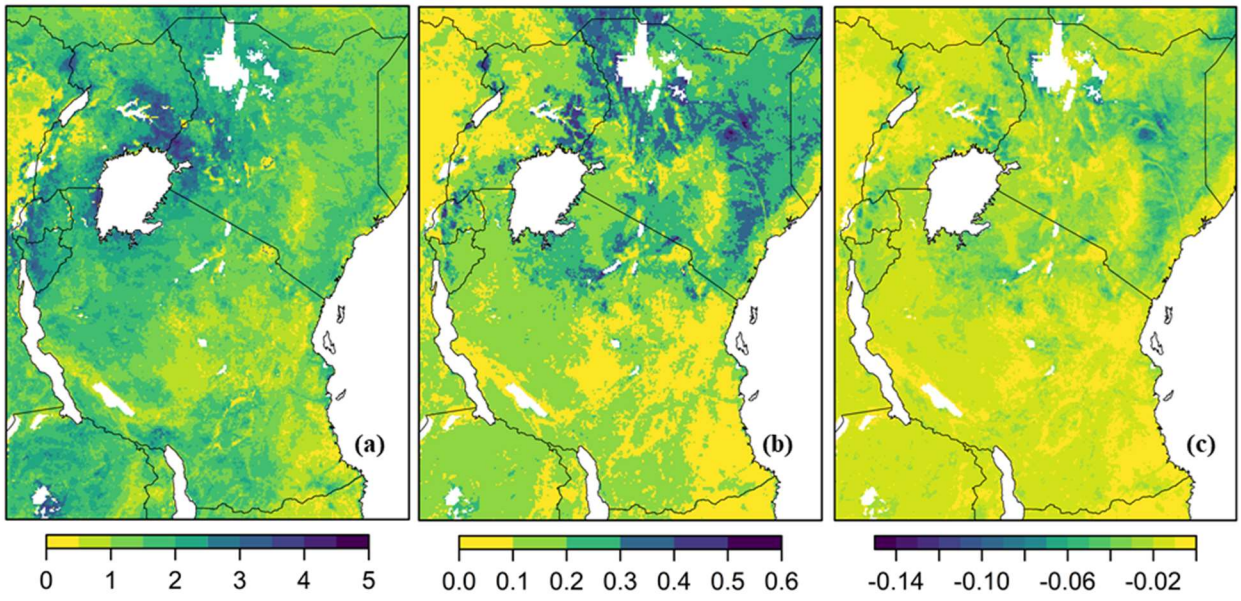

Figure 5-1: Spatial patterns of the changes in mean annual LAI (a), FVC (b) and albedo (c) due to the simulated land cover change.

5.4.1 Simulated land cover changes

Across the study area, LAI, FVC and albedo showed major seasonal variations. The area-averaged annual and seasonal changes in LAI, FVC and albedo are shown in Table 5-1. The annual mean LAI and FVC increased by 1.5 m^2m^{-2} and 0.16, respectively, while the albedo in land cover change

simulation is lower by 0.02. The mean LAI (FVC) in March-May and October-December seasons increased by 1.8 m^2m^{-2} (0.17) and 1.5 m^2m^{-2} (0.17) respectively (Table 5-1). Consequently, the surface albedo during these seasons decreased by 0.022 and 0.021 respectively (Table 5-1). The spatial patterns of annual changes in LAI, FVC and albedo between the present-day and land cover change simulations are shown in Figure 5-1. Major changes in the vegetation parameters were exhibited in areas with high bare area fractions as well as areas with short vegetation including grass, crops and shrubs as the main land cover types such as North eastern parts of Kenya, northern Tanzania and the Lake Victoria basin areas. Seasonally, strong spatial variations are shown in the LAI and FVC differences during the MAM and OND rain seasons (Figure A. 2 - Figure A. 4). Minimal albedo changes were exhibited across the seasons. During the JJAS season, which is the main dry season in most parts of the region, key vegetation changes were simulated in areas extending from northwestern Uganda through north of Lake Victoria into western Kenya. This area is particularly characterized by savanna and cropland cover types in the control simulation while in the LUCC simulation they are mainly covered by wooded savanna and crop/natural vegetation mosaics hence the strong increase in LAI and FVC.

5.4.2 Effects of land cover change

The changes in evapotranspiration, latent heat, sensible heat, ground heat, land surface temperature and vegetation canopy temperature fluxes averaged across the study area are also shown in Table 5-1. The simulated land cover changes showed statistically significant effects on all of the annual average water and energy fluxes shown in Table 5-1. The simulated increase in annual evapotranspiration (1.6 mm/month) is mainly attributed to an increase in vegetation transpiration (3.9 mm/month) and canopy evaporation (2.6 mm/month) and a corresponding decrease in soil evaporation (-4.9 mm/month). While the mean annual ground heat flux shows a decrease (by 0.19 Wm^{-2}) due to increased tree cover, the mean annual latent and sensible heat increased by1.5 Wm^{-2} and 9.7 Wm^{-2}, respectively. On the other hand, simulated annual mean canopy temperature decreased by 1.9 °C while land surface temperature decreased by 1.0 °C. The seasonal responses are also significant across all the water and energy fluxes. Latent heat represents the heat linked to physical evaporation (i.e., from soil and canopy surfaces) and transpiration through the stoma. Therefore, evapotranspiration acts a key link between the land surface water and energy balances.

Table 5-1: Differences in region-averaged water and energy balance fluxes between the control and the LUCC simulations for the annual, January-February, March-May, June-September and October-December periods. The changes in bold are statistically significant (t-test, $p < 0.05$)

Variable (units)	Annual	JF	MAM	JJAS	OND
LAI (m^2/m^2)	**1.5**	**1.7**	**1.8**	**1.3**	**1.5**
FVC (fraction)	**0.16**	**0.16**	**0.17**	**0.15**	**0.17**
Albedo (fraction)	**-0.02**	**-0.020**	**-0.022**	**-0.018**	**-0.021**
Total ET (mm/month)	**1.6**	**2.1**	**1.9**	**0.8**	**2.0**
Canopy Evap (mm/month)	**2.6**	**3.7**	**3.4**	**1.1**	**3.24**
Transpiration (mm/day)	**3.9**	**4.4**	**5.2**	**2.0**	**4.6**
Bare Evap (mm/day)	**-4.9**	**-5.9**	**-6.7**	**-2.3**	**-5.9**
Latent Heat (W/m^2)	**1.5**	**2.1**	**1.8**	**0.7**	**1.8**
Sensible Heat (W/m^2)	**9.7**	**10.0**	**8.9**	**10.4**	**9.5**
Ground Heat (W/m^2)	**-0.19**	**-0.24**	**-0.20**	**-0.17**	**-0.18**
LST (°C)	**-1.0**	**-1.1**	**-0.8**	**-1.1**	**-1.0**
Canopy Temperature (°C)	**-1.9**	**-2.0**	**-1.6**	**-2.1**	**-1.8**

It is noteworthy from Table 5-1 that the key vegetation changes were simulated in October- May period which coincides with the main rain seasons in most parts of the region. However, main changes between the simulations are expected where the significant changes in land cover properties occur. Thus, the regional average results presented in Table 5-1 may obscure key spatial variations in the simulated surface fluxes in the region. The subsequent sections focus on effects on surface water and energy fluxes during the seasons and discuss the corresponding mechanism of land cover change impacts. The multiyear mean as well as seasonal changes in total evapotranspiration and its various components was considered as an indication of the potential effects of tree cover increase on water balance in the region. As discussed in the previous chapter, the control simulation reproduced the MODIS evapotranspiration data effectively as indicated by consistency in the spatial and temporal patterns of the simulated ET. On the hand, effects of land cover change on energy balance were assessed based on changes in simulated latent heat, sensible heat, and land surface temperature and vegetation canopy temperature.

5.4.2.1 Effects on evapotranspiration

In order to evaluate the effects of land cover change on the water balance, we distinctly examined the three components of ET simulated by VIC (i.e vegetation transpiration, canopy interception

evaporation and bare soil evaporation). Figure 5-2 shows the spatial patterns of annual changes in vegetation transpiration, canopy evaporation, and bare soil evaporation due to land cover change while the seasonal changes are shown in Figure A. 5 to Figure A. 8 (in the appendices). Spatially, annual changes in vegetation transpiration and bare soil evaporation showed comparable responses to land cover change. As shown in Figure 5-2, substantial changes in all ET components are simulated in the Lake Victoria basin area, which is currently mainly covered by cropland and grassland. Due to intensive land use in this area, a strong decrease in bare soil evaporation rate was simulated under increased tree cover compared to other areas. Across the seasons, increase in tree cover shows large increase in transpiration rate as well as decrease in bare soil evaporation.

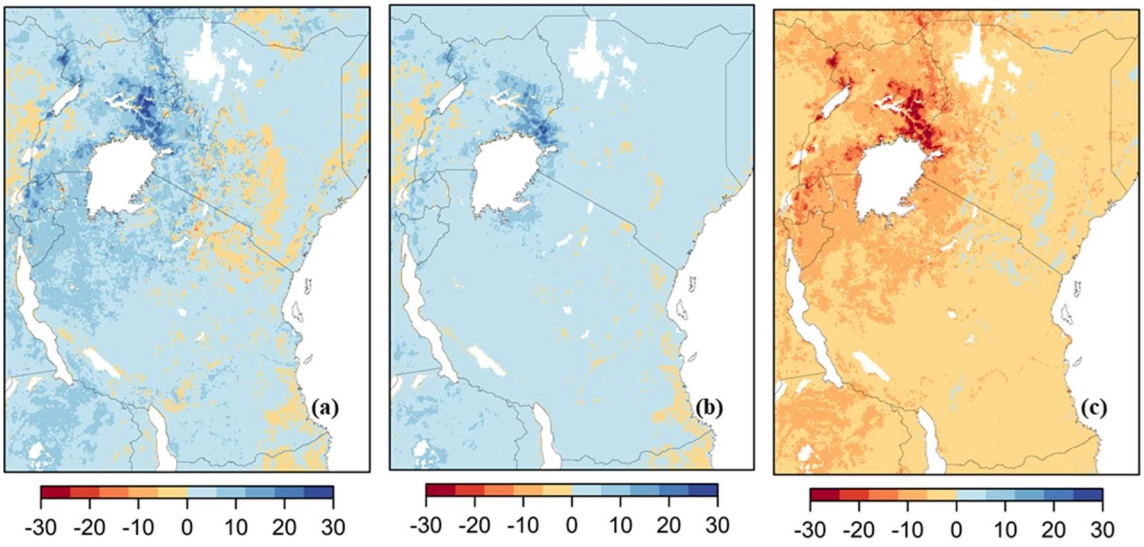

Figure 5-2: Mean annual changes (mm/month) in (a) vegetation transpiration, (b) canopy evaporation and (c)bare soil evaporation due to the simulated vegetation changes.

The mean total evapotranspiration in the MAM and OND rain seasons increased by 1.9 and 2.0 mm/month respectively (Table 5-1, Figure A. 5) which is mainly attributed to increased canopy evaporation and transpiration. During the June-September season, which is a dry season in the region, the simulated changes in ET components are minimal though statistically significant. As a result of phenological vegetation changes in the region, there is minimal difference in the prescribed LAI and FVC between the two simulations during this season (Table 5-1) which lowers the difference in simulated ET.

5.4.2.2 Effects on surface energy balance change

The changes in sensible and latent heat in this study were in the same direction in most parts of the study area, similar to the findings of other previous studies (Chen et al., 2012). Increasing tree cover increased sensible heat in most parts of the study domain across all the seasons (Table 5-1 and Figure A. 10). The strongest sensible heat changes between the control and land cover change simulations were exhibited in eastern parts of Kenya which are mainly characterized by grasslands and shrublands with high proportions of bare areas. Small areas with strong positive sensible heat changes were found northern parts of Tanzania during the four seasons. The sensitivity of the latent and sensible heat to changes in LAI is shown in Figure 5-3c-d as a function of mean annual precipitation and temperature. In these variables, high sensitivity is shown in areas with high mean temperature and low mean annual precipitation. These areas are particularly arid and semi-arid and key hotspots of vegetation degradation and intensive human activities leading to a decreasing trend in vegetation cover (Pricope et al., 2013). Thus, increasing tree cover in these areas will significantly increase the turbulent heat fluxes and thus contribute to a strong cooling effect.

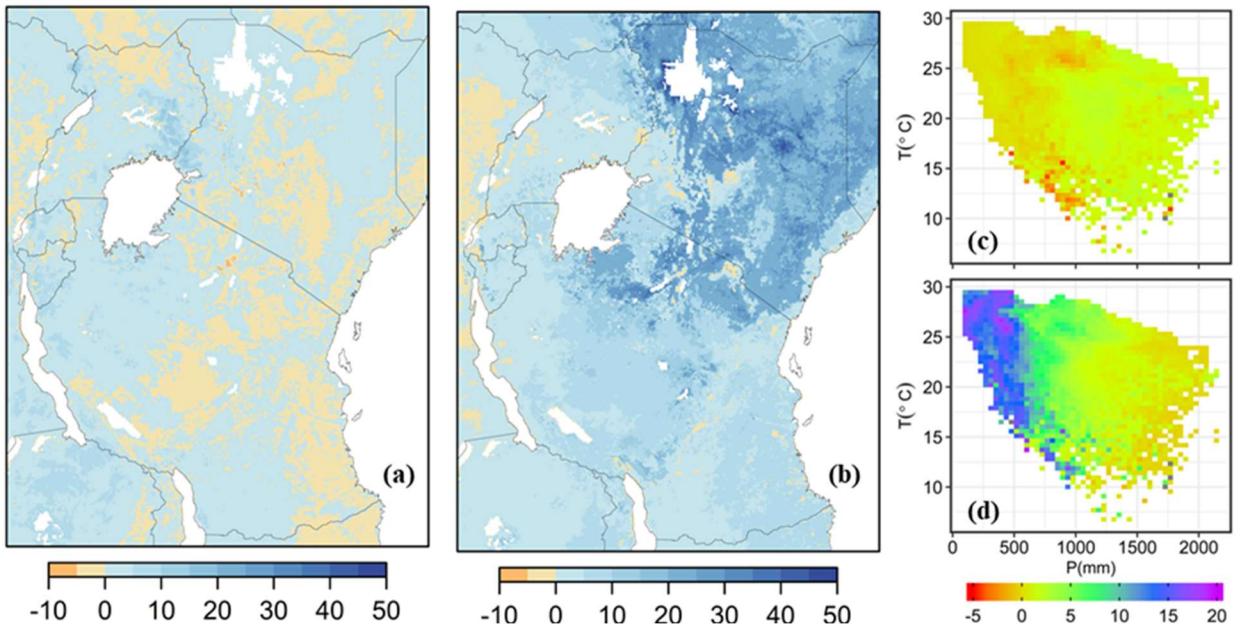

Figure 5-3: Mean annual changes (Wm^{-2}) in latent heat (a) and sensible heat (b) due to vegetation changes. The sensitivity of the latent heat and sensible heat changes to LAI changes binned as a function of climatological mean Precipitation (mm) and Temperature (°C) across the study region are shown in (c-d) in terms of ΔLE/ΔLAI and ΔH/ΔLAI, respectively.

Land surface temperature significantly decreased by 0.8°C and 1.0°C in MAM and OND over the study region (Table 5-1 and Figure A. 11). The decrease in vegetation canopy temperature is even greater during these seasons at 1.6°C and 1.8°C. The cooling effect of increased tree cover over the study region can be explained by the evapotranspiration, albedo and surface roughness mechanisms. The decrease in albedo due to increased LAI and FVC is expected to lower the proportion of surface upward shortwave flux thus warming the surface. However, the increase in total evapotranspiration leads to increased turbulent heat fluxes (by 1.5 Wm^{-2} for mean annual latent heat and 9.7 Wm^{-2} for mean annual sensible heat) at the surface leading to a net cooling effect. However, the intricate interplay between these mechanisms in east Africa still needs further study particularly based on fully coupled land surface and atmosphere models. The sensitivity of the land surface and canopy temperature to LAI change across different climatological gradients is particularly similar to the sensitivity of sensible and latent heat, respectively (Figure 5-3c-d and Figure 5-4c-d).

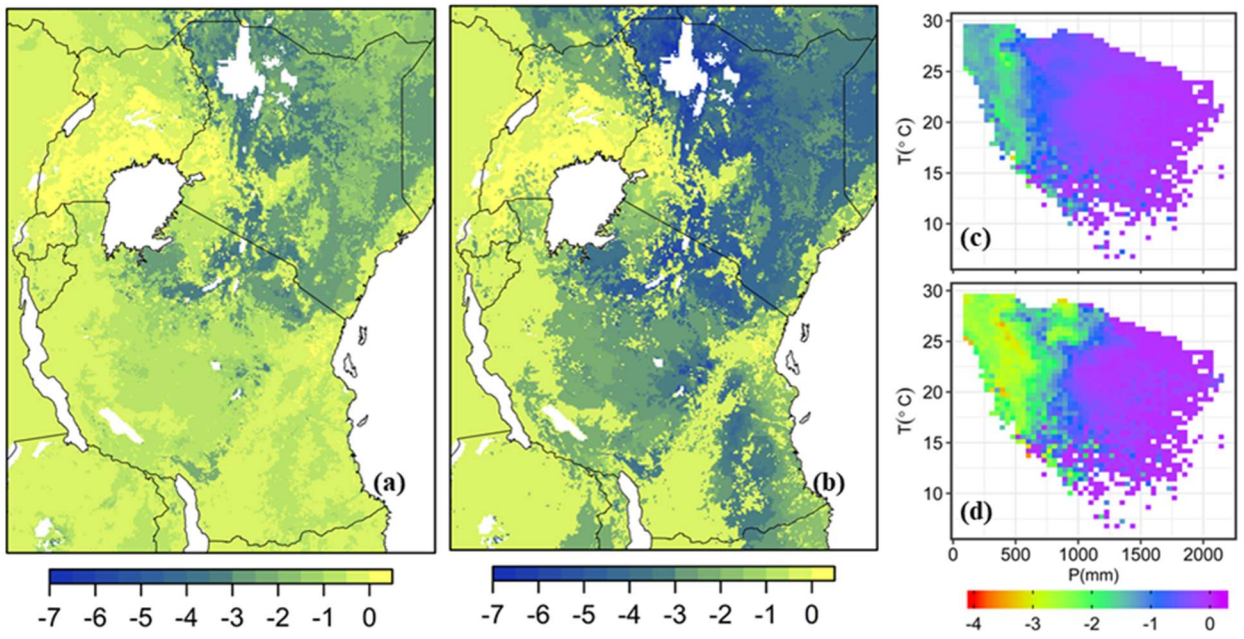

Figure 5-4: Mean annual changes (°C) in land surface temperature (a) and vegetation canopy temperature (b) due to vegetation changes. The sensitivity of the land surface and canopy temperature changes to LAI binned as a function of climatological mean Precipitation (mm) and Temperature (°C) across the study region are shown in (c-d) in terms of ΔLST/ΔLAI and ΔVEGT/ΔLAI, respectively.

Although our analysis focused on the mean surface and canopy temperature, the changes in minimum and maximum temperature are expected to show contrasting dynamics. The variations in LST and canopy temperature response to transitions across different land cover types is indicative of the different biophysical characteristics associated with the different cover types. For instance, open land cover types (i.e grassland, cropland, open shrubland and savanna) have less biophysical control on maximum LST due to their structure and surface roughness. Thus, increasing tree cover in this land cover types is accompanied by considerable decrease in maximum surface and canopy temperatures. On the other hand, increased tree cover leads to reduced albedo which is expected to cause a steady increase in minimum surface and canopy temperature.

5.5 Discussion

The terrestrial biosphere represents a vast and dynamic part of the Earth system which is presently undergoing widespread and significant changes due to human factors such as climate and land use change (Bondeau et al., 2007; Müller et al., 2006; Weber et al., 2009). The negative impacts of these factors present a serious risk on the key functions of the biosphere including the provisioning, regulating services such as local cooling, the terrestrial carbon sink, floral and faunal biodiversity, as well as accessible fresh water among others. On the other hand, multiple intervention measures have been formulated and implemented through various national, regional and global calls for action across the globe and particularly in the Africa continent. However, there is need for better understanding and modelling of current and future dynamics of the terrestrial biosphere. One of the major concerns East Africa is enhanced land cover changes mainly linked to expansion of croplands, overgrazing and climate induced vegetation mortality (Pricope et al., 2013). On the other hand, afforestation and/or reforestation have been widely encouraged as key strategies to address declining sustainability of the ecosystems as well as for climate change adaptation and mitigation in the region. The effects of these changes on the local climate, mainly through the accompanying biophysical changes such as albedo and ET, should be evaluated realistically to determine the extent to which they counteract or enforce the effect of greenhouse gases. In contrast to the effect of atmospheric greenhouse gases, the local climate sensitivity to land cover changes vary depending on the location, extent and type of land cover conversion (Anderson et al., 2011;

Devaraju et al., 2015; Duveiller et al., 2018c; Forzieri et al., 2018; Münch et al., 2019; Zhao and Jackson, 2014).

This study aimed to present an assessment of the potential impacts of land cover change on surface water and energy balance in East Africa based on VIC model through application of dynamic vegetation model (LPJ-mL) and a land surface model (VIC) at a 0.05° x 0.05° spatial resolution. The study therefore represents an improvement over the previous simulation studies in region as it resolves patterns of vegetation dynamics that may not well represented at coarser spatial resolutions. In addition, hypothetical land cover changes in region are represented through a hybrid diagnostic-dynamic vegetation approach which allows for growth and mortality of vegetation to vary over time based on a maximum projected cover per land cover type. As a result, the study was been able to provide a complete accounting of changes in surface properties based on an approach that is consistent with the simulation of biome shifts from dominantly herbaceous cover to increased tree cover.

5.5.1 Simulation of vegetation dynamics

The application of vegetation growth models in assessment of land cover change projections presents new possibilities for the evaluation of surface fluxes under a more broadly inclusive range of environmental changes compared to use static land cover maps to represent land cover change scenarios (Gerten et al., 2004). The simulated effects of increased tree cover show generally increase in LAI, FVC and decrease in albedo. However, the response of these variables to changes in tree cover is non-linear due to variations in vegetation response to temperature and water availability as well as the stochastic processes in the model such as vegetation establishment and mortality. Although different dynamic vegetation models are expected to show a generally similar results to LPJ-mL due to the common photosynthetic physiology, these models differ in many aspects such as fire-vegetation interactions, carbon allocation and growth, nitrogen cycling constraints, as well as vegetation responses to temperature and water availability (Sitch et al., 2008). These differences in model structures may influence the simulated vegetation composition and carbon storage. These uncertainties can be addressed by exploiting a range of models to simulate an ensemble of potential impacts of tree cover changes on vegetation properties (Weber et al., 2009). In addition, there is need for further analysis of vegetation sensitivity to CO_2

fertilization in the region. Nevertheless, this does not invalidate the general inference that increased tree cover is likely to contribute to changes in the surface water and energy balance in the region.

5.5.2 Impacts of tree cover change on water and energy flux

Natural and human-caused changes in land cover/use are a major influence of local climatic conditions through multiple mechanisms including changes in surface albedo and evapotranspiration. In this study, our analysis provides a critical perspective in the understanding of regional effects of land cover changes on local water and energy balance. Our results correspond with findings in earlier modeling and empirical studies on the effects of land cover type transitions on surface water and energy fluxes. The impacts of land cover changes on surface fluxes were particularly attributed to changes on biophysical properties such as surface albedo, evaporative capacity and surface roughness (Davin and de Noblet-Ducoudre, 2010). Despite the warming effect of decrease in albedo due to increased tree cover, the increase in total evaporation led to net cooling effect across the region. This cooling effect from increased tree cover is crucial as it could further reduce tree mortality induced by high temperatures and water stress. Moreover, multiple previous studies have noted that air temperature trends are closely related to average LST trends thus the impacts of land cover change on average LST and canopy temperature can be used to infer the potential effects on air temperature (Alkama and Cescatti, 2016; Fall et al., 2010; Li et al., 2016). However, the impact on LST has been shown to be higher than on air temperature (Alkama and Cescatti, 2016) thus more analysis is required to expound on the connection between LST and air temperature changes due to land cover change in East Africa. Nevertheless, the full extent of local influence of these mechanisms, particularly in arid areas such as in East Africa remains largely undetermined. As noted by Anderson et al. (2011), consideration of the biophysical effects of land cover changes is vital in development of climate policies as it helps to effectively estimate the climate benefits of forestry projects thus providing actual value of such projects. On the other hand, there is lack of consensus on the quantification of biophysical effects of land cover changes in comparison to the carbon sequestration impacts at various temporal and spatial scales. In addition, there is need for further evaluation of the multiple interactions and forcing from land cover changes both locally and through atmospheric teleconnections.

5.6 Conclusions

In this study, we analyze the impacts of increased tree cover on water and energy balance in East Africa. The approach adopted in the study provides a necessary assessment of the potential local impacts of afforestation and/or reforestation on land surface fluxes. Evaluation of potential impacts underscores spatio-temporal non-uniformity of land cover changes and therefore helps to better predict impacts of changes that have not yet occurred. The results of this study illuminate the need for use of more representative land cover scenarios in planning of forestry and agricultural development as well as assessment of the impacts of the subsequent vegetation changes. The use of a land surface model in simulation of surface fluxes allowed comparison of effects of forests and other cover types that are close in distance and that experience similar climatic conditions. Our findings are particularly useful in the planning and management of forest cover in the region which is continually threatened by a growing intensity of human activities. Through our results, we confirm the need for more concerted afforestation efforts in the region and provide a better understanding of the local impacts of these efforts. While our modelling approach can be useful in land surface water and energy balance studies, we acknowledge that the present study has some limitations. First the changes in the water and energy fluxes were based on prescribed non-interactive climatic forcing. Sensitivity of these fluxes to the climatic feedbacks can have substantial impact on their variance both in short and long-term. Second, the uncertainties in the model configuration particularly parameterization of the water and energy balance can have a significant effect on the simulated changes in these variables. Nevertheless, our results underscore the need for consideration of not only the carbon-related effects of land cover changes but also the biophysical effects which is gap in the most of the assessments of the climatic benefits of forestry activities in the region.

Chapter 6: General Discussion and Conclusions

6.1 General Discussion

This study focuses on assessment of land cover change impacts on water and energy balance in East Africa. To address the intricacy of the study topic, information from multiple sources, including climate data, remote sensing data, and a land surface model, was used. The first part of the thesis (Chapter 1 and 2) provides a general background information on the study and area of focus. The second part (chapter 3) assesses the vegetation dynamics in East Africa based on remote sensing data, thus providing input for the third part (Chapter 4 and 5) which explores the influence of parameterization of land surface dynamics on the simulation of regional water and energy fluxes as well as the potential effects of land cover change on surface water and energy balance from a modeling and observation perspective. The study process was guided by three research questions and the conclusions for each question are summarized in the following sections.

- *What are spatial and temporal patterns and trends in observed vegetation dynamics in East Africa, and how do they relate to climate anomalies?*

Observed LAI data over the 1982 -2011 period revealed a significant increase in about 25% of the region while significant decreasing trend in LAI was recorded in 4% of the region. However, analysis of the temporal consistency in the LAI trends showed that non-monotonic vegetation changes were widespread in the region, with about 78.3% of the study area showing statistically significant ($p<0.05$) abrupt changes in the general long-term trends during the study period. Widespread decreasing LAI trend found in Tanzania during the OND season coincides with Vrieling et al. (2013) finding of a decrease in the length of growing season. The vegetation-climate regression analysis provided a view of the interactions between vegetation and climate. The annual average water balance emerged as the key factor determining the level of vegetation resistance to drought anomalies compared to the human footprint. A high sensitivity of vegetation resistance coefficient across the region coincides with intermediate water balance areas. This relates with findings of Huxman et al. (2004) based on the correlation analysis of net primary production and annual precipitation data at sites sampled from major global biomes. However, due to the coarse spatial resolution of the data, the obtained vegetation response is comprised of the response by the dominant vegetation type as well contamination by spurious signal attributed to other vegetation

types in the pixels. The sensitivity of vegetation in drier areas has been linked to vegetation drought resistance strategies such as low specific leaf area, high root–shoot ratio and low stomatal conductance (Paruelo et al., 1999). While in wetter areas, the vegetation is also well-adapted to the temporary seasonal constraint in water availability (Camberlin et al., 2007). There is need for further analysis of the multifaceted connection between vegetation production patterns to human and climatic drivers in the region to account for the individual and coupled effects of both natural and anthropogenic determinants of terrestrial ecosystem functioning. With the availability of high-resolution remote sensing data such as Sentinel 1 and 2 products, such analysis can be carried focusing on the hotspot areas identified from the medium resolution datasets.

- *Can we simulate the current water and energy balance in East Africa better using an improved parameterization of spatial and temporal land surface heterogeneity?*

To study the effects of dynamic vegetation parameters on water and energy balance in East Africa, an improved parameterization of the vegetation phenology was developed and used as vegetation forcing in VIC model. Using the long-term vegetation parameter values, the model was applied across the region of study and the results were compared to remote sensing data. The simulation reproduced reasonable values for seasonal and interannual latent, sensible and ground heat fluxes as well as evapotranspiration. The impacts of interannual vegetation variability on the simulated water and energy fluxes over the region clearly varied from one subregion to another and from one land cover type to another. This is consistence with the findings of previous studies (Sacardi et al., 2015) and highlights role of not only vegetation characteristics but also climatic variability on water and energy portioning. The efficient use of satellite remote sensing data in land surface modelling is influenced by not only the quality of the data but also the interoperability between the model and data (Kumar et al., 2006; Rajib et al., 2020). The interoperability between the VIC model and MODIS data was addressed in terms of compatibility of the derived datasets with the model architecture (Bohn and Vivoni, 2019). In addition, regional land information systems can provide efficient and automated assimilation of satellite products in simulation of water and energy fluxes. Based on the changes in standard deviation of evapotranspiration, sensible and ground heat, varying vegetation parameters shows larger effects on interannual and spatial variability of water and energy fluxes in the region. Across the region, the effect of improved vegetation

parameterization is mainly exhibited in 64% - 92% of the region depending on the season. On the hand, effects of vegetation variability on energy fluxes is accounted for upto 90% of variance in latent and sensible heat fluxes. During the rain seasons (March-May and October-December), the exchange processes of water and energy at the land surface are strongly controlled by vegetation properties due to high LAI and FVC. The simulated water and energy fluxes in June-September season is only slightly affected due to low LAI values which disconnects the influence of vegetation on the surface fluxes.

With observations at biweekly temporal resolution at approximately 500 m spatial resolution, the MODIS based vegetation parameters ensure a higher level of stability of simulated biophysical variables. However, the retrieval of MODIS datasets is affected by atmospheric contaminations, particularly during the peak seasons. Appropriate corrections and smoothing approaches which not only preserves the peak values but also the seasonal cycles are therefore needed for an optimal use of these datasets in land surface models. The uncertainty in the land cover data has an effect in the retrieval of the MODIS vegetation parameters. For a correct evaluation of effects of land surface heterogeneity at a regional level, it is necessary to develop a land cover map with suitable accuracy in terms of locating, classifying and decomposing land cover types into common classes used in the land surface models. Further analysis is therefore recommended to compare the variables at reference pixels with considerably homogeneous land cover characteristics at the sub-pixel level. The parameters derived in this study and evaluated with the VIC model conform with the requirements for long-term applications in assessment of regional land surface water and energy balance. In this regard, the long-term vegetation parameters partially address impacts of the land conversion issues like deforestation or fires which are rampant in East Africa (Pfeifer et al., 2012). The regional application and evaluation of VIC model using the long-term vegetation parameter values was a basis for our assessment of impacts of LULC change. We conclude that the model presents a suitable framework for regional studies on impacts of vegetation dynamics on surface water and energy fluxes. Finally, this research could be extended by developing a new module in VIC model for dynamic vegetation growth, which would allow us to dynamically model the vegetation dynamics and feedbacks to climate anomalies in the region.

- *What are the potential effects of land cover change on the water and energy balance in East Africa?*

In this study, effects of land cover change were assessed based on the simulated changes in Leaf Area Index, fractional vegetation cover and albedo due to increased tree cover in the study region. The simulated land cover changes showed statistically significant effects on average water and energy fluxes. This impacts were linked to changes in surface properties including albedo, leaf area index, and fraction vegetation cover, which have been previously cited as key variable determining variability of surface fluxes (Anderson et al., 2011; Li et al., 2015b). The simulated increase in annual evapotranspiration was mainly attributed to an increase in vegetation transpiration and canopy evaporation and a corresponding decrease in soil evaporation. Increased tree cover in the study area led to an increase in total evapotranspiration. Although soil evaporation decreases with increased tree cover, its decline is less compared to the combined increase of canopy transpiration and evaporation of canopy-intercepted water (Table 5-1). While the mean annual ground heat flux showed a decrease due to increased tree cover, the mean annual latent and sensible heat increased by1.5 Wm^{-2} and 9.7 Wm^{-2}, respectively. The surface albedo decreases with increased tree cover, and there is a warming effect due to increase in net radiation, however, the effects of increased evapotranspiration surpasses the effect of albedo leading to a net cooling effect. The simulated annual mean canopy temperature decreased by 1.9 °C while land surface temperature decreased by 1.0 °C due to increased tree cover. The seasonal responses are also significant across all the water and energy fluxes. Latent heat represents the heat linked to physical evaporation (i.e., from soil and canopy surfaces) and transpiration through the stoma. Therefore, evapotranspiration acts a key link between the land surface water and energy balances. Our results provide a critical perspective in the understanding of regional effects of afforestation, reforestation and enhance forest management practices in climate change adaptation and mitigation in east Africa. Loss of tree cover due to logging, wild fires as well as drought-induced tree mortality is a main concern in East Africa. The warming effect from loss of tree cover compounded by high temperatures and water stress could lead to further deforestation in the region. In arid areas such as in East Africa, increased tree cover showed strong cooling effect.

6.2 Conclusions

This study focused on the assessment of vegetation dynamics and their impacts on water and energy fluxes in East Africa. The approach adopted entailed integration of climate observations, and remote sensing data on vegetation dynamics using a land surface model. While the surface process at a global scale play a key role in shaping regional processes, this study only addressed specifically the east Africa region. In addition, while impacts of land surface properties stem from both biophysical and geochemical processes, we only focused on the biophysical impacts of vegetation changes. Vegetation dynamics have local impacts but can also create teleconnections affecting land surface-atmosphere interactions in other areas. The findings presented in this study only showed the per-pixel impacts of variability in vegetation. However, we acknowledge the potential for advective effects of vegetation variability on surface water and energy fluxes in the region. The models adopted in this study do not currently address lateral transfer of water and energy flux between adjacent pixels. Therefore, although these models can be readily applied at fine spatial and temporal resolutions, it is crucial to address lateral transfers in future applications. However, as noted by Winckler et al. (2017a), at high spatial resolutions local effects are expected to dominate the overall biophysical impacts of land cover changes. Although the GIMMS LAI3g and MODIS LAI datasets used in this study have been widely used (Jiang et al., 2017; Pfeifer et al., 2014; Wu et al., 2016), the biases and uncertainties in the data in East Africa were not explored thus corresponding land surface processes could be biased. In addition, our simulations did not account for teleconnections and climate-vegetation feedbacks and this could be better studied through coupled application of VIC, dynamic vegetation model and a climate model. Despite the ongoing improvements in land surface modelling, simulation of impacts of changes in land surface in East Africa still require improved characterization of land surface heterogeneity at resolutions higher than current land cover maps and vegetation indices datasets. Integration of high-resolution remote sensing data and field observations may therefore be required to address the spatial and temporal uncertainties for better understanding of the biophysical mechanisms under different land cover properties across the region.

REFERENCES

Abera, T. A., Heiskanen, J., Pellikka, P., Rautiainen, M. and Maeda, E. E.: Clarifying the role of radiative mechanisms in the spatio-temporal changes of land surface temperature across the Horn of Africa, Remote Sens. Environ., 221, 210–224, doi:10.1016/j.rse.2018.11.024, 2019.

AghaKouchak, A., Farahmand, A., Melton, F. S., Teixeira, J., Anderson, M. C., Wardlow, B. D. and Hain, C. R.: Remote sensing of drought: progress, challenges and opportunities, Rev. Geophys., 53, 452–480, doi:10.1002/2014RG000456, 2015.

Albertson, J. D., Kustas, P. and Scanlon, M.: Large-eddy simulation over heterogeneous terrain with remotely sensed land surface conditions and LES (in the absence of free parameters) yields regionally averaged land surface height in the atmospheric surface atmosphere is shown to be scale-dependent, Water Resour. Res., 37(7), 1939–1953, 2001.

Alkama, R. and Cescatti, A.: Biophysical climate impacts of recent changes in global forest cover, Science, 351(6273), 600–604, 2016.

Anav, A., Ruti, P. M., Artale, V. and Valentini, R.: Modelling the effects of land-cover changes on surface climate in the Mediterranean region, Clim. Res., 41(2), 91–104, doi:10.3354/cr00841, 2010.

Anderson, R. G., Canadell, J. G., Randerson, J. T., Jackson, R. B., Hungate, B. A., Baldocchi, D. D., Ban-Weiss, G. A., Bonan, G. B., Caldeira, K., Cao, L., Diffenbaugh, N. S., Gurney, K. R., Kueppers, L. M., Law, B. E., Luyssaert, S. and O'Halloran, T. L.: Biophysical considerations in forestry for climate protection, Front. Ecol. Environ., 9(3), 174–182, doi:10.1890/090179, 2011.

Arola, A. and Lettenmaier, D. P.: Effects of subgrid spatial heterogeneity on GCM-scale land surface energy and moisture fluxes, J. Clim., 9(6), 1339–1349, doi:https://doi.org/10.1175/1520-0442(1996)009<1339:EOSSHO>2.0.CO;2, 1996.

Arora, V.: Modeling vegetation as a dynamic component in soil-vegetation-atmosphere transfer schemes and hydrological models, Rev. Geophys., 40(2), 1–26, doi:10.1029/2001RG000103, 2002.

Avissar, R.: A statistical-dynamical approach to parameterize subgrid-scale land-surface heterogeneity in climate models, Surv. Geophys., 12(1), 155–178, doi:10.1007/BF01903417, 1991.

Avissar, R.: Conceptual Aspects of a Statistical-Dynamical Approach to Represent Landscape Subgrid-Scale Heterogeneities in Atmospheric Models, J. Geophys. Res., 97(D3), 2729–2742, 1992.

Ayana, E. K., Ceccato, P., Fisher, J. R. B. and DeFries, R.: Examining the relationship between environmental factors and conflict in pastoralist areas of East Africa, Sci. Total Environ., 557–558, 601–611, doi:10.1016/j.scitotenv.2016.03.102, 2016.

Ayehu, G. T., Tadesse, T., Gessesse, B. and Dinku, T.: Validation of new satellite rainfall products over the Upper Blue Nile Basin, Ethiopia, Atmos. Meas. Tech., 11(4), 1921–1936, doi:10.5194/amt-11-1921-2018, 2018.

Bao, G., Qin, Z., Bao, Y., Zhou, Y., Li, W. and Sanjjav, A.: NDVI-Based Long-Term Vegetation Dynamics and Its Response to Climatic Change in the Mongolian Plateau, Remote Sens., 6(9), 8337–8358, doi:10.3390/rs6098337, 2014.

Berry, Z. C., Gotsch, S. G., Holwerda, F., Muñoz-Villers, L. E. and Asbjornsen, H.: Slope position influences vegetation-atmosphere interactions in a tropical montane cloud forest, Agric. For. Meteorol., 221, 207–218, doi:10.1016/j.agrformet.2016.02.012, 2016.

Bobée, C., Ottlé, C., Maignan, F., de Noblet-Ducoudré, N., Maugis, P., Lézine, a.-M. and Ndiaye, M.: Analysis of vegetation seasonality in Sahelian environments using MODIS LAI, in association with land cover and rainfall, J. Arid Environ., 84, 38–50, doi:10.1016/j.jaridenv.2012.03.005, 2012.

Bohn, T. J. and Vivoni, E. R.: Process-based characterization of evapotranspiration sources over the North American monsoon region, Water Resour. Res., 52, 358–384, doi:10.1002/2015WR017200.A, 2016.

Bohn, T. J. and Vivoni, E. R.: MOD-LSP, MODIS-based parameters for hydrologic modeling of North American land cover change, Sci. Data, 6(144), 1–13, doi:10.1038/s41597-019-0150-2, 2019.

Bonan, G. B.: Forests and climate change: forcings, feedbacks, and the climate benefits of forests., Science, 320(5882), 1444–1449, doi:10.1126/science.1155121, 2008.

Bondeau, A., Smith, P. C., Zaehle, S., Schaphoff, S., Lucht, W., Cramer, W., Gerten, D., Lotze-campen, H., Müller, C., Reichstein, M. and Smith, B.: Modelling the role of agriculture for the 20th century global terrestrial carbon balance, Glob. Chang. Biol., 13(3), 679–706, doi:10.1111/j.1365-2486.2006.01305.x, 2007.

Boschetti, M., Nutini, F., Brivio, P. A., Bartholomé, E., Stroppiana, D. and Hoscilo, A.: Identification of environmental anomaly hot spots in West Africa from time series of NDVI and rainfall, ISPRS J. Photogramm. Remote Sens., 78, 26–40, doi:10.1016/j.isprsjprs.2013.01.003, 2013.

Bright, R. M., Zhao, K., Jackson, R. B. and Cherubini, F.: Quantifying surface albedo and other direct biogeophysical climate forcings of forestry activities, Glob. Chang. Biol., 21(9), 3246–3266, doi:10.1111/gcb.12951, 2015.

Bright, R. M., Davin, E., O'Halloran, T., Pongratz, J., Zhao, K. and Cescatti, A.: Local temperature response to land cover and management change driven by non-radiative processes, Nat. Clim. Chang., 7(4), 296–302, doi:10.1038/nclimate3250, 2017.

Brink, A. B., Bodart, C., Brodsky, L., Defourney, P., Ernst, C., Donney, F., Lupi, A. and Tuckova,

K.: Anthropogenic pressure in East Africa-Monitoring 20 years of land cover changes by means of medium resolution satellite data, Int. J. Appl. Earth Obs. Geoinf., 28(1), 60–69, doi:10.1016/j.jag.2013.11.006, 2014.

Bronstert, A., Carrera, J., Kabat, P. and Lütkemeier, S., Eds.: Coupled Models for the Hydrological Cycle: Integrating Atmosphere, Biosphere and Pedosphere, Springer-Verlag, Berlin., 2005.

Brunsell, N., Mechem, D. B. and Anderson, M. C.: Surface heterogeneity impacts on boundary layer dynamics via energy balance partitioning, Atmos. Chem. Phys., 11(7), 3403–3416, doi:10.5194/acp-11-3403-2011, 2011.

Burakowski, E., Tawfik, A., Ouimette, A., Lepine, L., Novick, K., Ollinger, S., Zarzycki, C. and Bonan, G.: The role of surface roughness, albedo, and Bowen ratio on ecosystem energy balance in the Eastern United States, Agric. For. Meteorol., 249, 367–376, doi:10.1016/j.agrformet.2017.11.030, 2018.

Camberlin, P., Martiny, N., Philippon, N. and Richard, Y.: Determinants of the interannual relationships between remote sensed photosynthetic activity and rainfall in tropical Africa, Remote Sens. Environ., 106(2), 199–216, doi:10.1016/j.rse.2006.08.009, 2007.

Ceccherini, G., Ameztoy, I., Hernández, C. P. R. and Moreno, C. C.: High-resolution precipitation datasets in South America and West Africa based on satellite-derived rainfall, enhanced vegetation index and digital elevation model, Remote Sens., 7(5), 6454–6488, doi:10.3390/rs70506454, 2015.

Chaney, N. W., Sheffield, J., Villarini, G. and Wood, E. F.: Development of a high-resolution gridded daily meteorological dataset over sub-Saharan Africa: Spatial analysis of trends in climate extremes, J. Clim., 27(15), 5815–5835, doi:10.1175/JCLI-D-13-00423.1, 2014.

Chen, G. S., Notaro, M., Liu, Z. and Liu, Y.: Simulated local and remote biophysical effects of afforestation over the Southeast United States in boreal summer, J. Clim., 25(13), 4511–4522, doi:10.1175/JCLI-D-11-00317.1, 2012.

Chen, J., Jönsson, P., Tamura, M., Gu, Z., Matsushita, B. and Eklundh, L.: A simple method for reconstructing a high-quality NDVI time-series data set based on the Savitzky-Golay filter, Remote Sens. Environ., 91(3–4), 332–344, doi:10.1016/j.rse.2004.03.014, 2004.

Claussen, M.: Estimation of areally-averaged surface fluxes, Boundary-Layer Meteorol., 54(4), 387–410, doi:10.1007/BF00118868, 1991.

Cook, B. I. and Pau, S.: A global assessment of long-term greening and browning trends in pasture lands using the GIMMS LAI3g dataset, Remote Sens., 5(5), 2492–2512, doi:10.3390/rs5052492, 2013.

Crow, W. T., Wood, E. F. and Pan, M.: Multiobjective calibration of land surface model evapotranspiration predictions using streamflow observations and spaceborne surface radiometric temperature retrievals, J. Geophys. Res., 108(D23), 4725, doi:10.1029/2002JD003292, 2003.

Cuo, L., Zhang, Y., Piao, S. and Gao, Y.: Simulated annual changes in plant functional types and their responses to climate change on the northern Tibetan Plateau, Biogeosciences, 13(12), 3533–3548, doi:10.5194/bg-13-3533-2016, 2016.

Davin, E. L. and de Noblet-Ducoudre, N.: Climatic impact of global-scale Deforestation: Radiative versus nonradiative processes, J. Clim., 23(1), 97–112, doi:10.1175/2009JCLI3102.1, 2010.

Delire, C., de Noblet-Ducoudré, N., Sima, A. and Gouirand, I.: Vegetation dynamics enhancing long-term climate variability confirmed by two models, J. Clim., 24(9), 2238–2257, doi:10.1175/2010JCLI3664.1, 2011.

Dembélé, M. and Zwart, S. J.: Evaluation and comparison of satellite-based rainfall products in Burkina Faso, West Africa, Int. J. Remote Sens., 37(17), 3995–4014, doi:10.1080/01431161.2016.1207258, 2016.

Deng, X., Shi, Q., Zhang, Q., Shi, C. and Yin, F.: Impacts of land use and land cover changes on surface energy and water balance in the Heihe River Basin of China , 2000-2010, J. Phys. Chem. Earth, 2000–2010, doi:10.1016/j.pce.2015.01.002, 2015.

Devaraju, N., Bala, G. and Nemani, R.: Modelling the influence of land-use changes on biophysical and biochemical interactions at regional and global scales, Plant, Cell Environ., 38(9), 1931–1946, doi:10.1111/pce.12488, 2015.

Donohue, R. J., Roderick, M. L. and McVicar, T. R.: On the importance of including vegetation dynamics in Budyko's hydrological model, Hydrol. Earth Syst. Sci. Discuss., 3(4), 1517–1551, doi:10.5194/hessd-3-1517-2006, 2006.

Droogers, P. and Allen, R. G.: Estimating reference evapotranspiration under inaccurate data conditions, Irrig. Drain. Syst., 16, 33–45, doi:10.1023/A:1015508322413, 2002.

Duveiller, G., Hooker, J. and Cescatti, A.: A dataset mapping the potential biophysical effects of vegetation cover change, Sci. Data, 5, 1–15, doi:10.1038/sdata.2018.14, 2018a.

Duveiller, G., Forzieri, G., Robertson, E., Li, W., Georgievski, G., Lawrence, P., Wiltshire, A., Ciais, P., Pongratz, J., Sitch, S., Arneth, A. and Cescatti, A.: Biophysics and vegetation cover change: A process-based evaluation framework for confronting land surface models with satellite observations, Earth Syst. Sci. Data, 10(3), 1265–1279, doi:10.5194/essd-10-1265-2018, 2018b.

Duveiller, G., Hooker, J. and Cescatti, A.: The mark of vegetation change on Earth's surface energy balance, Nat. Commun., 9(1), doi:10.1038/s41467-017-02810-8, 2018c.

Esserya, R. L. H., Besta, M. J., Bettsa, R. A., Coxa, P. M. and Taylorb, C. M.: Explicit Representation of Subgrid Heterogeneity in a GCM Land-Surface Scheme, J. Hydrometeorol., 4, 530–545, 2003.

Fall, S., Niyogi, D., Gluhovsky, A., Pielke, R. A., Kalnay, E. and Rochon, G.: Impacts of land use land cover on temperature trends over the continental United States: Assessment using the North

American Regional Reanalysis, Int. J. Climatol., 30(13), 1980–1993, doi:10.1002/joc.1996, 2010.

Fatichi, S. and Ivanov, V. Y.: Interannual variability of evapotranspiration and vegetation productivity, Water Resour. Res., 50(4), 3275–3294, doi:10.1002/2013WR015044, 2014.

Fensholt, R. and Proud, S. R.: Evaluation of Earth Observation based global long term vegetation trends - Comparing GIMMS and MODIS global NDVI time series, Remote Sens. Environ., 119, 131–147, doi:10.1016/j.rse.2011.12.015, 2012.

Fensholt, R., Langanke, T., Rasmussen, K., Reenberg, A., Prince, S. D., Tucker, C., Scholes, R. J., Le, Q. B., Bondeau, A., Eastman, R., Epstein, H., Gaughan, A. E., Hellden, U., Mbow, C., Olsson, L., Paruelo, J., Schweitzer, C., Seaquist, J. and Wessels, K.: Greenness in semi-arid areas across the globe 1981-2007 - an Earth Observing Satellite based analysis of trends and drivers, Remote Sens. Environ., 121, 144–158, doi:10.1016/j.rse.2012.01.017, 2012.

Fensholt, R., Rasmussen, K., Kaspersen, P., Huber, S., Horion, S. and Swinnen, E.: Assessing Land Degradation/Recovery in the African Sahel from Long-Term Earth Observation Based Primary Productivity and Precipitation Relationships, Remote Sens., 5(2), 664–686, doi:10.3390/rs5020664, 2013.

Foley, J. A., Levis, S., Prentice, I. C., Pollard, D. and Thompson, S. L.: Coupling dynamic models of climate and vegetation, Glob. Chang. Biol., 4(5), 561–579, doi:10.1046/j.1365-2486.1998.00168.x, 1998.

Foley, J. A., Levis, S., Costa, M. H., Cramer, W. and Pollard, D.: Incorporating Dynamic Vegetation Cover within Global Climate Models, Ecol. Appl., 10(6), 1620–1632, 2000.

Ford, T. W. and Quiring, S. M.: Influence of MODIS-Derived Dynamic Vegetation on VIC-Simulated Soil Moisture in Oklahoma, J. Hydrometeorol., 14(2007), 1910–1921, doi:10.1175/JHM-D-13-037.1, 2013.

Forkel, M., Carvalhais, N., Schaphoff, S., Bloh, W. V., Migliavacca, M., Thurner, M. and Thonicke, K.: Identifying environmental controls on vegetation greenness phenology through model-data integration, Biogeosciences, 11(23), 7025–7050, doi:10.5194/bg-11-7025-2014, 2014.

Forkel, M., Drüke, M., Thurner, M., Dorigo, W., Schapho, S., Thonicke, K., Bloh, W. Von and Carvalhais, N.: Constraining modelled global vegetation dynamics and carbon turnover using multiple satellite observations, Sci. Rep., 9(18757), 1–12, doi:10.1038/s41598-019-55187-7, 2019.

Forzieri, G., Duveiller, G., Georgievski, G., Li, W., Robertson, E., Kautz, M., Lawrence, P., Garcia San Martin, L., Anthoni, P., Ciais, P., Pongratz, J., Sitch, S., Wiltshire, A., Arneth, A. and Cescatti, A.: Evaluating the Interplay Between Biophysical Processes and Leaf Area Changes in Land Surface Models, J. Adv. Model. Earth Syst., 10(5), 1102–1126, doi:10.1002/2018MS001284, 2018.

Franchini, M. and Pacciani, M.: Comparative analysis of several conceptual rainfall-runoff

models, J. Hydrol., 122, 161–219, 1991.

Funk, C., Peterson, P., Landsfeld, M., Pedreros, D., Verdin, J., Shukla, S., Husak, G., Rowland, J., Harrison, L., Hoell, A. and Michaelsen, J.: The climate hazards infrared precipitation with stations—a new environmental record for monitoring extremes, Sci. Data, 2, 150066, doi:10.1038/sdata.2015.66, 2015.

Gerten, D., Schaphoff, S., Haberlandt, U., Lucht, W. and Sitch, S.: Terrestrial vegetation and water balance - Hydrological evaluation of a dynamic global vegetation model, J. Hydrol., 286(1–4), 249–270, doi:10.1016/j.jhydrol.2003.09.029, 2004.

Ghilain, N., Arboleda, A., Sepulcre-Cantò, G., Batelaan, O., Ardö, J. and Gellens-Meulenberghs, F.: Improving evapotranspiration in a land surface model using biophysical variables derived from MSG/SEVIRI satellite, Hydrol. Earth Syst. Sci., 16(8), 2567–2583, doi:10.5194/hess-16-2567-2012, 2012.

Giorgi, F.: An Approach for the Representation of Surface Heterogeneity in Land Surface Models. Part I: Theoretical Framework, Mon. Weather Rev., 125(8), 1885–1899, doi:10.1175/1520-0493(1997)125<1885:AAFTRO>2.0.CO;2, 1997.

Giorgi, F. and Avissar, R.: Representation of Heterogeneity Effects in Earth System Modeling: Experience from Land Surface Modeling, Am. Geophys. Union, 35(97), 413–438, 1997.

Grace, K., Husak, G. and Bogle, S.: Estimating agricultural production in marginal and food insecure areas in Kenya using very high resolution remotely sensed imagery, Appl. Geogr., 55, 257–265, doi:10.1016/j.apgeog.2014.08.014, 2014.

Guillevic, P., Koster, R. D., Suarez, M. J., Bounoua, L., Collatz, G. J., Los, S. O. and Mahanama, S. P. P.: Influence of the Interannual Variability of Vegetation on the Surface Energy Balance — A Global Sensitivity Study, J. Hydrometeorol. AMS, 3, 617–629, doi:10.1175/1525-7541(2002)003<0617:IOTIVO>2.0.CO;2, 2002.

Guo, Y. and Shen, Y.: Quantifying water and energy budgets and the impacts of climatic and human factors in the Haihe River Basin, China: 2. Trends and implications to water resources, J. Hydrol., 527, 251–261, doi:10.1016/j.jhydrol.2015.04.071, 2015a.

Guo, Y. and Shen, Y.: Quantifying water and energy budgets and the impacts of climatic and human factors in the Haihe River Basin , China : 1 . Model and validation, J. Hydrol., 528, 206–216, doi:10.1016/j.jhydrol.2015.06.039, 2015b.

Hargreaves, G. H.: Defining and using reference evapotranspiration, J. Irrig. Drain. Eng., 120(6), 1132–1139, doi:10.1061/(ASCE)0733-9437(1994)120:6(1132), 1994.

Hastie, T. and Tibshirani, R.: Generalized Additive Models, Chapman and Hall, London., 1990.

Hawinkel, P., Thiery, W., Lhermitte, S., Swinnen, E., Verbist, B., Van Orshoven, J. and Muys, B.: Vegetation response to precipitation variability in East Africa controlled by biogeographical

factors, J. Geophys. Res. G Biogeosciences, 121(9), 2422–2444, doi:10.1002/2016JG003436, 2016.

He, F., Vavrus, S. J., Kutzbach, J. E., Ruddiman, W. F., Kaplan, J. O. and Krumhardt, K. M.: Simulating global and local surface temperature changes due to Holocene anthropogenic land cover change, Geophys. Res. Lett., 41, 623–631, doi:10.1002/2013GL058085, 2014.

Hély, C., Bremond, L., Alleaume, S., Smith, B., Sykes, M. T. and Guiot, J.: Sensitivity of African biomes to changes in the precipitation regime, Glob. Ecol. Biogeogr., 15(3), 258–270, doi:10.1111/j.1466-822X.2006.00235.x, 2006.

Hibbard, K., Janetos, A., Van Vuuren, D. P., Pongratz, J., Rose, S. K., Betts, R., Herold, M. and Feddema, J. J.: Research priorities in land use and land-cover change for the Earth system and integrated assessment modelling, Int. J. Climatol., 30(13), 2118–2128, doi:10.1002/joc.2150, 2010.

Hoscilo, A., Balzter, H., Bartholomé, E., Boschetti, M., Brivio, P. A., Brink, A., Clerici, M. and Pekel, J. F.: A conceptual model for assessing rainfall and vegetation trends in sub-Saharan Africa from satellite data, Int. J. Climatol., 35(12), 3582–3592, doi:10.1002/joc.4231, 2015.

Hu, Z., Yu, G., Zhou, Y., Sun, X., Li, Y., Shi, P., Wang, Y., Song, X., Zheng, Z., Zhang, L. and Li, S.: Partitioning of evapotranspiration and its controls in four grassland ecosystems: Application of a two-source model, Agric. For. Meteorol., 149(9), 1410–1420, doi:10.1016/j.agrformet.2009.03.014, 2009.

Huxman, T. E., Smith, M. D., Fay, P. A., Knapp, A. K., Shaw, M. R., Loik, M. E., Smith, S. D., Tissue, D. T., Zak, J. C., Weltzin, J. F., Pockman, W. T., Sala, O. E., Haddad, B. M., Harte, J., Koch, G. W., Schwinning, S., Small, E. E. and Williams, D. G.: Convergence across biomes to a common rain-use efficiency, Nature, 429(6992), 651–654, doi:10.1038/nature02561, 2004.

Ivanov, V. Y., Bras, R. L. and Vivoni, E. R.: Vegetation-hydrology dynamics in complex terrain of semiarid areas: 2. Energy-water controls of vegetation spatiotemporal dynamics and topographic niches of favorability, Water Resour. Res., 44(3), 1–20, doi:10.1029/2006WR005595, 2008.

Jacobson, A., Dhanota, J., Godfrey, J., Jacobson, H., Rossman, Z., Stanish, A., Walker, H. and Riggio, J.: A novel approach to mapping land conversion using Google Earth with an application to East Africa, Environ. Model. Softw., 72, 1–9, doi:10.1016/j.envsoft.2015.06.011, 2015.

Jarvis, A., Reuter, H. I., Nelson, A. and Guevara, E.: Hole-filled SRTM for the globe Version 4, available from the CGIAR-CSI SRTM 90m Database (http://srtm.csi.cgiar.org), 2008.

Jiang, C., Ryu, Y., Claverie, M. and Zhu, Z.: Inconsistencies of interannual variability and trends in long-term satellite leaf area index products, Glob. Chang. Biol., 23, 4133–4146, doi:10.1111/gcb.13787, 2017.

Jiapaer, G., Liang, S., Yi, Q. and Liu, J.: Vegetation dynamics and responses to recent climate

change in Xinjiang using leaf area index as an indicator, Ecol. Indic., 58, 64–76, doi:10.1016/j.ecolind.2015.05.036, 2015.

de Jong, R. and de Bruin, S.: Linear trends in seasonal vegetation time series and the modifiable temporal unit problem, Biogeosciences, 9(1), 71–77, doi:10.5194/bg-9-71-2012, 2012.

de Jong, R., de Bruin, S., de Wit, A., Schaepman, M. E. and Dent, D. L.: Analysis of monotonic greening and browning trends from global NDVI time-series, Remote Sens. Environ., 115(2), 692–702, doi:10.1016/j.rse.2010.10.011, 2011.

De Jong, R., Verbesselt, J., Zeileis, A. and Schaepman, M. E.: Shifts in global vegetation activity trends, Remote Sens., 5(3), 1117–1133, doi:10.3390/rs5031117, 2013.

Julien, Y. and Sobrino, J. a.: Global land surface phenology trends from GIMMS database, Int. J. Remote Sens., 30(13), 3495–3513, doi:10.1080/01431160802562255, 2009.

Jung, M., Henkel, K., Herold, M. and Churkina, G.: Exploiting synergies of global land cover products for carbon cycle modeling, Remote Sens. Environ., 101(4), 534–553, doi:10.1016/j.rse.2006.01.020, 2006.

Jung, M., Koirala, S., Weber, U., Ichii, K., Gans, F., Gustau-Camps-Valls, Papale, D., Schwalm, C., Tramontana, G. and Reichstein, M.: The FLUXCOM ensemble of global land-atmosphere energy fluxes, , 1–14, doi:10.1038/s41597-019-0076-8, 2018.

Ke, Y., Leung, L. R., Huang, M., Coleman, A. M., Li, H. and Wigmosta, M. S.: Development of high resolution land surface parameters for the Community Land Model, Geosci. Model Dev., 5(6), 1341–1362, doi:10.5194/gmd-5-1341-2012, 2012.

De Keersmaecker, W., Lhermitte, S., Tits, L. and Honnay, O.: A model quantifying global vegetation resistance and resilience to short-term climate anomalies and their relationship with vegetation cover, Glob. Ecol. Biogeogr., 24, 539–548, doi:10.1111/geb.12279, 2015.

De Keersmaecker, W., Lhermitte, S., Hill, M. J., Tits, L., Coppin, P. and Somers, B.: Assessment of regional vegetation response to climate anomalies: A case study for australia using GIMMS NDVI time series between 1982 and 2006, Remote Sens., 9(1), 1–17, doi:10.3390/rs9010034, 2017.

Kim, D. Y., Thomas, V., Olson, J., Williams, M. and Clements, N.: Statistical trend and change-point analysis of land-cover-change patterns in East Africa, Int. J. Remote Sens., 34(19), 6636–6650, doi:10.1080/01431161.2013.804224, 2013.

Kim, W., Agata, Y. and Oki, T.: Simulation of potential impacts of land use/cover changes on surface water fluxes in the Chaophraya river basin, Thailand, J. Geophys. Res., 110(D8110), doi:10.1029/2004JD004825, 2005.

Koster, R. D. and Suarez, M. J.: A comparative-analysis of two land surface heterogeneity representations, J. Clim., 5(12), 1379–1390, doi:https://doi.org/10.1175/1520-

0442(1992)005<1379:ACAOTL>2.0.CO;2, 1992a.

Koster, R. D. and Suarez, M. T.: Modeling the Land Surface Boundary in Climate Models as a Composite of Independent Vegetation Stands, J. Geophys. Res., 97, 2697–2715, 1992b.

Kumar, S. V, Peters-lidard, C. D., Tian, Y., Houser, P. R., Geiger, J., Olden, S., Lighty, L., Eastman, J. L., Doty, B., Dirmeyer, P., Adams, J., Mitchell, K., Wood, E. F. and Sheffield, J.: Land information system : An interoperable framework for high resolution land surface modeling, Environ. Model. Softw., 21, 1402–1415, doi:10.1016/j.envsoft.2005.07.004, 2006.

Kure, S., Kavvas, M. and Ohara, N.: Upscaling of Coupled Land Surface Process Modeling for Heterogeneous Landscapes: Stochastic Approach, J. Hydrol., (December), 1017–1029, doi:10.1061/(ASCE)HE.1943-5584.0000163., 2010.

Kure, S., Kavvas, M., Ohara, N. and Jang, S.: Upscaling of Coupled Land Surface Process Modeling for Heterogeneous Landscapes: Stochastic Approach, J. Hydrol. Eng., 16, 1017–1029, 2011.

Lakshmi, V.: Remote sensing of soil moisture, ISRN Soil Sci., 2013, 33, 2013.

Lambin, E. F., Geist, H. J. and Lepers, E.: Dynamics of Land -Use and Land -Cover Change in Tropical Regions, Annu. Rev. Environ. Resour., 28(1), 205–241, doi:10.1146/annurev.energy.28.050302.105459, 2003.

Landmann, T. and Dubovyk, O.: Mapping vegetation productivity dynamics and degradation trends over East Africa using a decade of medium Resolution MODIS time-series data, Int. Geosci. Remote Sens. Symp., 1801–1804, doi:10.1109/IGARSS.2013.6723149, 2013.

Lee, E., He, Y., Zhou, M. and Liang, J.: Potential feedback of recent vegetation changes on summer rainfall in the Sahel, Phys. Geogr., 36(6), 449–470, doi:10.1080/02723646.2015.1120139, 2015.

Lee, X., Goulden, M. L., Hollinger, D. Y., Barr, A., Black, T. A., Bohrer, G., Bracho, R., Drake, B., Goldstein, A., Gu, L., Katul, G., Kolb, T., Law, B. E., Margolis, H., Meyers, T., Monson, R., Munger, W., Oren, R., Paw U, K. T., Richardson, A. D., Schmid, H. P., Staebler, R., Wofsy, S. and Zhao, L.: Observed increase in local cooling effect of deforestation at higher latitudes, Nature, 479(7373), 384–387, doi:10.1038/nature10588, 2011.

Lhomme, J.-P.: Energy balance of heterogeneous terrain: averaging the controlling parameters, Agric. For. Meteorol., 61(1), 11–21, 1992.

Li, A., Zhao, W. and Deng, W.: A Quantitative Inspection on Spatio-Temporal Variation of Remote Sensing-Based Estimates of Land Surface Evapotranspiration in South Asia, Remote Sens., 7, 4726–4752, doi:10.3390/rs70404726, 2015a.

Li, F., Lawrence, D. M. and Bond-Lamberty, B.: Impact of fire on global land surface air temperature and energy budget for the 20th century due to changes within ecosystems, Environ. rese, 12, 2017.

Li, Y., Zhao, M., Motesharrei, S., Mu, Q., Kalnay, E. and Li, S.: Local cooling and warming effects of forests based on satellite observations, Nat. Commun., 6, 1–8, doi:10.1038/ncomms7603, 2015b.

Li, Y., Zhao, M., Mildrexler, D. J., Motesharrei, S., Mu, Q., Kalnay, E., Zhao, F., Li, S. and Wang, K.: Potential and actual impacts of deforestation and afforestation on land surface temperature, J. Geophys. Res., 121(24), 14372–14386, doi:10.1002/2016JD024969, 2016.

Li, Z. L., Tang, B. H., Wu, H., Ren, H., Yan, G., Wan, Z., Trigo, I. F. and Sobrino, J. A.: Satellite-derived land surface temperature: Current status and perspectives, Remote Sens. Environ., 131, 14–37, doi:10.1016/j.rse.2012.12.008, 2013.

Liang, X., Lettenmaier, D. P., Wood, E. F. and Burges, S. J.: A simple hydrologically based model of land surface water and energy fluxes for general circulation models, J. Geophys. Res., 99(D7), 14415–14428, 1994.

Lin, P.-L. and Brunsell, N.: Assessing Regional Climate and Local Landcover Impacts on Vegetation with Remote Sensing, Remote Sens., 5(9), 4347–4369, doi:10.3390/rs5094347, 2013.

Liu, Y., Li, Y., Li, S. and Motesharrei, S.: Spatial and temporal patterns of global NDVI trends: Correlations with climate and human factors, Remote Sens., 7(10), 13233–13250, doi:10.3390/rs71013233, 2015.

Lucia, P., Luca, C., Sergio, M., Alessandro, C., Benjamin, Q., Nathalie de, N.-D., Johanna, I. H. and Almut, A.: Biophysical effects on temperature and precipitation due to land cover change, Environ. Res. Lett., 12(5), 53002 [online] Available from: http://stacks.iop.org/1748-9326/12/i=5/a=053002, 2017.

Maitima, J. M., Mugatha, S. M., Reid, R. S., Gachimbi, L. N., Majule, A., Lyaruu, H., Pomery, D., Mathai, S. and Mugisha, S.: The linkages between land use change, land degradation and biodiversity across East Africa, African J. Environ. Sci. Technol., 3(10), 310–325, 2009.

Mallick, K., Jarvis, A., Wohlfahrt, G., Kiely, G., Hirano, T., Miyata, A., Yamamoto, S. and Hoffmann, L.: Components of near-surface energy balance derived from satellite soundings – Part 2 : Noontime latent heat flux, Biogeosciences, 11, 7369–7382, doi:10.5194/bg-11-7369-2014, 2014.

Maneta, M. P. and Silverman, N. L.: A spatially distributed model to simulate water, energy, and vegetation dynamics using information from regional climate models, Earth Interact., 17(11), doi:10.1175/2012EI000472.1, 2013.

Mao, J., Shi, X., Thornton, P. E., Hoffman, F. M., Zhu, Z. and Myneni, R. B.: Global Latitudinal-Asymmetric Vegetation Growth Trends and Their Driving Mechanisms: 1982–2009, Remote Sens., 5, 1484–1497, doi:10.3390/rs5031484, 2013.

Marshall, M., Funk, C. and Michaelsen, J.: Examining evapotranspiration trends in Africa, Clim. Dyn., 38(9–10), 1849–1865, doi:10.1007/s00382-012-1299-y, 2012.

McNally, A., Shukla, S., Arsenault, K. R., Wang, S., Peters-Lidard, C. D. and Verdin, J. P.: Evaluating ESA CCI soil moisture in East Africa, Int. J. Appl. Earth Obs. Geoinf., 48, 1–14, doi:10.1016/j.jag.2016.01.001, 2016.

Melton, J. R. and Arora, V. K.: Sub-grid scale representation of vegetation in global land surface schemes: Implications for estimation of the terrestrial carbon sink, Biogeosciences, 11(4), 1021–1036, doi:10.5194/bg-11-1021-2014, 2014.

Meng, X. H., Evans, J. P. and McCabe, M. F.: The influence of inter-annually varying albedo on regional climate and drought, Clim. Dyn., 42(3–4), 787–803, doi:10.1007/s00382-013-1790-0, 2014.

Milly, P. C. D., Malyshev, S. L., Shevliakova, E., Dunne, K. a., Findell, K. L., Gleeson, T., Liang, Z., Phillips, P., Stouffer, R. J. and Swenson, S.: An enhanced model of land water and energy for global hydrologic and earth-system studies, J. Hydrometeorol., 140602152715002, doi:10.1175/JHM-D-13-0162.1, 2014.

Molod, A. and Salmun, H.: A global assessment of the mosaic approach to modeling land surface heterogeneity, J. Geophys. Res., 107(D14, 4217), 2002.

Montaldo, N., Albertson, J. D. and Mancini, M.: Vegetation dynamics and soil water balance in a water-limited Mediterranean ecosystem on Sardinia, Italy, Hydrol. Earth Syst. Sci. Discuss., 5, 219–255, doi:10.5194/hessd-5-219-2008, 2008.

Moriasi, D. N., Arnold, J., Liew, M. W. Van, Bingner, R. L., Harmel, R. D. and Veith, T. L.: Model Evaluation Guidelines for Systematic Quantification of Accuracy in Watershed Simulations, Trans. ASABE, 50(3), 885–900, 2007.

Mu, Q., Zhao, M. and Running, S. W.: Improvements to a MODIS global terrestrial evapotranspiration algorithm, Remote Sens. Environ., 115(8), 1781–1800, doi:10.1016/j.rse.2011.02.019, 2011.

Mu, Q., Zhao, M. and Running, S. W.: Algorithm Theoretical Basis Document: MODIS Global Terrestrial Evapotranspiration (ET) Product (NASA MOD16A2/A3) Collection 5. NASA Headquarters., 2013.

Mueller, T., Dressler, G., Tucker, C., Pinzon, J., Leimgruber, P., Dubayah, R., Hurtt, G., Böhning-Gaese, K. and Fagan, W.: Human Land-Use Practices Lead to Global Long-Term Increases in Photosynthetic Capacity, Remote Sens., 6(6), 5717–5731, doi:10.3390/rs6065717, 2014.

Müller, C., Bondeau, A., Lotze-Campen, H., Cramer, W. and Lucht, W.: Comparative impact of climatic and nonclimatic factors on global terrestrial carbon and water cycles, Global Biogeochem. Cycles, 20(4), doi:10.1029/2006GB002742, 2006.

Münch, Z., Gibson, L. and Palmer, A.: Monitoring Effects of Land Cover Change on Biophysical Drivers in Rangelands Using Albedo, Land, 8(2), 33, doi:10.3390/land8020033, 2019.

Murray, S. J., Foster, P. N. and Prentice, I. C.: Evaluation of global continental hydrology as simulated by the Land-surface Processes and eXchanges Dynamic Global Vegetation Model, Hydrol. Earth Syst. Sci., 15(1), 91–105, doi:10.5194/hess-15-91-2011, 2011.

Ning, T., Liu, W., Lin, W. and Song, X.: NDVI Variation and Its Responses to Climate Change on the Northern Loess Plateau of China from 1998 to 2012, Adv. Meteorol., 2015, 2015.

Olson, J. M., Alagarswamy, G., Andresen, J. A., Campbell, D. J., Davis, A. Y., Ge, J., Huebner, M., Lofgren, B. M., Lusch, D. P., Moore, N. J., Pijanowski, B. C., Qi, J., Thornton, P. K., Torbick, N. M. and Wang, J.: Integrating diverse methods to understand climate-land interactions in East Africa, Geoforum, 39(2), 898–911, doi:10.1016/j.geoforum.2007.03.011, 2008.

Ottlé, C., Lescure, J., Maignan, F., Poulter, B., Wang, T. and Delbart, N.: Use of various remote sensing land cover products for plant functional type mapping over Siberia, Earth Syst. Sci. Data, 5(2), 331–348, doi:10.5194/essd-5-331-2013, 2013.

Overgaard, J., Rosbjerg, D. and Butts, M.: Land-surface modelling in hydrological perspective – a review, Biogeosciences, 3(2), 229–241, doi:10.5194/bg-3-229-2006, 2006.

Paruelo, J. M., Lauenroth, W. K., Burke, I. C. and Sala, O. E.: Grassland precipitation-use efficiency varies across a resource gradient, Ecosystems, 2(1), 64–68, doi:10.1007/s100219900058, 1999.

Peng, D., Zhang, B., Liu, L., Chen, D., Fang, H. and Hu, Y.: Seasonal dynamic pattern analysis on global FPAR derived from AVHRR GIMMS NDVI, Int. J. Digit. Earth, 5(5), 439–455, doi:10.1080/17538947.2011.596579, 2012.

Peng, S.-S., Piao, S., Zeng, Z., Ciais, P., Zhou, L., Li, L. Z. X., Myneni, R. B., Yin, Y. and Zeng, H.: Afforestation in China cools local land surface temperature, Proc. Natl. Acad. Sci., 111(8), 2915–2919, doi:10.1073/pnas.1315126111, 2014.

Pfeifer, M., Platts, P. J., Burgess, N. D., Swetnam, R. D., Willcock, S., Lewis, S. L. and Marchant, R.: Land use change and carbon fluxes in East Africa quantified using earth observation data and field measurements, Environ. Conserv., 40(3), 241–252, doi:10.1017/S0376892912000379, 2012.

Pfeifer, M., Lefebvre, V., Gonsamo, A., Pellikka, P. K. E., Marchant, R., Denu, D. and Platts, P. J.: Validating and linking the GIMMS leaf area index (LAI3g) with environmental controls in tropical Africa, Remote Sens., 6(3), 1973–1990, doi:10.3390/rs6031973, 2014.

Pinzon, J. and Tucker, C.: A Non-Stationary 1981–2012 AVHRR NDVI3g Time Series, Remote Sens., 6(8), 6929–6960, doi:10.3390/rs6086929, 2014.

Pitman, A. J.: Sensitivity of the Land Surface to Sub-Grid Scale Processes: Implications for Climate Simulations, Vegetatio, 91, 121–134, 1991.

Pitman, A. J.: The evolution of, and revolution in, land surface schemes designed for climate models, Int. J. Climatol., 23(5), 479–510, doi:10.1002/joc.893, 2003.

Pongratz, J., Reick, C., Raddatz, T. and Claussen, M.: A reconstruction of global agricultural areas and land cover for the last millennium, Global Biogeochem. Cycles, 22, GB3018, doi:10.1029/2007GB003153, 2008.

Pongratz, J., Reick, C. H., Raddatz, T. and Claussen, M.: Biogeophysical versus biogeochemical climate response to historical anthropogenic land cover change, Geophys. Res. Lett., 37(8), 1–5, doi:10.1029/2010GL043010, 2010.

Prevedello, J. A., Winck, G. R., Weber, M. M., Nichols, E. and Sinervo, B.: Impacts of forestation and deforestation on local temperature across the globe, PLoS One, 14(3), 1–18, doi:10.1371/journal.pone.0213368, 2019.

Pricope, N. G., Husak, G., Lopez-Carr, D., Funk, C. and Michaelsen, J.: The climate-population nexus in the East African Horn: Emerging degradation trends in rangeland and pastoral livelihood zones, Glob. Environ. Chang., 23(6), 1525–1541, doi:10.1016/j.gloenvcha.2013.10.002, 2013.

Quéré, C., Andrew, R., Friedlingstein, P., Sitch, S., Hauck, J., Pongratz, J., Pickers, P., Ivar Korsbakken, J., Peters, G., Canadell, J., Arneth, A., Arora, V., Barbero, L., Bastos, A., Bopp, L., Ciais, P., Chini, L., Ciais, P., Doney, S., Gkritzalis, T., Goll, D., Harris, I., Haverd, V., Hoffman, F., Hoppema, M., Houghton, R., Hurtt, G., Ilyina, T., Jain, A., Johannessen, T., Jones, C., Kato, E., Keeling, R., Klein Goldewijk, K., Landschützer, P., Lefèvre, N., Lienert, S., Liu, Z., Lombardozzi, D., Metzl, N., Munro, D., Nabel, J., Nakaoka, S. I., Neill, C., Olsen, A., Ono, T., Patra, P., Peregon, A., Peters, W., Peylin, P., Pfeil, B., Pierrot, D., Poulter, B., Rehder, G., Resplandy, L., Robertson, E., Rocher, M., Rödenbeck, C., Schuster, U., Skjelvan, I., Séférian, R., Skjelvan, I., Steinhoff, T., Sutton, A., Tans, P., Tian, H., Tilbrook, B., Tubiello, F., Van Der Laan-Luijkx, I., Van Der Werf, G., Viovy, N., Walker, A., Wiltshire, A., Wright, R., Zaehle, S. and Zheng, B.: Global Carbon Budget 2018, Earth Syst. Sci. Data, 10(4), 2141–2194, doi:10.5194/essd-10-2141-2018, 2018.

Rajib, A., Kim, I. L., Golden, H. E., Lane, C. R., Kumar, S. V., Yu, Z. and Jeyalakshmi, S.: Watershed Modeling with Remotely Sensed Big Data: MODIS Leaf Area Index Improves Hydrology and Water Quality Predictions, Remote Sens., 12(2148), 1–17, 2020.

Ren, X., He, H., Moore, D. J. P., Zhang, L., Liu, M., Li, F., Yu, G. and Wang, H.: Uncertainty analysis of modeled carbon and water fluxes in a subtropical coniferous plantation, J. Geophys. Res. Biogeosciences, 118, 1674–1688, doi:10.1002/2013JG002402, 2013.

Renner, M. and Bernhofer, C.: Applying simple water-energy balance frameworks to predict the climate sensitivity of streamflow over the continental United States, Hydrol. Earth Syst. Sci., 16(8), 2531–2546, doi:10.5194/hess-16-2531-2012, 2012.

Sacardi, M., Louis, G., Gomes, N., Henrique, P., Arruda, Z. De, Aparecido, G., Neves, R., Almeida, F. De, Michael, C., Neale, U. and Souza, J. De: Patterns of energy exchange for tropical ecosystems across a climate gradient in Mato Grosso , Brazil, Agric. For. Meteorol., 202, 112–124, doi:10.1016/j.agrformet.2014.12.008, 2015.

Sato, H., Ito, A., Ito, A., Ise, T. and Kato, E.: Current status and future of land surface models, Soil

Sci. Plant Nutr., 61(1), 34–47, doi:10.1080/00380768.2014.917593, 2015.

Saxton, K. E. and Rawls, W. J.: Soil Water Characteristic Estimates by Texture and Organic Matter for Hydrologic Solutions, Soil Sci. Soc. Am. J., 70(5), 1569, doi:10.2136/sssaj2005.0117, 2006.

Schaaf, C. B., Gao, F., Strahler, A. H., Lucht, W., Li, X., Tsang, T., Strugnell, N. C., Zhang, X., Jin, Y., Muller, J. P., Lewis, P., Barnsley, M., Hobson, P., Disney, M., Roberts, G., Dunderdale, M., Doll, C., D'Entremont, R. P., Hu, B., Liang, S., Privette, J. L. and Roy, D.: First operational BRDF, albedo nadir reflectance products from MODIS, Remote Sens. Environ., 83(1–2), 135–148, doi:10.1016/S0034-4257(02)00091-3, 2002.

Schaphoff, S., von Bloh, W., Rammig, A., Thonicke, K., Biemans, H., Forkel, M., Gerten, D., Heinke, J., Jägermeyr, J., Knauer, J., Langerwisch, F., Lucht, W., Müller, C., Rolinski, S. and Waha, K.: LPJmL4 – a dynamic global vegetation model with managed land – Part 1: Model description, Geosci. Model Dev., 11(4), 1343–1375, doi:10.5194/gmd-11-1343-2018, 2018.

Sellers, P. J., Randall, D. A., Collatz, G. J., Berry, J. A., Field, C. B., Dazlich, D. A., Zhang, C., Collelo, G. D. and Bounoua, L.: A revised land surface parameterization (SiB2) for atmospheric GCMs. Part I: Model formulation, J. Clim., 9(4), 676–705, doi:10.1175/1520-0442(1996)009<0676:ARLSPF>2.0.CO;2, 1996.

Seth, A., Giorgi, F. and Dickinson, R. E.: Simulating fluxes from heterogeneous land surface - Explicit subgrid method employing the biosphere-atmosphere transfer scheme (BATS), J. Geophys. Res., 99(D9), 18651–18667, 1994.

Sheffield, J., Goteti, G. and Wood, E. F.: Development of a 50-year high-resolution global dataset of meteorological forcings for land surface modeling, J. Clim., 19(13), 3088–3111, doi:10.1175/JCLI3790.1, 2006.

Sitch, S., C, H., N, G., E, L. P., M, L., S, P., R, B., P, C., P, C., P, F., Jones, C. D., Prentice, I. C. and Woodwards, F. I.: Evaluation of the terrestrial carbon cycle, future plant geography and climate-carbon cycle feedbacks using five Dynamic Global Vegetation Models (DGVMs), Glob. Chang. Biol., 14, 2015–2039, doi:10.1111/j.1365-2486.2008.01626.x, 2008.

Sleeter, B. M., Liu, J., Daniel, C., Rayfield, B., Sherba, J., Hawbaker, T. J., Zhu, Z., Selmants, P. C. and Loveland, T. R.: Effects of contemporary land-use and land-cover change on the carbon balance of terrestrial ecosystems in the United States, Environ. Res. Lett., 13, doi:10.1088/1748-9326/aab540, 2018.

Smith, B., Wärlind, D., Arneth, A., Hickler, T., Leadley, P., Siltberg, J. and Zaehle, S.: Implications of incorporating N cycling and N limitations on primary production in an individual-based dynamic vegetation model, Biogeosciences, 11(7), 2027–2054, doi:10.5194/bg-11-2027-2014, 2014.

Snyder, P. K., Foley, J. A., Hitchman, M. H. and Delire, C.: Analyzing the effects of complete tropical forest removal on the regional climate using a detailed three-dimensional energy budget: An application to Africa, J. Geophys. Res. D Atmos., 109(21), doi:10.1029/2003JD004462, 2004.

Stoll, R. and Porte´-Agel, F.: Surface Heterogeneity Effects on Regional-Scale Fluxes in the Stable Boundary Layer: Aerodynamic Roughness Length Transitions, J. Atmos. Sci., 66, 412–431, doi:10.1007/s10546-013-9839-5, 2009.

Strengers, B. J., Müller, C., Schaeffer, M., Haarsma, R. J., Severijns, C., Gerten, D., Schaphoff, S., Van Den Houdt, R. and Oostenrijk, R.: Assessing 20th century climate-vegetation feedbacks of land-use change and natural vegetation dynamics in a fully coupled vegetation-climate model, Int. J. Climatol., 30(13), 2055–2065, doi:10.1002/joc.2132, 2010.

Su, Z., Pelgrum, H. and Menenti, M.: Aggregation effects of surface heterogeneity in land surface processes, Hydrol. Earth Syst. Sci., 3(4), 549–563, 1999.

Tagesson, T., Fensholt, R., Guiro, I., Rasmussen, M. O., Huber, S., Mbow, C., Garcia, M., Horion, S., Sandholt, I., Holm-Rasmussen, B., Gottsche, F. M., Ridler, M. E., Olen, N., Lundegard Olsen, J., Ehammer, A., Madsen, M., Olesen, F. S. and Ardo, J.: Ecosystem properties of semiarid savanna grassland in West Africa and its relationship with environmental variability, Glob. Chang. Biol., 21(1), 250–264, doi:10.1111/gcb.12734, 2015.

Teferi, E., Uhlenbrook, S. and Bewket, W.: Inter-annual and seasonal trends of vegetation condition in the Upper Blue Nile (Abay) Basin : dual-scale time, Earth Syst. Dyn., 6, 617–636, doi:10.5194/esd-6-617-2015, 2015.

Toté, C., Patricio, D., Boogaard, H., van der Wijngaart, R., Tarnavsky, E. and Funk, C.: Evaluation of satellite rainfall estimates for drought and flood monitoring in Mozambique, Remote Sens., 7(2), 1758–1776, doi:10.3390/rs70201758, 2015.

Townshend, J. R. G., Carroll, M., Dimiceli, C., Hansen, R., M., S. and DeFries., R.: Vegetation Continuous Fields MOD44B, 2001 Percent Tree Cover, Collection 5, 2011.

Twine, T. E., Kucharik, C. J. and Foley, J. a.: Effects of Land Cover Change on the Energy and Water Balance of the Mississippi River Basin, J. Hydrometeorol., 5(4), 640–655, doi:10.1175/1525-7541(2004)005<0640:EOLCCO>2.0.CO;2, 2004.

Verbesselt, J., Hyndman, R., Newnham, G. and Culvenor, D.: Detecting trend and seasonal changes in satellite image time series, Remote Sens. Environ., 114(1), 106–115, doi:10.1016/j.rse.2009.08.014, 2010.

Verhoef, A., Ottlé, C., Cappelaere, B., Murray, T., Saux-Picart, S., Zribi, M., Maignan, F., Boulain, N., Demarty, J. and Ramier, D.: Spatio-temporal surface soil heat flux estimates from satellite data; results for the AMMA experiment at the Fakara (Niger) supersite, Agric. For. Meteorol., 154, 55–66, doi:10.1016/j.agrformet.2011.08.003, 2012.

Verma, M., Friedl, M. A., Law, B. E., Bonal, D., Kiely, G., Black, T. A., Wohlfahrt, G., Moors, E. J., Montagnani, L., Marcolla, B., Toscano, P., Varlagin, A., Roupsard, O., Cescatti, A., Arain, M. A. and D'Odorico, P.: Improving the performance of remote sensing models for capturing intra- and inter-annual variations in daily GPP: An analysis using global FLUXNET tower data, Agric. For. Meteorol., 214–215, 416–429, doi:10.1016/j.agrformet.2015.09.005, 2015.

Vicente-Serrano, S. M., Beguería, S. and López-Moreno, J. I.: A multiscalar drought index sensitive to global warming: The standardized precipitation evapotranspiration index, J. Clim., 23(7), 1696–1718, doi:10.1175/2009JCLI2909.1, 2010.

Vicente-Serrano, S. M., Gouveia, C., Julio, J., Beguería, S., Trigo, R., López-Morenoa, J. I., César Azorín-Molinaa, E. P., Lorenzo-Lacruza, J., Revueltoa, J. and Enrique Morán-Tejedaa, A. S.-L.: Response of vegetation to drought time-scales across global land biomes, PNAS, 110(1), 52–57, doi:https://doi.org/10.1073/pnas.1207068110, 2013.

Vrieling, A., de Leeuw, J. and Said, M.: Length of Growing Period over Africa: Variability and Trends from 30 Years of NDVI Time Series, Remote Sens., 5(2), 982–1000, doi:10.3390/rs5020982, 2013.

Wan, Z.: New refinements and validation of the collection-6 MODIS land-surface temperature/emissivity product, Remote Sens. Environ., 140, 36–45, doi:10.1016/j.rse.2013.08.027, 2014.

Wang, W., Chen, Y., Becker, S. and Liu, B.: Linear Trend Detection in Serially Dependent Hydrometeorological Data Based on a Variance Correction Spearman Rho Method, Water, 7, 7045–7065, doi:10.3390/w7126673, 2015.

WCS and CIESIN: Last of the Wild Project, Version 2, 2005 (LWP-2): Global Human Footprint Dataset (Geographic), [online] Available from: http://dx.doi.org/10.7927/H4M61H5F, 2005.

Weber, U., Jung, M., Reichstein, M., Beer, C., Braakhekke, M. C., Lehsten, V., Ghent, D., Kaduk, J., Viovy, N., Ciais, P., Gobron, N. and Rödenbeck, C.: The interannual variability of Africa's ecosystem productivity: a multi-model analysis, Biogeosciences, 6(2), 285–295, doi:10.5194/bg-6-285-2009, 2009.

White, F.: The vegetation of Africa—a descriptive memoir to accompany the Unesco/ AETFAT/UNSO vegetation map of Africa. Natural Resources Research Report XX., Paris, France., 1983.

Williams, M., Richardson, a. D., Reichstein, M., Stoy, P. C., Peylin, P., Verbeeck, H., Carvalhais, N., Jung, M., Hollinger, D. Y., Kattge, J., Leuning, R., Luo, Y., Tomelleri, E., Trudinger, C. and Wang, Y.-P.: Improving land surface models with FLUXNET data, Biogeosciences Discuss., 6(2), 2785–2835, doi:10.5194/bgd-6-2785-2009, 2009.

Winckler, J., Reick, C. H. and Pongratz, J.: Robust Identification of Local Biogeophysical Effects of Land-Cover Change in a Global Climate Model, J. Clim., 30(3), 1159–1176, doi:10.1175/JCLI-D-16-0067.1, 2017a.

Winckler, J., Reick, C. H. and Pongratz, J.: Why does the locally induced temperature response to land cover change differ across scenarios?, Geophys. Res. Lett., 44(8), 3833–3840, doi:10.1002/2017GL072519, 2017b.

Wood, E. F., Lettenmaier, D. P. and Zartarian, V. G.: A Land-Surface Hydrology Parameterization

With Subgrid Variability for General Circulation Models, J. Geophys. Res., 97(D3), 2717–2728, 1992.

Wu, M., Schurgers, G., Rummukainen, M., Smith, B., Samuelsson, P., Jansson, C., Siltberg, J. and May, W.: Vegetation-climate feedbacks modulate rainfall patterns in Africa under future climate change, Earth Syst. Dyn., 7(3), 627–647, doi:10.5194/esd-7-627-2016, 2016.

Wu, Z. Y., Lu, G. H., Wen, L. and Lin, C. A.: Reconstructing and analyzing China's fifty-nine year (1951 – 2009) drought history using hydrological model simulation, Hydrol. Earth Syst. Sci., 2881–2894, doi:10.5194/hess-15-2881-2011, 2011.

Xin, X. and Liu, Q.: The Two-layer Surface Energy Balance Parameterization Scheme (TSEBPS) for estimation of land surface heat fluxes, Hydrol. Earth Syst. Sci., 14(3), 491–504, doi:10.5194/hess-14-491-2010, 2010.

Xinmin, Z., Ming, Z. and Bingkai, S.: A numerical study on effects of land-surface heterogeneity from "combined approach" on atmospheric process Part I: Principle and method, Adv. Atmos. Sci., 17(1), 103–120, doi:10.1007/s00376-000-0047-0, 2000.

Yang, Z.: Modeling land surface processes in short-term weather and climate studies, in Observation, Theory and Modeling of Atmospheric Variability, edited by X. Zhu, X. Li, M. Cai, S. Zhou, Y. Zhu, F.-F. Jin, X. Zou, and M. Zhang, pp. 288–313, World Scientific, New Jersey., 2004.

Yue, S. and Wang, C. Y.: Applicability of prewhitening to eliminate the influence of serial correlation on the Mann-Kendall test, Water Resour. Res., 38(6), 4-1-4–7, doi:10.1029/2001WR000861, 2002.

Yue, S., Pilon, P., Phinney, B. and Cavadias, G.: The influence of autocorrelation on the ability to detect trend in hydrological series, Hydrol. Process., 16(9), 1807–1829, doi:10.1002/hyp.1095, 2002.

Zeide, B.: Primary Unit of the Tree Crown, Ecology, 74(5), 1598–1602, 1993.

Zeng, X.: Global Vegetation Root Distribution for Land Modeling, J. Hydrometeorol., 2, 525–530, doi:10.1175/1525-7541(2001)002<0525:gvrdfl>2.0.co;2, 2001.

Zhang, M., Lee, X., Yu, G., Han, S., Wang, H., Yan, J., Zhang, Y., Li, Y., Ohta, T., Hirano, T., Kim, J., Yoshifuji, N. and Wang, W.: Response of surface air temperature to small-scale land clearing across latitudes, Environ. Res. Lett., 9(3), doi:10.1088/1748-9326/9/3/034002, 2014.

Zhao, F., Zhang, L., Chiew, F. H. S., Vaze, J. and Cheng, L.: The effect of spatial rainfall variability on water balance modelling for south-eastern Australian catchments, J. Hydrol., 493, 16–29, doi:10.1016/j.jhydrol.2013.04.028, 2013.

Zhao, K. and Jackson, R. B.: Biophysical forcings of land-use changes from potential forestry activities in North America, Ecol. Monogr., 84(2), 329–353, doi:10.1890/12-1705.1, 2014.

Zhao, W. and Li, A.: A Review on Land Surface Processes Modelling over Complex Terrain, Adv. Meteorol., 2015, 1–17, doi:http://dx.doi.org/10.1155/2015/607181, 2015.

Zhu, Z., Bi, J., Pan, Y., Ganguly, S., Anav, A., Xu, L., Samanta, A., Piao, S., Nemani, R. R. and Myneni, R. B.: Global data sets of vegetation leaf area index (LAI)3g and fraction of photosynthetically active radiation (FPAR)3g derived from global inventory modeling and mapping studies (GIMMS) normalized difference vegetation index (NDVI3G) for the period 1981 to 2, Remote Sens., 5(2), 927–948, doi:10.3390/rs5020927, 2013.

Zhu, Z., Piao, S., Myneni, R. B., Huang, M., Zeng, Z., Canadell, J. G., Ciais, P., Sitch, S., Friedlingstein, P., Arneth, A., Cao, C., Cheng, L., Kato, E., Koven, C., Li, Y., Lian, X., Liu, Y., Liu, R., Mao, J., Pan, Y., Peng, S., Peuelas, J., Poulter, B., Pugh, T. A. M., Stocker, B. D., Viovy, N., Wang, X., Wang, Y., Xiao, Z., Yang, H., Zaehle, S. and Zeng, N.: Greening of the Earth and its drivers, Nat. Clim. Chang., 6(8), 791–795, doi:10.1038/nclimate3004, 2016.

APPENDICES

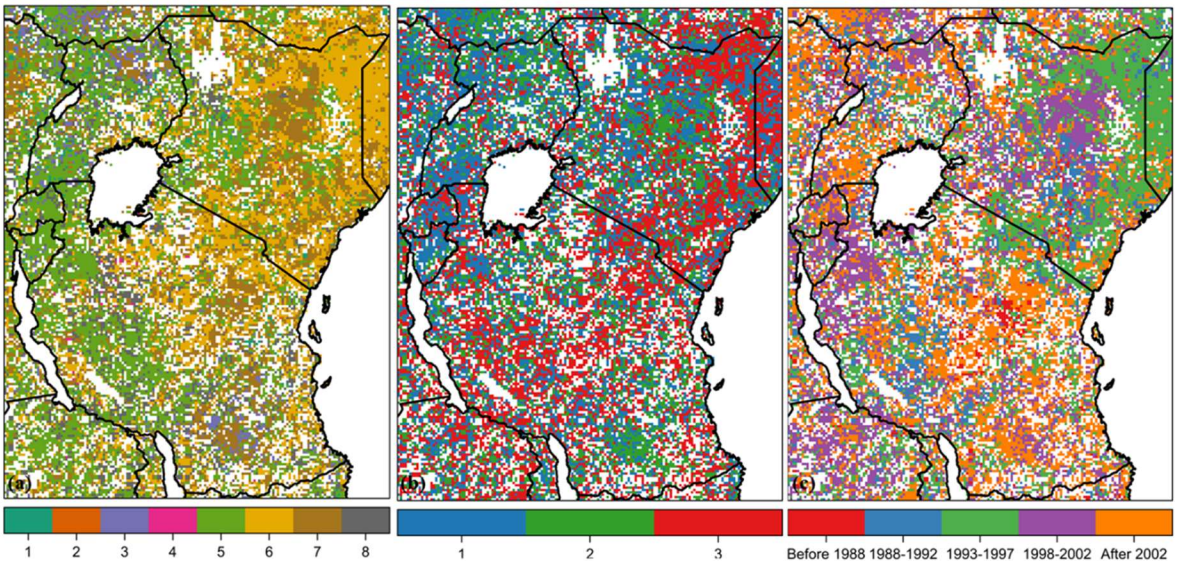

Figure A. 1: (a) Type, (b) significance and (c) timing of trend shift in monthly LAI time series. Trends and breaks are considered as significant when P-value is below 0.05. Pixels with no significant (P < 0.05) change for all segments and/or no significant (P < 0.05) breakpoint are not shown. The trend shifts types in (a) are: (1) monotonic increase, (2) monotonic decrease, (3) monotonic increase (with positive break), (4) monotonic decrease (with negative break), (5) interruption: increase with negative break, (6) interruption: decrease with positive break, (7) reversal: increase to decrease, and (8) reversal: decrease to increase. The significance classes are: (1) both segments significant (or no break and significant), (2) only first segment significant, and (3) only 2nd segment significant.

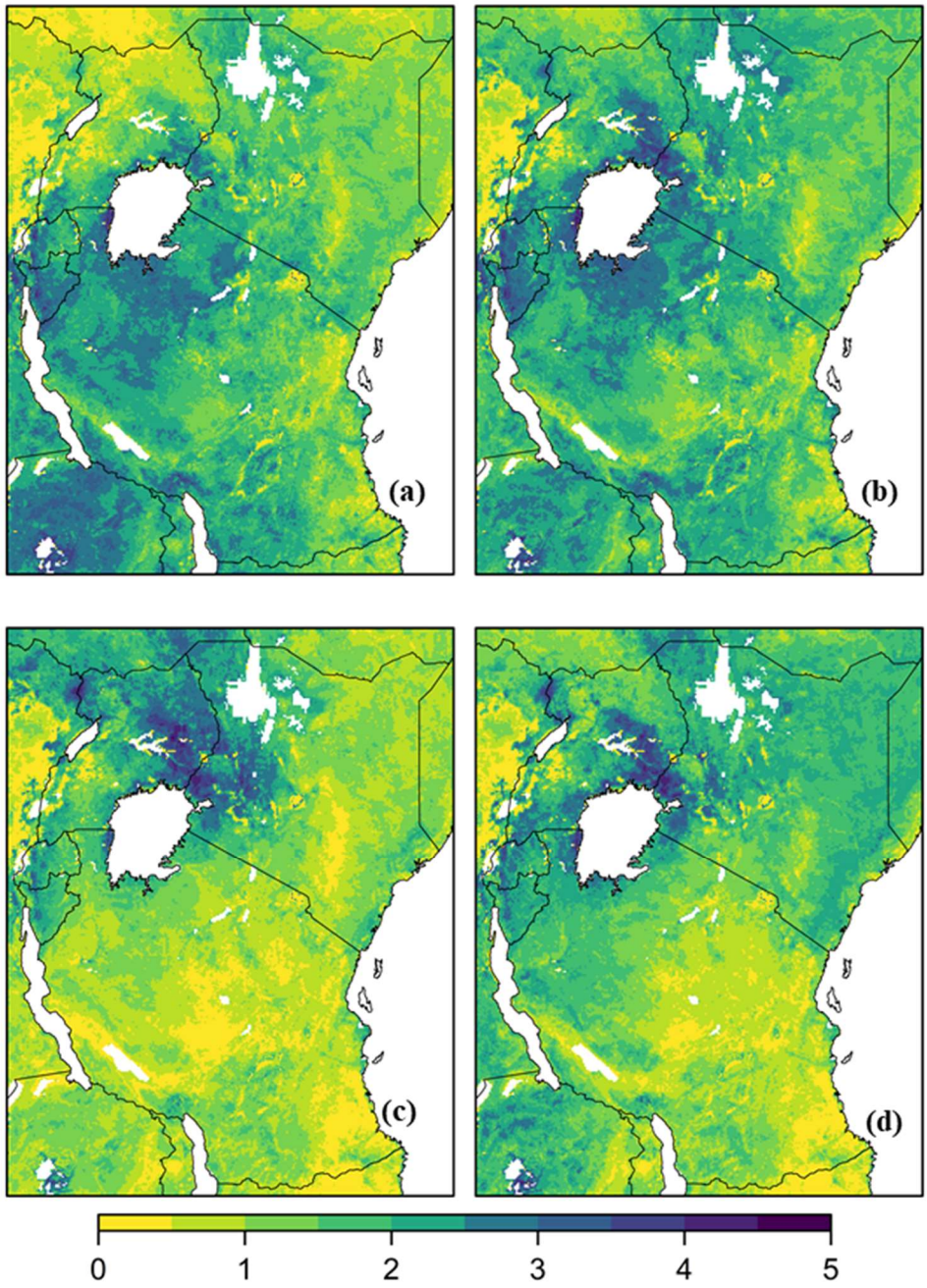

Figure A. 2: Mean seasonal changes in LAI (m^2/m^2) during (a) January-February, (b) March-May, (c) June-September and (d)October-December seasons.

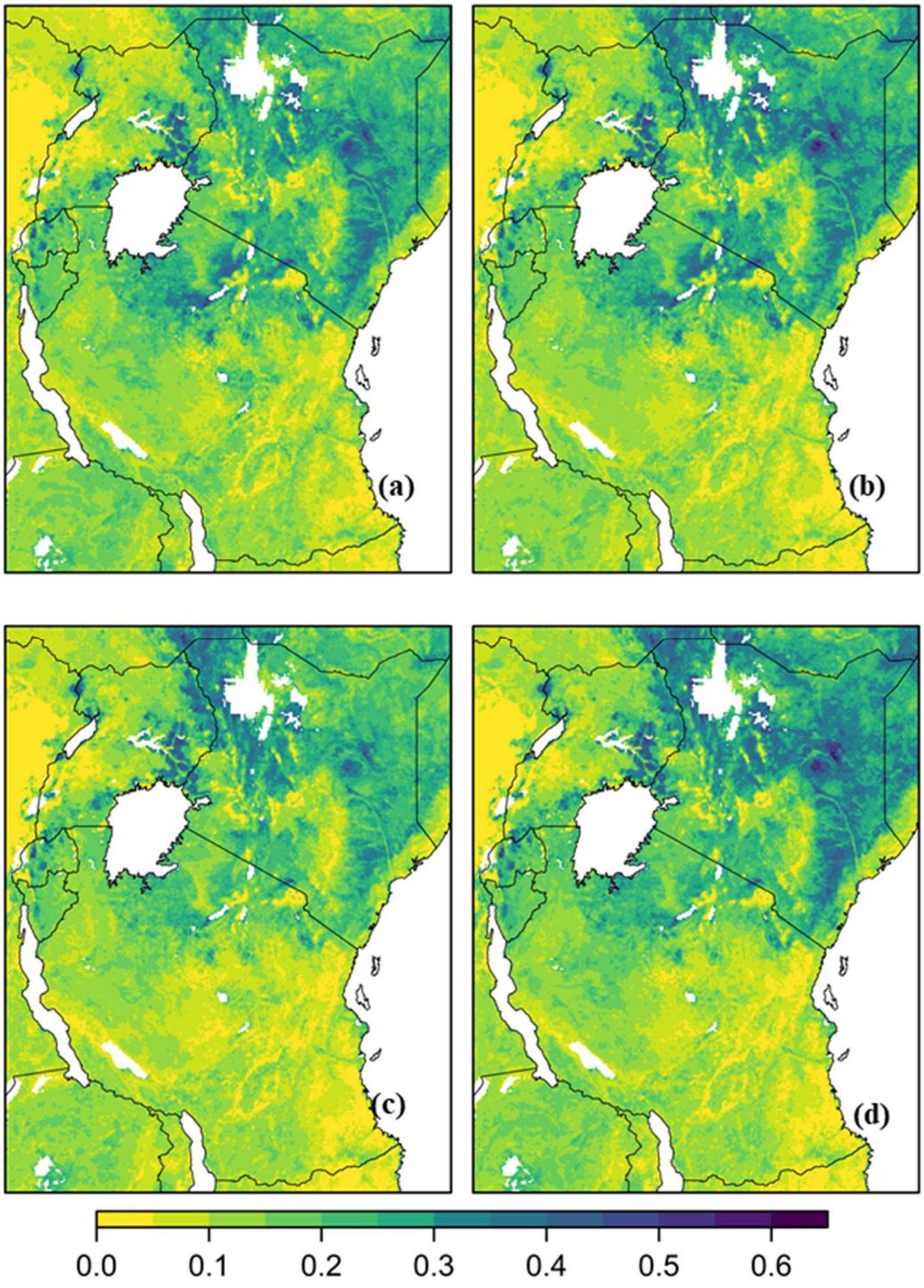

Figure A. 3: Mean seasonal changes in Fractional vegetation cover during (a) January-February, (b) March-May, (c) June-September and (d)October-December seasons.

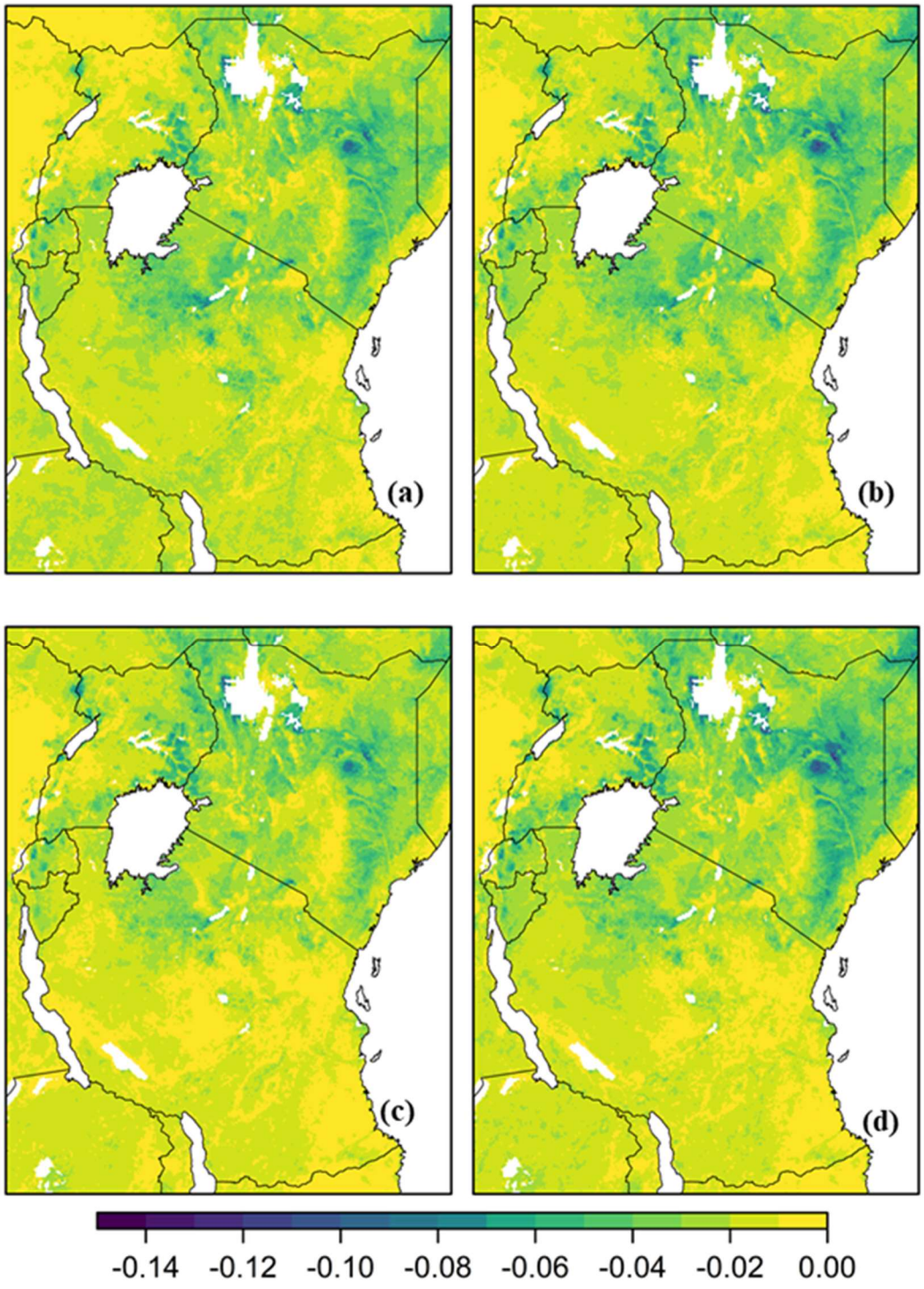

Figure A. 4: Mean seasonal changes in albedo during (a) January-February, (b) March-May, (c) June-September and (d)October-December seasons

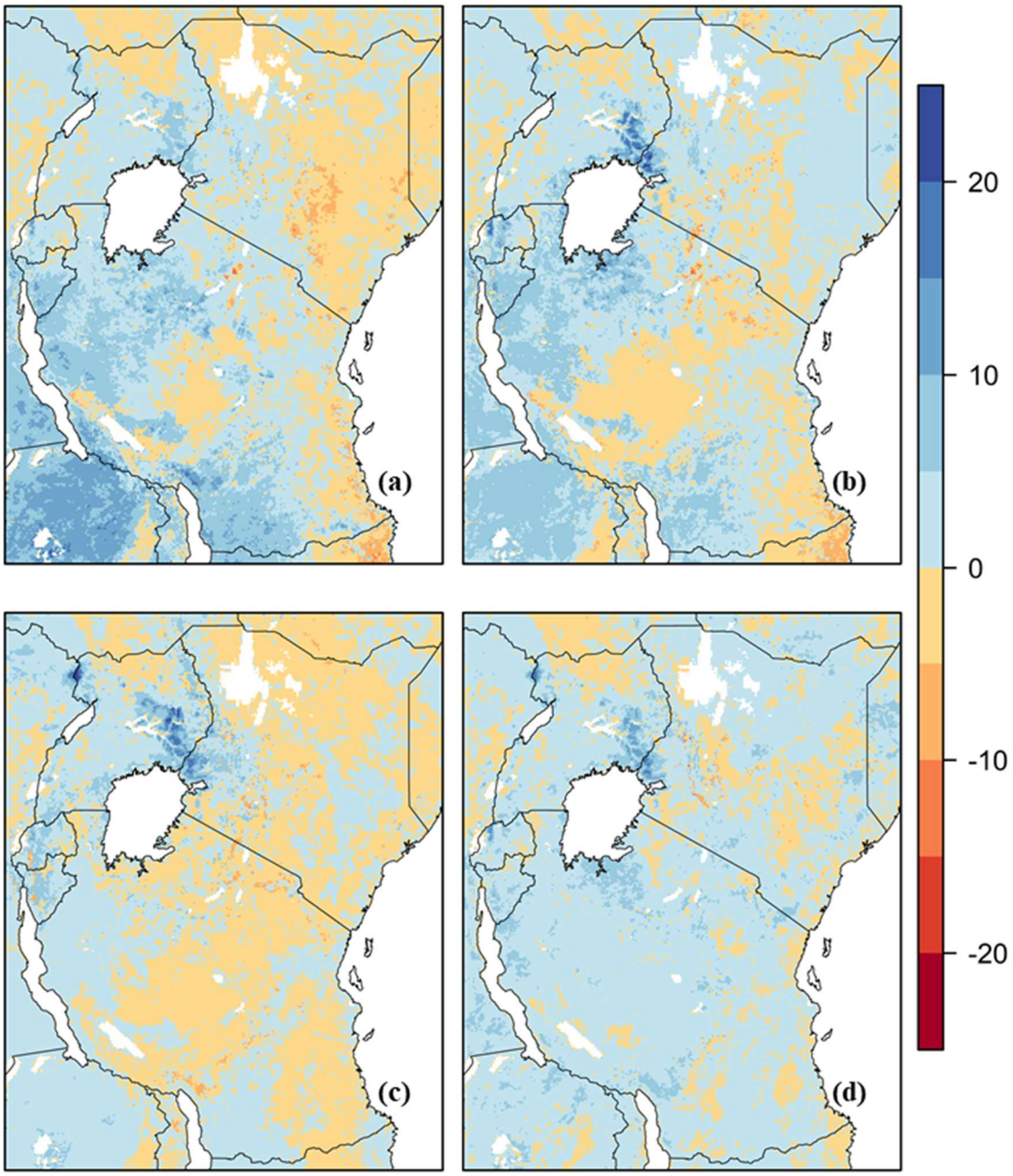

Figure A. 5: Mean seasonal changes in total evapotranspiration (mm/month) during (a) January-February, (b) March-May, (c) June-September and (d)October-December seasons.

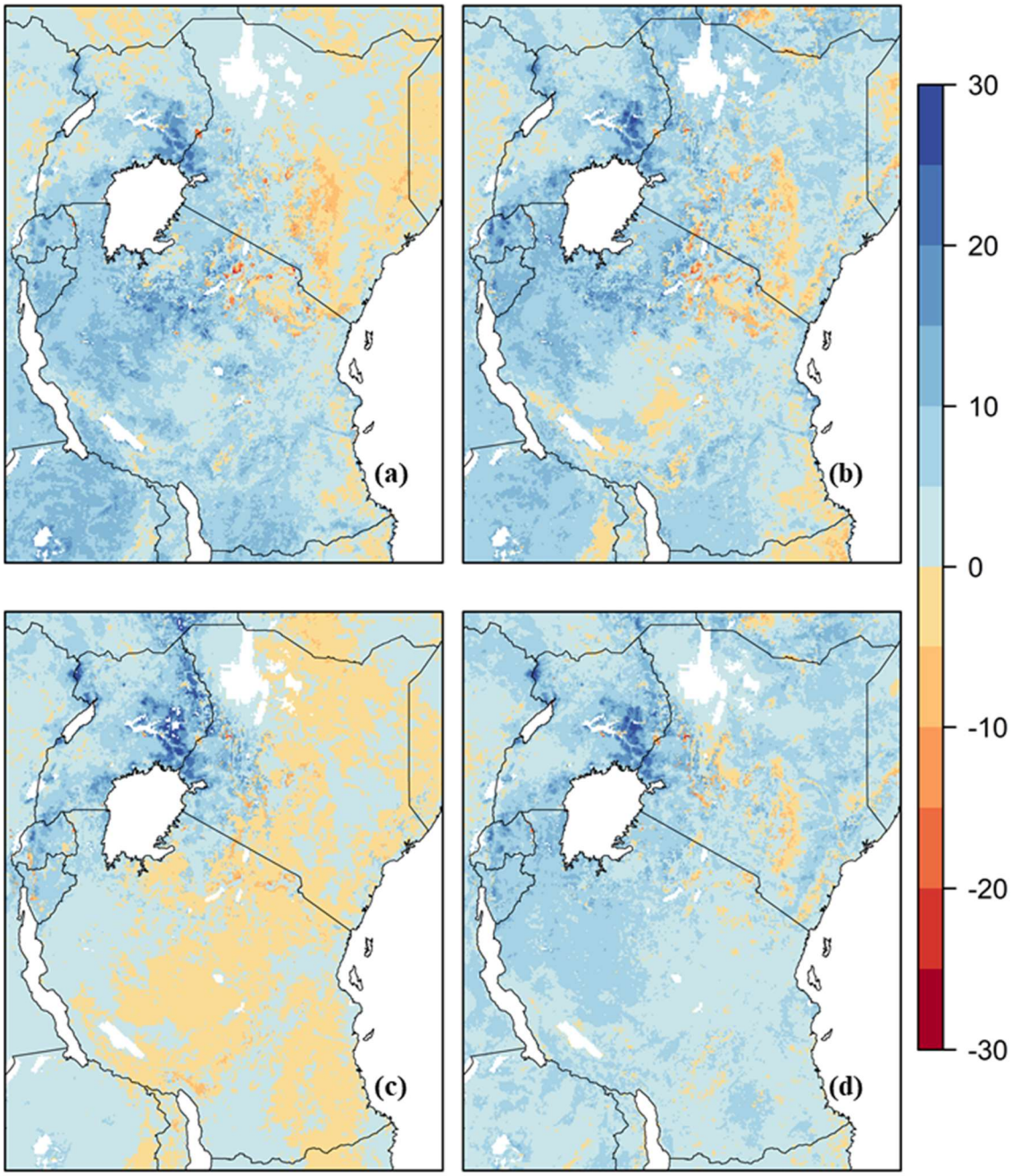

Figure A. 6: Mean seasonal changes in vegetation transpiration (mm/month) during (a) January-February, (b) March-May, (c) June-September and (d)October-December seasons.

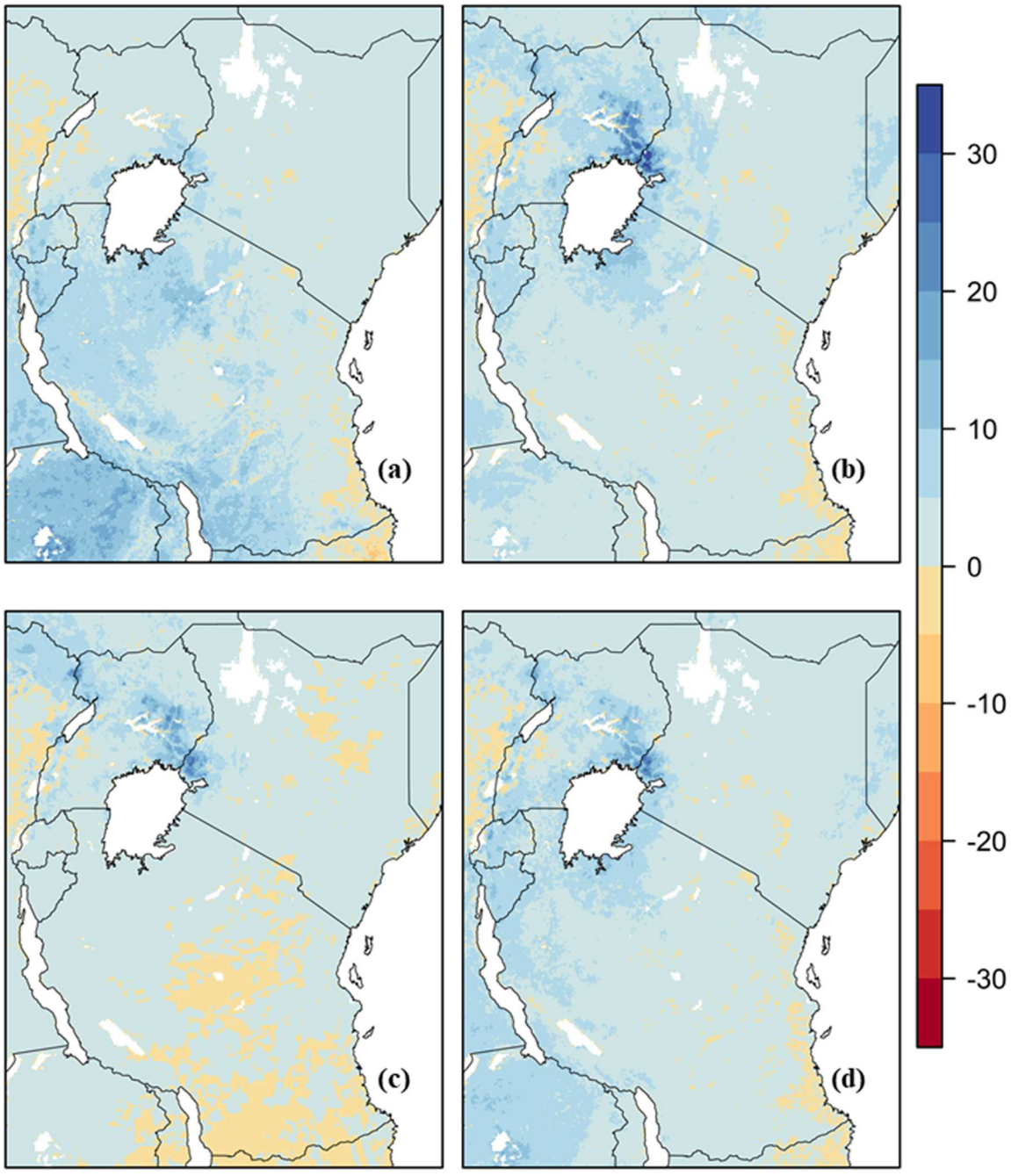

Figure A. 7: Mean seasonal changes in vegetation canopy evaporation (mm/month) during (a) January-February, (b) March-May, (c) June-September and (d)October-December seasons.

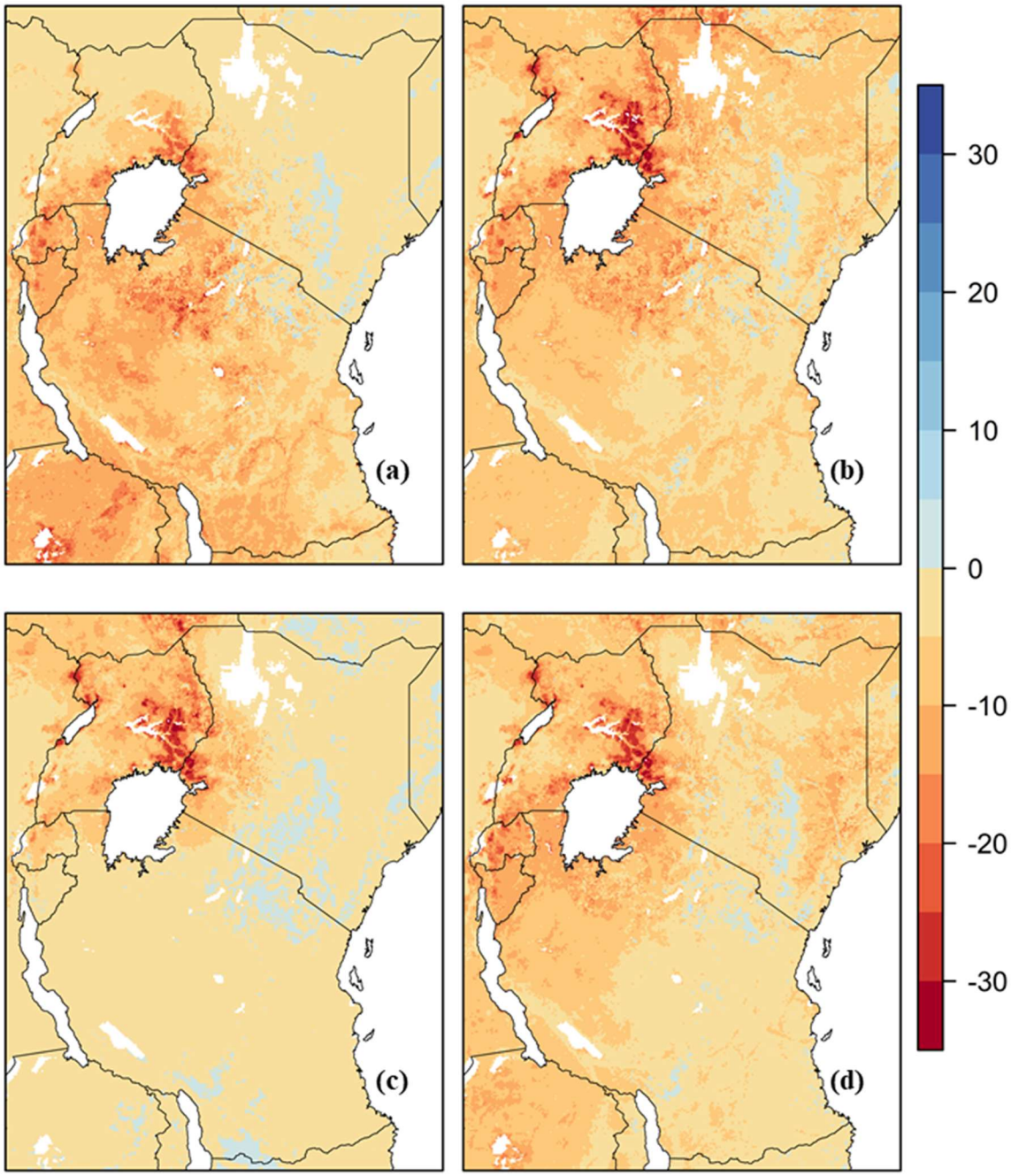

Figure A. 8: Mean seasonal changes in bare soil evaporation (mm/month) during (a) January-February, (b) March-May, (c) June-September and (d)October-December seasons.

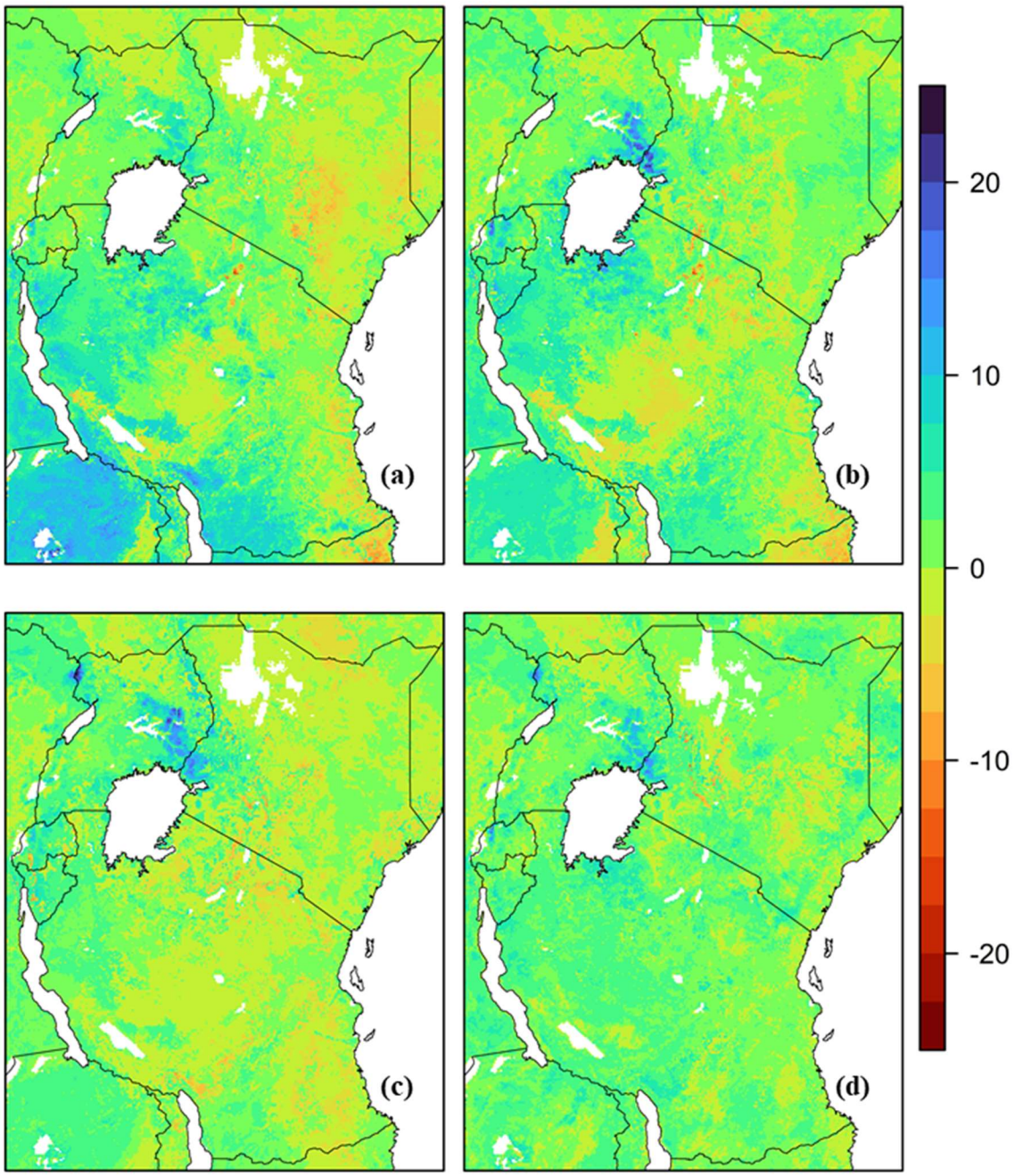

Figure A. 9: Mean seasonal changes in latent heat (Wm^{-2}) during (a) January-February, (b) March-May, (c) June-September and (d)October-December seasons.

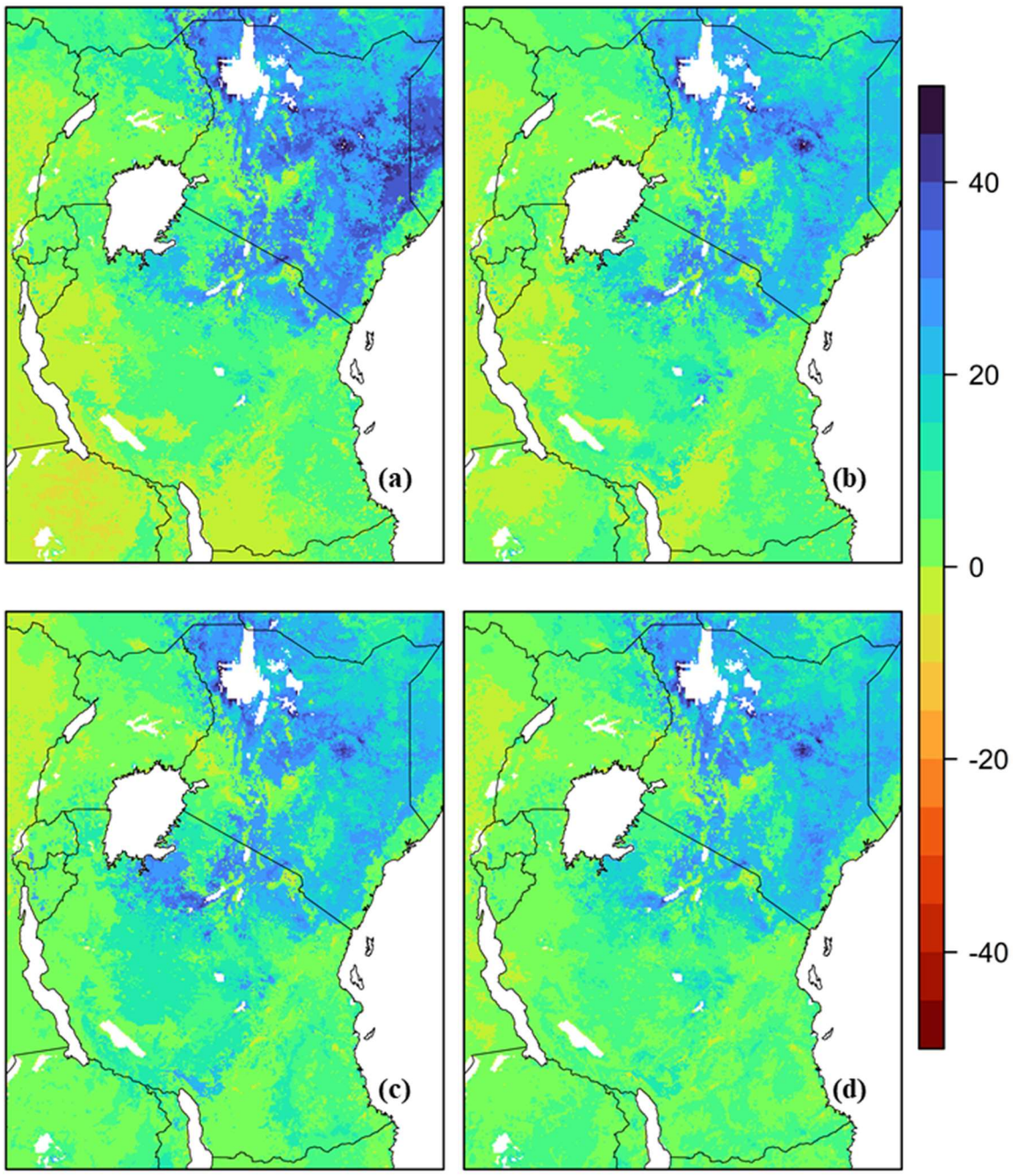

Figure A. 10: Mean seasonal changes in sensible heat (Wm^{-2}) during (a) January-February, (b) March-May, (c) June-September and (d)October-December seasons.

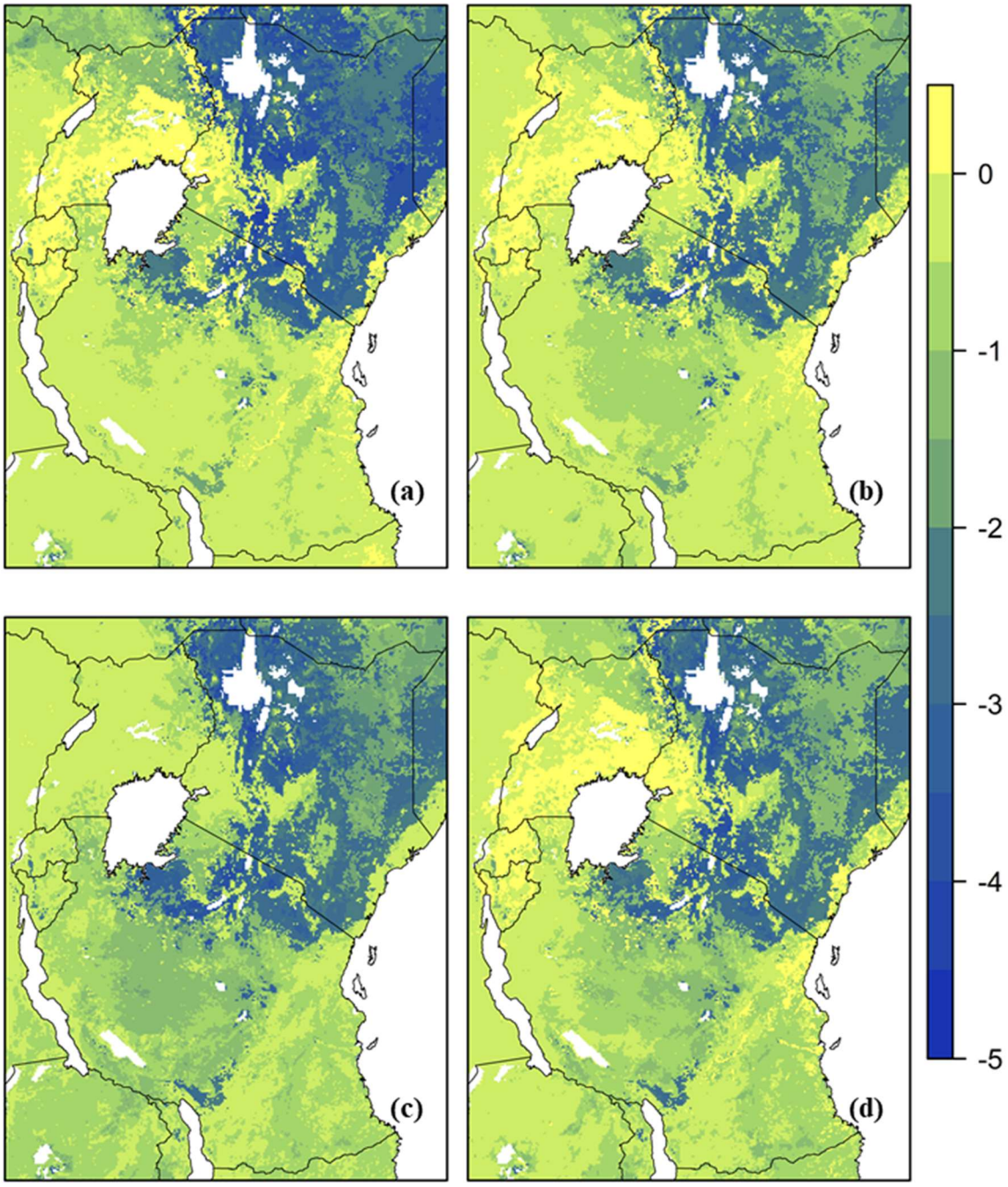

Figure A. 11: Mean seasonal changes in land surface temperature (°C) during (a) January-February, (b) March-May, (c) June-September and (d)October-December seasons.

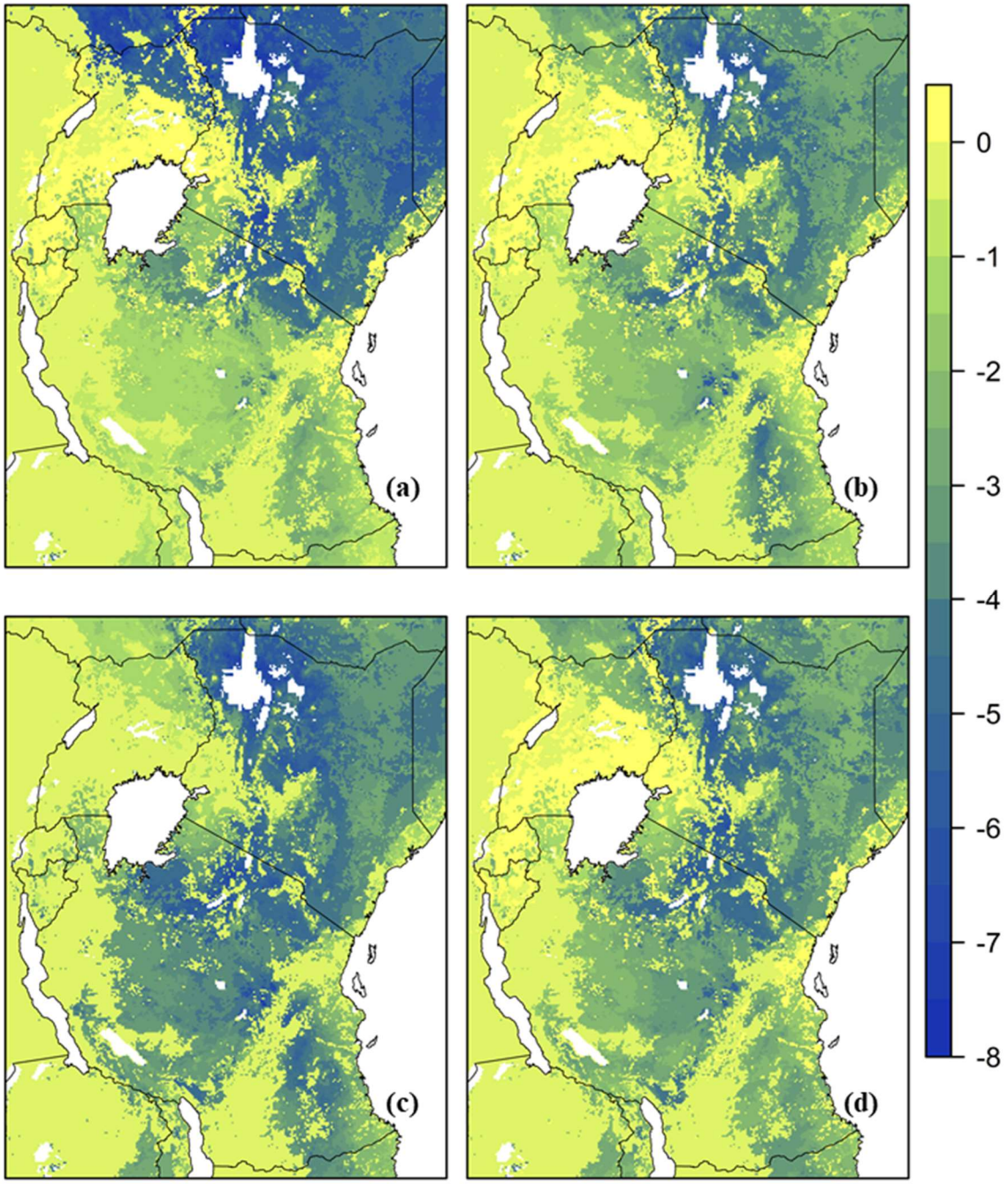

Figure A. 12: Mean seasonal changes in vegetation canopy temperature (°C) during (a) January-February, (b) March-May, (c) June-September and (d)October-December seasons.